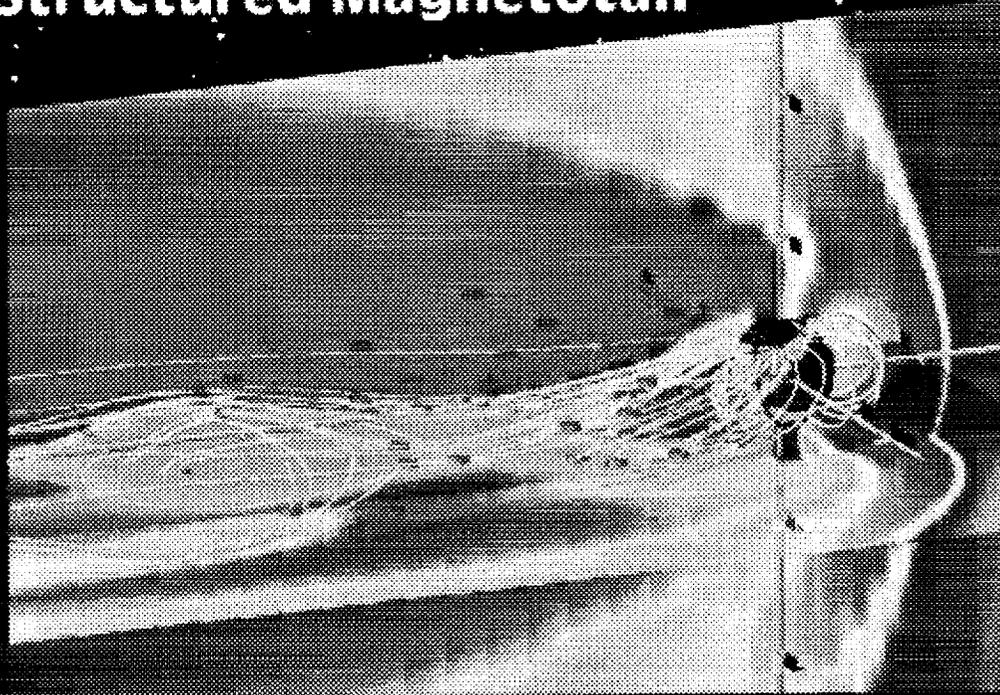The Magnetospheric Constellation Mission

Dynamic Response and Coupling Observatory (DRACO):

Understanding the Global Dynamics of the Structured Magnetotail

Report of the NASA
Magnetospheric Constellation
Science and Technology
Definition Team

REPORT DOCUMENTATION PAGE

Public reporting burden for this collection of information is estimated to average 1 hour per response, including the time for reviewing instructions, searching existing data sources, gathering and maintaining the data needed, and completing and reviewing the collection of information. Send comments regarding this burden estimate or any other aspect of this collection of information, including suggestions for reducing this burden, to Washington Headquarters Services, Directorate for Information Operations and Reports, 1215 Jefferson Davis Highway, Suite 1204, Arlington, VA 22202-4302, and to the Office of Management and Budget, Paperwork Reduction Project (0704-0188), Washington, DC 20503.

1. AGENCY USE ONLY *(Leave blank)*	2. REPORT DATE May 2001	3. REPORT TYPE AND DATES COVERED Technical Memorandum

4. TITLE AND SUBTITLE
The Magnetospheric Constellation Mission
Dynamic Response And Coupling Observatory (DRACO):
Understanding the Global Dynamics of the Structured Magnetotail

5. FUNDING NUMBERS
460

6. AUTHOR(S)
Report of the NASA Science and Technology Definition Team for the
Magnetospheric Constellation Mission DRACO

7. PERFORMING ORGANIZATION NAME(S) AND ADDRESS (ES)

Goddard Space Flight Center
Greenbelt, Maryland 20771

8. PEFORMING ORGANIZATION REPORT NUMBER
2001-00790-0

9. SPONSORING / MONITORING AGENCY NAME(S) AND ADDRESS (ES)

National Aeronautics and Space Administration
Washington, DC 20546-0001

10. SPONSORING / MONITORING AGENCY REPORT NUMBER
TM—2001–209985

11. SUPPLEMENTARY NOTES

12a. DISTRIBUTION / AVAILABILITY STATEMENT
Unclassified–Unlimited
Subject Category: 46
Report available from the NASA Center for AeroSpace Information,
7121 Standard Drive, Hanover, MD 21076-1320. (301) 621-0390.

12b. DISTRIBUTION CODE

13. ABSTRACT *(Maximum 200 words)*

Magnetospheric Constellation Dynamic Response and Coupling Observatory (DRACO) is the Solar Terrestrial Probe (STP) designed to understand the nonlinear dynamics, responses, and connections within the Earth's structured magnetotail, using a constellation of ~50-100 distributed vector measurement spacecraft. DRACO will reveal magnetotail processes operating within a domain extending 20 Earth radii (R_E) across the tail and 40 R_E down the tail, on spatial and time scales accessible to global circulation models, i.e., ~2 R_E and 10 seconds.

14. SUBJECT TERMS
DRACO, magnetotail, plasma, nanosatellite.

15. NUMBER OF PAGES
43

16. PRICE CODE

17. SECURITY CLASSIFICATION OF REPORT Unclassified	18. SECURITY CLASSIFICATION OF THIS PAGE Unclassified	19. SECURITY CLASSIFICATION OF ABSTRACT Unclassified	20. LIMITATION OF ABSTRACT UL

NSN 7540-01-280-5500

Standard Form 298 (Rev. 2-89)
Prescribed by ANSI Std. Z39 18
298-102

The NASA STI Program Office ... in Profile

Since its founding, NASA has been dedicated to the advancement of aeronautics and space science. The NASA Scientific and Technical Information (STI) Program Office plays a key part in helping NASA maintain this important role.

The NASA STI Program Office is operated by Langley Research Center, the lead center for NASA's scientific and technical information. The NASA STI Program Office provides access to the NASA STI Database, the largest collection of aeronautical and space science STI in the world. The Program Office is also NASA's institutional mechanism for disseminating the results of its research and development activities. These results are published by NASA in the NASA STI Report Series, which includes the following report types:

- TECHNICAL PUBLICATION. Reports of completed research or a major significant phase of research that present the results of NASA programs and include extensive data or theoretical analysis. Includes compilations of significant scientific and technical data and information deemed to be of continuing reference value. NASA's counterpart of peer-reviewed formal professional papers but has less stringent limitations on manuscript length and extent of graphic presentations.

- TECHNICAL MEMORANDUM. Scientific and technical findings that are preliminary or of specialized interest, e.g., quick release reports, working papers, and bibliographies that contain minimal annotation. Does not contain extensive analysis.

- CONTRACTOR REPORT. Scientific and technical findings by NASA-sponsored contractors and grantees.

- CONFERENCE PUBLICATION. Collected papers from scientific and technical conferences, symposia, seminars, or other meetings sponsored or cosponsored by NASA.

- SPECIAL PUBLICATION. Scientific, technical, or historical information from NASA programs, projects, and mission, often concerned with subjects having substantial public interest.

- TECHNICAL TRANSLATION. English-language translations of foreign scientific and technical material pertinent to NASA's mission.

Specialized services that complement the STI Program Office's diverse offerings include creating custom thesauri, building customized databases, organizing and publishing research results . . . even providing videos.

For more information about the NASA STI Program Office, see the following:

- Access the NASA STI Program Home Page at http://www.sti.nasa.gov/STI-homepage.html

- E-mail your question via the Internet to help@sti.nasa.gov

- Fax your question to the NASA Access Help Desk at (301) 621-0134

- Telephone the NASA Access Help Desk at (301) 621-0390

- Write to:
  NASA Access Help Desk
  NASA Center for AeroSpace Information
  7121 Standard Drive
  Hanover, MD 21076-1320

NASA/TM—2001-209985

The Magnetospheric Constellation Mission
Dynamic Response And Coupling Observatory (DRACO):
Understanding the Global Dynamics of the Structured Magnetotail

Report of the NASA Science and Technology Definition Team
for the Magnetospheric Constellation Mission DRACO

May 2001

For more information on the Magnetospheric Constellation mission contact:
Thomas E. Moore, Code 692.0, NASA Goddard Space Flight Center, Greenbelt, MD 20771
thomas.e.moore@gsfc.nasa.gov (301) 286-5236

Science and Technology Definition Team (STDT)

Chair
Harlan Spence
Dept. of Astronomy and Center for Space Physics
Boston University
Boston, MA

Project Study Scientist
Thomas Moore
Laboratory for Extraterrestrial Physics
NASA Goddard Space Flight Center
Greenbelt, MD

Project Formulation Manager
Mary DiJoseph
NASA Goddard Space Flight Center
Greenbelt, MD

Acting Project Formulation Manager
Robert Buchanan
NASA Goddard Space Flight Center
Greenbelt, MD

Committee Members
Brian Anderson
Applied Physics Laboratory
Johns Hopkins University
Laurel, MD

Vassilis Angelopoulos
Space Sciences Laboratory
University of California, Berkeley
Berkeley, CA

Wolfgang Baumjohann
Max Planck Institute for
Extraterrestrial Physics
Garching, Germany

Joseph Borovsky
Space and Atmospheric Science
Los Alamos National Laboratory
Los Alamos, NM

Robert Carovillano
Department of Physics
Boston College
Chestnut Hill, MA

Paul Craven
Space Science Department
NASA Marshall Space Flight Center
Huntsville, AL

Joseph Fennell
Space Particles and Fields
The Aerospace Corporation
El Segundo, CA

Charles Goodrich
Department of Physics and Astronomy
University of Maryland
College Park, MD

Michael Hesse
Electrodynamics Branch
NASA Goddard Space Flight Center
Greenbelt, MD

Xinlin Li
Laboratory for Atmospheric and Space Physics
University of Colorado, Boulder
Boulder, CO

Kristina Lynch
Department of Physics
University of New Hampshire
Durham, NH

Peter Panetta
Systems, Technology, and Advanced Concepts
NASA Goddard Space Flight Center
Greenbelt, MD

Joachim Raeder
Institute for Geophysics and Planetary Physics
University of California, Los Angeles
Los Angeles, CA

Geoffrey Reeves
Space and Atmospheric Science
Los Alamos National Laboratory
Los Alamos, NM

David Sibeck
Applied Physics Laboratory
Johns Hopkins University
Laurel, MD

George Siscoe
Dept. of Astron. and Center for Space Physics
Boston University
Boston, MA

Nikolai Tsyganenko
Raytheon
NASA Goddard Space Flight Center
Greenbelt, MD

Solar Terrestrial Probes Senior Project Scientist
Richard Vondrak
NASA Goddard Space Flight Center
Greenbelt, MD

Solar Terrestrial Probes
Senior Project Scientist for Geospace
James Slavin
NASA Goddard Space Flight Center
Greenbelt, MD

Magnetospheric Constellation Program Scientist
James Spann
NASA Headquarters
Washington, DC

Acknowledgments

The Magnetospheric Constellation Science and Technology Definition Team (MCSTDT) would especially like to thank the unwavering support, bold direction, and visionary leadership provided by the following NASA team members:

Dana Brewer, Advanced Technology and Mission Studies, NASA Headquarters

George Withbroe, Solar Terrestrial Probes Program Scientist, NASA Headquarters

Lawrence Zanetti, Magnetotail Constellation Program Scientist, NASA Headquarters

Without their dedicated and deliberate service to the space science community, the financial resources, administrative support, and agency impetus, this study and mission would clearly not have been possible.

In addition, the MCSTDT gratefully thanks the previous pioneering efforts of Magnetospheric Constellation planning provided by NASA's Geospace Multiprobes Science and Technology Definition Team. We would also like to thank both the former and the current NASA Office of Space Science Roadmap Teams. As part of the

Roadmap effort, we especially recognize the Sun-Earth Connection Advisory Subcommittee (SECAS) for their efforts in helping to define, refine, and clarify this report. We also gratefully acknowledge the considerable mission development efforts that have sprung from the grass-roots community. Contributions from within the space science community-at-large are manifestly visible through presentations made at several special sessions at scientific meetings and published in refereed publications. Those documented efforts have figured largely in the conceptualization and implementation of this report.

We also acknowledge the editorial efforts of Vassilis Angelopoulos and Peter Panetta in assembling the papers presented at a special session of the fall 1997 meeting of the American Geophysical Union, in a volume published by the University of California at Berkeley [1998]. These papers point the way to future constellation class missions, including Magnetospheric Constellation DRACO.

Finally, we should like to recognize all those scientists and engineers who, over the past 40 years of research and development, have provided the scientific basis, technological readiness, and insights needed to embark on this millennium mission.

> "Looking to the future I believe that progress requires bunches of satellites, though these are as yet in no published program. One is continually conscious of this need for reasons which have a direct analogue on the ground...[S]ince satellites are being launched singly, the scientific returns are less than they could be." *J. Dungey [1966]*[1]
>
> "Most of the important phenomena involve simultaneous variations in space and time. In some cases simultaneous measurements made at two well-chosen locations will provide unambiguous results. In other cases, it may be necessary to make simultaneous measurements at several hundred locations." *C. E. McIlwain [1967]*[2]
>
> *...Yesterday's Future is Now!*

[1] from "Inaugural Lecture as Professor of Physics at Imperial College," 1966; quote courtesy of W. J. Hughes.
[2] from "Comments and Speculations Concerning the Radiation Belts," page 303 (Proceedings of the Joint IQSY/COSPAR Symposium, London, 1967, Part 1), MIT Press, 1967; quote courtesy of R. B. Sheldon.

Contents

Executive Summary

Magnetospheric Constellation Dynamic Response and Coupling Observatory (DRACO) is the Solar Terrestrial Probe (STP) designed to understand the nonlinear dynamics, responses, and connections within the Earth's structured magnetotail, using a constellation of ~ 50-100 distributed vector measurement spacecraft. DRACO will reveal magnetotail processes operating within a domain extending 20 Earth radii (R_E) across the tail and 40 R_E down the tail, on spatial and time scales accessible to global circulation models, i.e., ~ 2 R_E and 10 seconds. Visualizing and understanding them will require observations analogous to a network of weather stations distributed within this domain. DRACO will reveal simultaneously for the first time both the global spatial structures and the time variations of the magnetotail. It will determine which phenomena are responses to solar wind inputs and which occur as a result of internal instabilities. In particular, it will reveal the locations and extents of the instabilities that trigger the explosive release of solar wind energy, mass, and momentum stored within the magnetotail, how these entities are transported, and the means by which magnetotail phenomena are propagated between regions and to the auroral ionosphere.

The magnetotail is a critical volume of the geospace environment wherein global circulation of magnetic fields and plasmas is regulated in response to changing solar wind conditions. In it, impulsive localized flow bursts launch and dissipate, powerful electrical currents form and evolve abruptly, and magnetic energy is explosively converted to particle energy. The fundamental plasma process known as magnetic reconnection is thought to occur during substorms, an important building block of "space weather." These are recurrent energy releases that become more frequent during magnetospheric storms. The dynamism and turbulent evolution of the magnetotail have humbled our efforts to observe and understand it using individual spacecraft. The magnetotail magnetic fields and plasmas do possess an underlying, slowly varying coherent structure, but strongly turbulent flows and fields are usually large compared to the mean field or flow. Thus, globally coherent pictures of the system dynamics become lost in the "noise" of individual measurements. Despite over 30 years of research with ever more sophisticated instrumentation on ever larger and more complex spacecraft, fundamental questions concerning the dynamic response of the magnetotail remain unanswerable. Accordingly, scientific progress has slowed. Intelligent, reasonable scientists cannot reach consensus on these issues, not for lack of models and theories, but because of a lack of relevant measurements. Neither current single spacecraft nor tight groups of spacecraft can resolve these fundamental controversies.

To provide the first ever global time-evolving vector field and streamline images of this important region, DRACO will use rapidly developing technologies to deploy a "constellation" of nanospacecraft. With resources of ~ 10-20 kg and 10 W apiece, 50-100 nanosatellites will be deployed in highly elliptical, equatorial orbits with common perigees of 3 R_E, and apogees distributed from 7 to 40 R_E, yielding mean inter-spacecraft separation of ~ 1-2 R_E.

The nominal DRACO mission has a design lifetime of 2 years, and is currently scheduled for a 2010 launch. While the enabling technologies for DRACO are developed or in development for the ST-5 Nanosat Constellation Trailblazer mission of the New Millennium Program, additional resources are required to demonstrate mass manufacturability and to optimize miniaturization while preserving functionality. With such resources, DRACO development could be accelerated with the launch as early as 2008.

Magnetospheric Constellation DRACO represents the logical outgrowth of a sequence of STP missions, designed to explore plasma transport and energy conversion processes over spatial sizes ranging from the distance to the Sun to the size of low-energy particle gyro-orbits. The Magnetospheric Multiscale (MMS) mission will focus on the smallest scale, microphysical processes occurring within and near magnetospheric boundary layers: magnetic reconnection, charged particle acceleration, and eddy turbulence. It will serve as the plasma physical "microscope," investigating scales too small to be resolved by global circulation models. In contrast, DRACO is designed to be a "meso/macro-scope" for the magnetotail. It will resolve persistent controversies by providing the required observations. Ultimately, it will yield a new understanding on which we shall build a predictive science of next-generation magnetospheric meteorology, adding to our collective body of knowledge relating to complex nonlinear dynamical systems.

Magnetospheric Constellation DRACO Highlights:

- DRACO will answer the following questions: How does the magnetotail control energy flow? What processes control magnetotail structure and dynamics? How do the physical processes and regions couple over the hierarchy of scales?

- Leads to closure of crucial magnetotail controversies that have remained unresolved for more than 30 years, owing to lack of coordinated multipoint observations.

- Single Delta launch creates a magnetotail constellation with possible launch in mid-2010 or earlier.

- 50-100 spacecraft with 10 sec time resolution, at mean separation of ~ 1-2 R_E over ~ 20 x ~ 30 R_E domain, resolve all features of global circulation models.

- Primary science accomplished annually when the constellation sweeps through the magnetotail. Ancillary magnetospheric/magnetosheath/solar wind science accomplished during balance of each year.

- New technology requirement is for miniaturization and mass manufacturability of nanosatellites and their instrument payloads.

1.0 Introduction and Science Objectives

1.1 Magnetotail Configuration

The geomagnetic field carves out a three-dimensional cavity in the flow of solar wind plasma, known as the magnetosphere, as illustrated in **Figure 1**. Supersonic solar wind plasmas stream away from the Sun and are heated, deflected, and decelerated at the bow shock. Within the magnetosheath, the slowed plasma flows around the magnetopause, the locus of positions where the incident solar wind pressure balances that of the geomagnetic field. The magnetopause is not a perfectly impenetrable boundary, though. A small fraction of the solar wind mass, energy, and momentum enter the cavity, resulting in the transfer of energy to the magnetosphere. The amount of energy and the locations for entry are controlled by constantly varying solar wind conditions. The transferred energy is stored principally in the region called the magnetotail, a vast re-

gion of dynamically evolving magnetic fields and plasmas stretching far from the Earth in the anti-solar direction.

The Earth's magnetotail consists of several distinct regions (ref. **Figure 1**). Much of the plasma in the magnetotail resides in the plasma sheet, a region of hot plasma extending across the tail from the dawn to the dusk edge, and extending from the distant tail into the inner magnetosphere. The thermal pressure of the plasma sheet is substantial and supports a delicate balance between the plasma sheet and the stretched field lines of the low-density northern and southern tail lobes. Enshrouding the northern and southern lobes are the plasma mantles or High Latitude Boundary Layers (HLBL). The HLBL are regions of dense, cool plasma flowing along the magnetic field lines in the anti-Sunward direction. They contain plasma mainly of solar wind origin with a minor component that has escaped from the ionosphere. On the dawn and dusk flanks of the magnetosphere are the Low-Latitude Boundary Layers (LLBL), regions of anti-Sunward
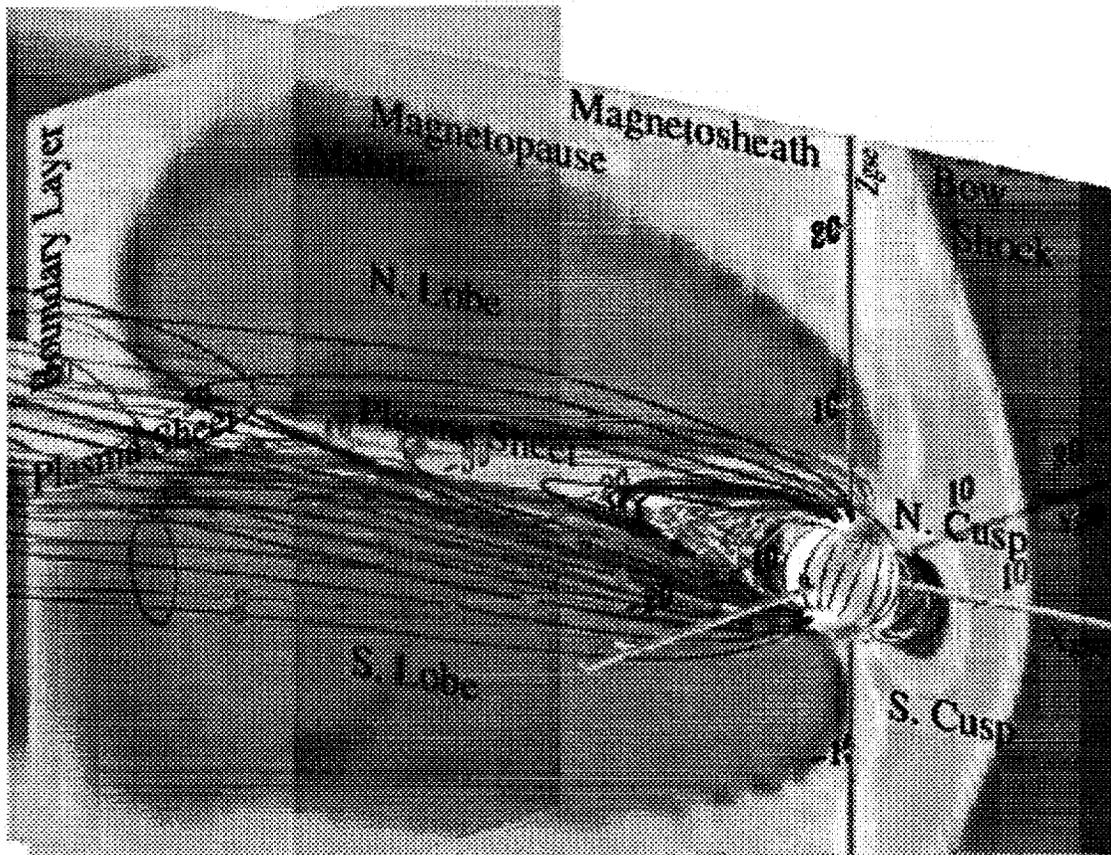
Figure 1. The figure illustrates the computed magnetotail and its major component regions and boundaries in three dimensions; figure was generated from the results of magnetohydrodynamic global simulation modeling. Color-coding indicates plasma density on intersecting planes at Y=0, and at X= 40 Earth radii. Labels indicate significant boundaries and other features. Light blue magnetic field lines originate from geomagnetic mid-latitudes, while dark blue field lines originate in the polar cap region. Red dots indicate typical constellation spacecraft positions near the plasma sheet (green color on the Y=0 plane). Figure is provided courtesy of J. Raeder, UCLA.

flowing plasma of solar wind origin, again mixed with magnetospheric plasma. Finally, the northern and southern Plasma-Sheet Boundary Layers (PSBL) lie between the plasma sheet and the lobes. The PSBL typically contains magnetic-field-aligned beams of electrons and ions that originate from magnetic reconnection farther down the tail. These seemingly disparate regions are globally interconnected. This intricately linked system responds dynamically to external boundary conditions as well as to internal reconfigurations on short time scales.

Much of the plasma of mixed internal and external origin becomes trapped within the geomagnetic field and is unable to escape directly downstream. This plasma participates in the global circulation of the magnetosphere. In the closed field region of the magnetotail, the magnetic field lines are stretched into a long plasma tail. Curvature forces in the stretched field lines ultimately cause the entrained plasmas to convect Sunward back toward the dayside magnetosphere from which they came, thereby completing the cycle of global circulation. The earliest models of the magnetosphere cast this process as a simple time-independent circulation. Today, we know that the Earthward, return flow is both highly variable in time and highly structured in space. Consequently, single spacecraft studies have faced overwhelming challenges in unambiguously describing the fundamentals of this flow. The flow is a vital link in understanding how the solar wind energy propagates through and thereby affects geospace. Accordingly, it is a focal point of the DRACO mission.

With the exception of global magnetohydrodynamic (MHD) models, global magnetospheric models are static [Tsyganenko, 1989, 1995]. The large magnetic field variability in the databases that are used as input to those models [Stern and Tsyganenko, 1992] suggests that a significant part of the physics that determines the most probable magnetospheric state is missed. Most often, severe modification of the model currents is necessary away from expected state [i.e., for the measured Kp or AE parameter] when actual time-dependent situations are considered [Pulkkinen, 1991; Baker et al,. 1993]. It is impossible for a static model parameterized on global indices to capture

the complexity, the richness and the physics of the instantaneous magnetospheric configuration. However, a large array of measurements from magnetospheric probes can produce, when inverted using techniques available from statistical [Tsyganenko and Usmanov, 1982], simulation [Berchem et al., 1995] and atmospheric [Ghil and Malanotte-Rizzoli, 1997] models, an instantaneous "image" of currents and fields that is consistent with the average tail structure but representative of the instantaneous measured fields. This can produce a far clearer picture of the magnetospheric current systems, their sources and sinks and their temporal evolution. Parameterization versus substorm-phases and upstream conditions can produce the "typical" substorm sequence, i.e., a time history of the magnetospheric system's response to qualitatively different drivers.

1.2 The 'Quiet' Plasma Sheet

Global Versus Turbulent Transport and Thermodynamics — Magnetospheric Constellation DRACO will provide the critical new observations for visualizing and understanding large-scale plasma transport within the magnetotail. Single spacecraft missions have explored this region comprehensively over time, but we still have only a poor understanding of its global, quiet-time, instantaneous behavior. Indeed, past single-satellite observations have presented important glimpses into the underlying texture of the near-Earth magnetotail. It is known, for instance, that the magnetic field of the plasma sheet has large fluctuations and that its plasma flows are highly erratic [Hayakawa et al., 1982; Borovsky et al., 1997].

While the most dramatic flow events are associated with geomagnetically active times, the most probable state of the plasma sheet (90-95% of the time) is the state possessing no significant bulk flow [Baumjohann et al., 1989, 1990]. That state exhibits random flow directions with peak-to-peak amplitude many times larger than the average flow itself [Angelopoulos et al., 1993]. Despite the large flow variability, the average flow pattern exhibits behavior that can be understood in simple 2-fluid theory [Angelopoulos et al., 1993] or single particle orbits [Spence et al., 1993a, 1993b]
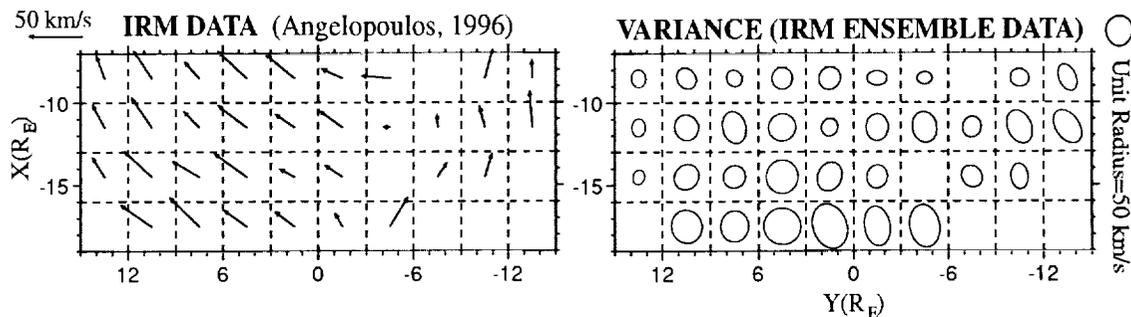
Figure 2. The mean flow and variability of the magnetotail, showing that a Sunward/duskward circulation prevails (in the positive X and Y directions), but that the variability of the flow is as large or larger than the mean flow speeds (right panel). Figure is courtesy of V. Angelopoulos.

(**Figure** 2). Significant variability about the magnetic field average also exists [*Stern and Tsyganenko*, 1992], rendering orbit integration schemes vulnerable to criticism [*Cattell et al.*, 1995]. Is the variability the consequence of nearby high-speed flows [*Angelopoulos et al.*, 1994; *Borovsky et al.*, 1997] or the result of nonadiabatic ion trajectories under steady external conditions [*Ashour-Abdalla et al.*, 1995]? Both theories are viable yet presently unresolvable with available observations. DRACO will provide the comprehensive view of plasma sheet flows needed to unravel these questions. Furthermore, what role does the flow variability have on resolving the long-standing, "pressure balance inconsistency" which arises in models of time-independent, laminar tail convection?

As noted above, statistical treatments reveal an average Earthward flow in the plasma sheet, but with fluctuations as large or larger than the average flow. Indeed, this irregular flow of the plasma sheet may become fully turbulent. Turbulence data-analysis methods have been applied to single-satellite measurements of fields and flows [*Borovsky et al.*, 1997]. Models of the magnetotail morphology based upon turbulent transport have been developed, and models of auroral activity driven by flow turbulence in the plasma sheet have been constructed [*Swift*, 1981; *Song and Lysak*, 1988].

Velocity auto-correlation times are of the order of 2 to 3 minutes and mixing lengths of the order of 1-2 R_E. This suggests that although large-scale eddies are occasionally observed in the plasma sheet [*Hones et al.*, 1978, 1981] underlying effective mixing also takes place at shorter scale lengths. In order to characterize this state of the plasma sheet, correlative measurements at many points of the system are necessary in order to measure the wavelength spectrum of the plasma sheet flows. This will tell us whether substorm processes generate the variability or whether it is an inherent, fundamental property of the convecting plasma sheet. Distribution functions are necessary in order to ascertain whether the flow variability is due to particle bunching or a velocity shift of the entire particle distribution.

Recent results from the International Solar Terrestrial Project (ISTP)-era indicate that beyond ~ 30 R_E the magnetic field configuration is tail-like and the plasma beta is high. Present observations indicate that in this region the flow is reasonably laminar. Closer in, the Earthward-jetting plasma encounters the deflecting effect of the Earth's rigid dipolar field [*Baumjohann*, 2000]. In this transition region, the flow is observed to grow more turbulent. The transition from laminar to turbulent, which may additionally involve bursty and localized reconnection, can only be realistically studied using a constellation of spacecraft.

The fundamental thermodynamic properties of the plasma sheet are also not clearly understood. *Huang et al.* [1992] have shown that plasma sheet temperature increases after substorm onset represent an important plasma sheet response to geomagnetic activity but that they do not al-

ways correlate with flow enhancements. Although single particle approaches [*Spence*, 1993a, 1993b; *Ashour-Abdalla et al.*, 1994] have led to certain predictive pictures of the plasma sheet pressure, temperature and density spatial profiles, such profiles have not been reported except in energetic particles [*Krimigis and Sarris*, 1979]. Thus, there is a need to observe the system and its evolution at many points simultaneously for a given thermodynamic state. This entails fine spatial resolution observations of the instantaneous flow pattern, density and temperature to observe the source and propagation of the resulting heating.

The reason for the fine spatial resolution is twofold: First, the acceleration regions are localized in space [*Krimigis and Sarris*, 1979; *Sergeev et al.*, 1986b, 1996; *Angelopoulos et al.*, 1997]. Second, the plasma sheet flow and thus particle trajectories are variable at inferred spatial scales of ~ 2 R_E. Without a dedicated constellation mission, it has been shown to be unlikely that two spacecraft will have many chances of crossing the same flow line at a given time. The high spatial density and high-time resolution distribution functions provided by DRACO are necessary to resolve this problem.

Attempts to characterize the detailed thermodynamics of the plasma sheet (such as measuring its polytropic index) have been made [*Baumjohann and Paschmann*, 1989; *Huang et al.*, 1989; *Goertz and Baumjohann*, 1991]. However, there is always a great uncertainty in any inferred result, because with a single spacecraft we cannot observe the evolution of a single flux tube. Multiprobe studies that utilize two (or more) spacecraft traversing plasma streamlines will be able to answer the aforementioned question. However, discoveries from such a multiprobe mission may result in a complete change of mindset regarding this issue; if the plasma flow is nonlaminar, the concept of a streamline may be invalid.

1.3 Global Aspects of Magnetic Reconnection

Magnetic reconnection is one of the most important energy transfer mechanisms operating throughout the magnetosphere, yet we have little knowledge of how it is triggered and what its consequences are globally. It is thought to be the driver by which energy enters the magnetosphere from the solar wind, and important for the ultimate release of this transferred energy which builds up episodically in the magnetotail. Over long enough time intervals and integrated over the entire spatial volume, dayside and nightside reconnection rates must balance so that no magnetic flux is permanently added to or removed from the Earth's magnetosphere. Transient increases of one rate over the other are important drivers of short-term magnetotail dynamics in which the magnetotail moves from one state to another. The magnetotail varies in response to constantly varying solar wind conditions imposed on the magnetopause boundary. Some of these responses occur in direct relation to the external drivers, while others are tied

to internal global instabilities. Despite the vastness of the three-dimensional magnetotail, its regions are closely linked electrodynamically, and respond globally in complex ways. The Magnetospheric Constellation DRACO mission is designed to resolve these important features of the magnetotail.

Based on the analysis of a vast quantity of single spacecraft data, the following is a phenomenological model of how the solar wind driver, through magnetic reconnection, sets the magnetotail toward a global instability known as a magnetospheric *substorm*. Magnetic reconnection at the dayside magnetopause breaks open closed geomagnetic field lines and "reconnects" each end to solar wind field lines, coupling and mixing the solar wind and internal plasmas. The motion of the solar wind drags the plasma on these "open" field lines downstream and into the magnetotail. The field lines are added to the northern and southern lobes and stored there as excess magnetic energy, further squeezing and stretching the fields in the plasma sheet.

The stretching continues until some yet undetermined instability occurs. The excess open field lines in the lobe must eventually reconnect a second time to conserve flux; this time going from an open to a closed topology. It is this reconnection in the tail between magnetic flux tubes once concentrated in the lobes that most likely powers geomag-

netic substorms — the most common dynamical magnetotail event. The solar wind and ionospheric ends of lobe field lines decouple, releasing stored energy, and restoring closed field lines within the magnetosphere and interplanetary magnetic fields in the solar wind. The extended closed magnetic field lines, and the plasma on them, then collapse back closer to a dipolar configuration. The process creates a magnetic bubble of plasma, a *plasmoid*, downstream of the reconnection region that moves back into the solar wind [*Hoshino et al.*, 1996; *Mukai et al.*, 1996; *Slavin et al.*, 1998]. **Figure 3** is a cartoon depicting the gross morphology of the magnetotail just after the global substorm instability has occurred.

While the stretching, growth phase of a substorm can be gradual (~ 1 hour), the relaxation toward a dipolar configuration, or dipolarization, is typically abrupt and dramatic (~ 1 minute), characterized by high inductive electric fields and fast plasma flows. The magnetic energy once stored in the lobe fields is converted rapidly at substorm onset to particle energy that is then released through the plasma sheet. Some particles are accelerated to high energies and injected into the inner magnetosphere. Others precipitate to form auroras at high latitudes.

While initially a regionalized phenomenon, magnetospheric substorm effects become demonstrably global and evolve rapidly through the entire volume. Syntheses of single point
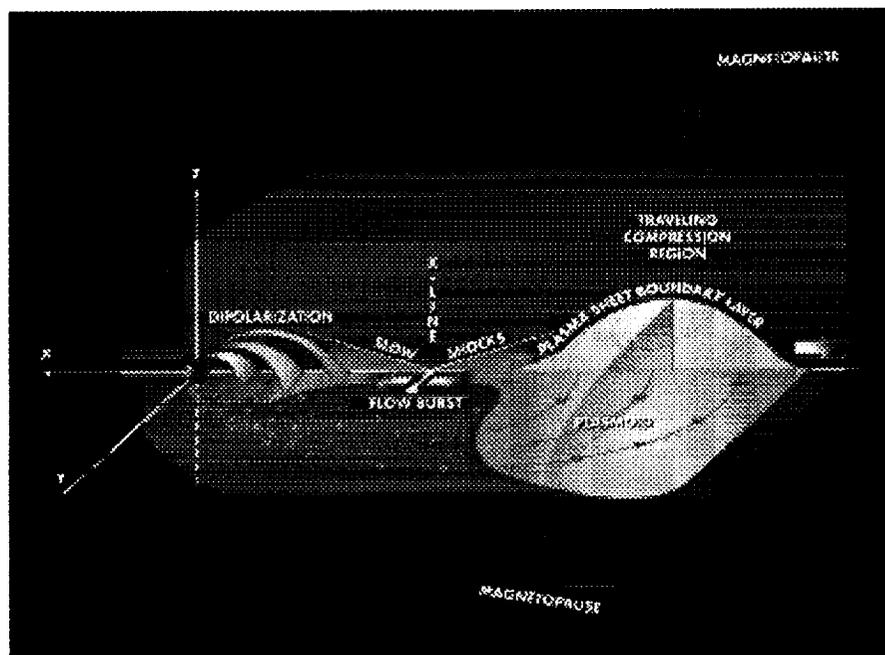
Figure 3. A cartoon of the global consequences of tail reconnection during a substorm. After a reconnection site has formed near Earth, fast flows propagate Sunward accompanied by a rapid dipolarization. A plasmoid has formed and is traveling downstream, creating a traveling compression region in the magnetic lobes. DRACO nanosatellites are shown schematically throughout the plasma sheet. Courtesy of J. Slavin/NASA Goddard Space Flight Center (GSFC).

measurements have led to statistical cartoons such as that shown above. While significant insights into tail dynamics have come from such analyses, our views have been limited and competing theories have remained untested. To compensate for this observational deficit, further insights into substorm dynamics have been gleaned by appealing to MHD models. The macroscopic structures illustrated schematically in **Figure 3** are present in virtually all MHD models of the dynamic magnetotail (**Figure 4**). These numerical models reveal intricacies of the magnetic topologies and complexities in the flows not only during substorm intervals, but also during the relatively quiet resting state of the magnetotail. They also predict dramatic variability of their time evolution that certainly confounds analysis by single, or even several, tightly clustered spacecraft. From the MHD model results, it is clear that magnetic reconnection plays a major role in the configuration and dynamics of the magnetotail, and that reconnection is likely both bursty and patchy.

The magnetospheric research community relies on a concept of magnetotail structure that has been constructed by averaging measurements taken by various single satellites. In large measure, we rely on understanding the magnetotail's global dynamics through computer simulations having relatively coarse spatial resolution and sometimes incomplete parameterization. The community has come to realize that deficiencies of this magnetotail conceptualization are impeding progress in understanding how the magnetosphere actually behaves. DRACO will,

for the first time, reveal in three dimensions the true instantaneous evolution of the elusive substorm sequence in the magnetotail that we have only seen glimpses of in sparse data and physical models.

1.4 The Substorm Problem: Chronology and Associated Mesoscale Structures

As detailed earlier, the Earth's magnetotail is a complex and dynamic region of the magnetosphere. Intense, small-scale plasma flows typically conceal the large-scale flow pattern within the plasma sheet. The magnetic field in the plasma sheet often exhibits small-scale kinks and tangles. However, during certain intervals, the Earth's magnetosphere undergoes large coherent changes in its global morphology, events we call *substorms* and *magnetic storms*. These phenomena are not fundamental physical processes in themselves, but rather a collection of chronologically ordered physical processes that repeat episodically in some quasi-regular way. MHD models suggest that there is substantial coherence within these global reconfigurations, a feature that is extremely hard to arrive at from single point measurements. The meta-process of a substorm represents the most frequent mode of significant magnetospheric dynamics, and thus provides a practical context for understanding the consequences of the underlying microphysics. While substorms have galvanized the community's interest, a consensus understanding of the substorm has been hampered by data sparseness.
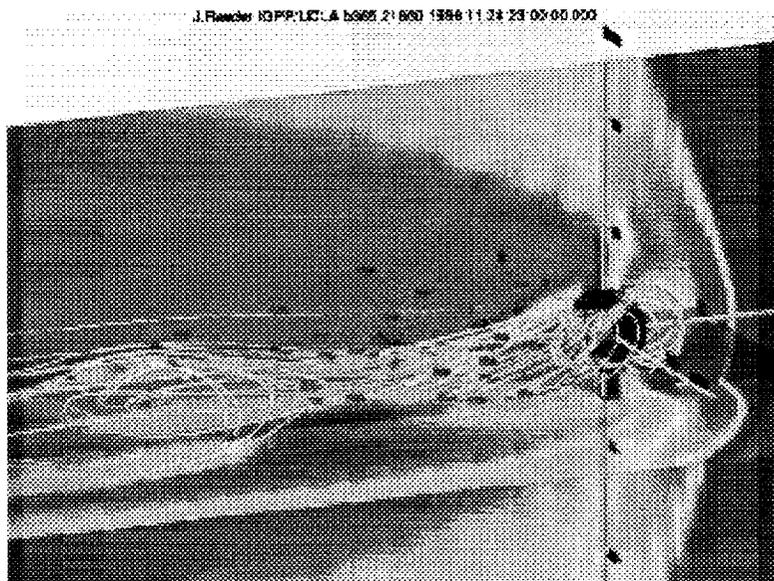
Figure 4. A snapshot from an MHD simulation of the dynamic magnetosphere. Sunward of a reconnection site near Earth, field lines are rapidly depolarizing, while a recently formed plasmoid is being ejected farther down the tail. Courtesy of J. Raeder/ UCLA.

1.4.1 Chronology and Causality

Ever since *Syun Akasofu* [1964] showed that auroral phenomena could be organized into characteristic recurrent patterns called "auroral substorms," substorms have been a topic of vigorous debate. In the ionosphere, a global picture can be obtained with all-sky cameras, radars, and magnetometer networks; in space, we depend on statistical analyses to compose a time history of events. There is broad consensus that the magnetotail exhibits a characteristic behavior during magnetospheric substorms, defined by diverse observed aspects including auroral expansion, magnetic field dipolarization, current wedge formation, dispersionless particle injections, bursty bulk flows, and current disruption. There is, however, no consensus on the physics of substorms, as suggested by the persistence of a designation that is only useful for classification and conveys little understanding of physical basis.

Recently, the debate has centered on the first few minutes of the substorm expansion phase: the so-called "substorm onset." The first sign of substorm activity should be located close to the causative source. From a few fortuitous multispacecraft conjunctions, we have learned that the field dipolarization starts at a localized region of the order of 1-2 R_E [*Ohtani et al.*, 1992]. The field dipolarization propagates longitudinally [*Nagai*, 1982] at a speed of an hour of local time every 1-3 minutes and radially tailward [*Jacquey et al.*, 1993; *Ohtani et al.*, 1991, 1992] with a speed of ~ 250 km/s, or 2.5 R_E/minute. Tailward flows are also observed during substorms and most often at distances greater than 19 R_E; Earthward flows are observed closer to Earth [*Baumjohann et al.*, 1990; *Angelopoulos et al.*, 1994]. These flows have been interpreted as signatures of magnetic reconnection. However, the time and location of the first magnetospheric signature of substorm onset and its relationship with the ground observables still remain a mystery. The present lack of an observational resolution of this point, in turn, inhibits theoretical progress in the understanding of the physics that govern the phenomenon. Two theories, each associated with a different initial location of substorm onset have been proposed, and each predicts a different chronology and causality that is testable by the DRACO mission.

One theory [*Lui*, 1991, 1996] holds that substorms start near or slightly outside geosynchronous orbit. Theories in this class suggest that the electrical current that produces the stretching of tail field lines is disrupted from flowing across the tail, instead flowing down along magnetic field lines and through the ionosphere. This forms the "substorm current wedge" [*McPherron et al.*, 1973] — a transient substorm feature inferred from magnetometer measurements near geosynchronous orbit. The new current system allows the local magnetic field to relax and become more dipolar, launching a rarefaction wave that propagates down the magnetotail [*Jacquey et al.*, 1993; *Lopez et al.*, 1993]. Some 20-30 Earth radii down the tail, it initiates increased magnetic reconnection of the type that turns open

lobe field lines back into closed field lines in the magnetosphere. This causes plasma to rush Earthward through the plasma sheet, allowing the plasma sheet to quickly reestablish itself and recover its plasma pressure and cross-tail current.

The other theory [e.g., *Schindler*, 1974; *Birn et al.*, 1996; *Baker et al.*, 1996; *McPherron et al.*, 1973; *Hones and Schindler*, 1979] argues that substorms start with increases in reconnection at a distance of 20-30 R_E. The stretched lobe magnetic field is reconnected, creating a burst of plasma flow that launches captured plasma and field toward the Earth, at the same time forming a plasmoid that is shed downstream [*Slavin et al.*, 1993; 1998]. The Earthward burst launches a compression wave toward Earth [*Moore et al.*, 1981; *Reeves et al.*, 1996; *Li et al.*, 1998], creating a flow of particles with a wide range of energies (100's of eV to 100's of keV) that runs into denser plasma and stronger magnetic field and is slowed and deflected as a result. The braking of the flow creates the observed substorm current wedge in this scenario. Also, at the same time, energetic particles up to ~ 500 keV are injected from the inner edge of the magnetotail to the trapping regions of the inner magnetosphere.

Both of these theories seek to account for the characteristics of a substorm in the magnetotail, including the dipolarization (relaxation) of the magnetic field to a less stressed state, the substorm current wedge, and the acceleration and injection of plasma into the dipolar region. However, the two have completely opposite flows of causality: one case, from the tail toward the Earth; the other, from near the Earth out into the magnetotail. **Figure 5** shows these two models schematically [*Baumjohann*, 2000]. The difficulty lies in the localization of the initial phenomena both in space (1-2 R_E) and in time (10-20 sec) and its subsequent propagation over great distances (10-20 R_E). Single spacecraft within the vast magnetospheric system have little chance of being at the key region at the exact time of substorm onset. More importantly, the lack of simultaneous measurements from adjacent "pixels" of this vast system prohibits placing the observed phenomenon in the context of the global magnetotail evolution. Many simulation results support the idea that the initial substorm disturbance originates farther out in the magnetotail and then propagates inward as described above in the second theory. Limited observations [*Ohtani*, 1998] show that the field configuration changes propagate inward at a speed less than the sound speed, suggesting that they are not accomplished by a hydromagnetic compression wave. Other observations suggest that the changes are simply convected by fast plasma flows (100's km/s), but field configuration accompanied by energetic particle injections were observed to travel as slowly as 25 km/s from 6.6 R_E to 4.5 R_E. Lack of consistent observational confirmation indicates that neither theory can be declared false, nor accepted as definitive. Thus, the most prevalent and important physical process in the magnetotail continues to escape scientific identification.
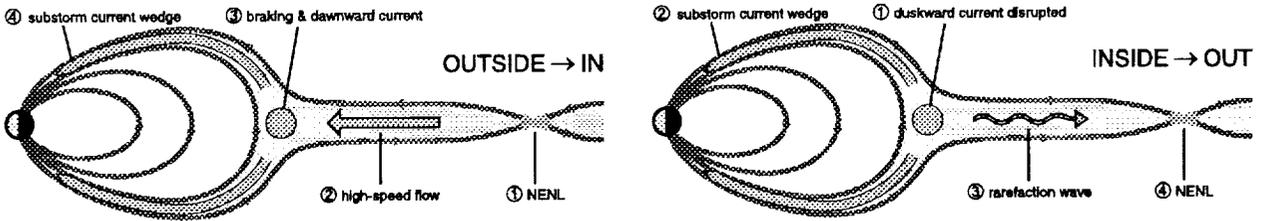
Figure 5. *DRACO will resolve a long-standing ambiguity in substorm chronology, illustrated in this figure. It will determine whether the magnetotail reconfigures rarefactively, from the inside out (right panel) or compressively, from the outside in (left panel).*

The maximum altitude of the spacecraft necessary to capture the reconnection process is determined from previous statistical studies of fast plasma sheet flows. Such studies [*Hayakawa et al.,* 1982; *Nakamura et al.,* 1994; *Hones and Schindler,* 1979] indicate that at a distance of ~ 35 R_E anywhere between 25% and 80% of fast flows observed were tailward; the variability is due to the selection criteria and methodology. Recent Geotail results place the most likely position of observation of the near-Earth neutral line at around X=-25 R_E [*Nishida et al.,* 1995] while they confirm that on the average the flows are tailward at distances of 30-60 R_E [*Frank and Paterson,* 1994]. Since tailward motion of the neutral line occurs, the neutral line is likely to start most often Earthward of X=-40 R_E at substorm onset. Thus, it is in the region between 7-40 R_E that onset and evolution of current disruption and near-Earth neutral line can be compared during the time of expansion phase onset of magnetospheric substorms. A suite of spacecraft at cross-tail separations ranging between 1 and 20 R_E and at downtail position between 7 to 40 R_E are a necessary and sufficient condition for the study of the magnetospheric evolution during the course of a substorm. Quantities necessary and sufficient are high time resolution (1-5 s) magnetic field and 3-D ion moment measurements.

1.4.2 Mesoscale Processes and Structures

Particle Acceleration Fronts—Substorms are a primary mechanism of energization of the nightside ionosphere and the ring current. Although the ultimate source of energy during substorms is the solar wind, the transfer of that energy to the plasma sheet particles is not well understood. Modeling of geosynchronous injections during substorms as broad spatial fronts of Earthward-collapsing particles [*Moore et al.,* 1981; *Mauk,* 1986] (based on measured electric fields observed in the near-Earth plasma sheet [*Aggson et al.,* 1983; *Maynard et al.,* 1996]) has produced fairly good agreement between theory [*Quinn and Southwood,* 1982] and observations. In that scenario, it is the braking of the Earthward flows [*Haerendel,* 1992] resulting from either the current disruption or the reconnection process that causes the near-Earth signatures of substorms. Until now, flow braking is established only statistically in that the occurrence rate drops with distance along the tail. DRACO can establish the instantaneous pattern of this phenomenon, which is a vital clue to its source. In the flow-brak-

ing region (10-15 R_E), the flow causes pressure gradients and, perhaps, vorticity, which is the source of the Substorm Current Wedge (SCW). The azimuthal gradient has been established statistically by observations and in simulations. DRACO will for the first time establish the instantaneous pattern.

Current Wedge — The longitudinal spread of the substorm current wedge [*Nagai,* 1982] is coupled to the evolution of the westward traveling surge in the ionosphere [*Roux et al.,* 1991; *Robert et al.,* 1984; *Maynard et al.,* 1996]. The extent in Y of the SCW at distances far from geosynchronous is neither known, nor possible to document with single spacecraft because it is a 3-dimensional system. *Lopez and Lui* [1990] used AMPTE/IRM and Charge Composition Explorer (CCE) observations to show that the SCW is irregular in space. In addition, substorms take place most often as a series of consecutive, isolated activations. The near-Earth and ground response is the integral response to the resulting consecutive elemental current wedges. Such individual activations have been proposed to be the elemental processes [*Lui et al.,* 1991; *Sergeev et al.,* 1986a, 1986b] that compose substorms. Multispacecraft observations will result in resolving the ambiguities associated with the number, location and extent of such activations.

In fact, ISTP studies [*Angelopoulos et al.,* 1997; *Slavin et al.,* 1997; *Fairfield et al.,* 1998] are already providing direct measurements of the extreme localization of the elemental activations and their relationship to the ionosphere. Despite the limited number of near-by conjunctions of ISTP spacecraft while in the magnetotail, it is possible with these to glimpse the complexity and richness of the magnetotail plasma when studied at intermediate spatial scales. Perhaps, though, the most important lesson learned from ISTP is the scarcity of fortuitous conjunctions and the need for a distributed satellite system even when the goal is the study of the microstructures and macrostructures. The subliminal, and prevailing, understanding is that the current wedge maps to the entire width of the aurora and that its outermost boundary is the location where the current feeds from the magnetosphere to the ionosphere. Thus, the SCW is an important key in the chain of energy from the plasma sheet plasma to the ionospheric Joule heating. Understanding the three-dimensional evolution of the substorm current wedge system promises to solidify estimates of the magnetospheric-ionospheric energy cou-

pling during a substorm, and in addition probe simultaneously its component activations and their ionospheric mapping.

"Bursty Bulk Flows" — The most prominent plasma sheet transport phenomena occur during short intervals and correlate well with substorm activity. Short-lived, high-velocity "bursty bulk flows" (BBF's) are observed within $|Y| < 10\ R_E$ from the midtail axis [Baumjohann et al., 1990; Angelopoulos et al., 1994]. In the magnetotail tailward of $X = -15\ R_E$, and close to the neutral sheet, fast plasma sheet flows are thought to be a significant if not dominant part of the long-term average transport of the plasma sheet energy, particle and magnetic flux [Angelopoulos et al., 1994]. Present estimates for the important spatial and temporal scales are about $\sim 2\ R_E$ and ~ 1 sec for flow bursts.

A significant impediment to understanding their significance is the uncertainty in their physical dimensions. Without knowledge of that critical parameter, we have only a vague understanding of how much flux and plasma they transport. Are the fast flows that are observed at substorm onset of sufficient energy to account for substorm energization of the near-Earth environment and the ionosphere? The answer depends on the 3-D evolution of the magnetotail flows. Given the extreme localization in Y of some of the fast flow events observed so far [Sergeev et al., 1996; Angelopoulos et al., 1996; Angelopoulos et al., 1997], simultaneous multipoint measurements over an extent of $dY \sim 20\ R_E$ and at a probe density of 1 measurement per 1-3 R_E in Y are necessary.

MHD models demonstrate similar mesoscale features and an example is shown in **Figure 6**. Four panels are shown of the equatorial plasma sheet. Flow vectors (arrows) and parallel current densities (color coded) are shown throughout the magnetotail at four different times during a substorm simulation. A flow burst is seen to race Earthward in the post midnight region and then brake as it reaches the inner magnetosphere. As the flow brakes, a current wedge appears that couples to the ionosphere. While the effects of this flow burst and wedge are prominent in the post-midnight region, little effect is seen in the midnight or premidnight sectors. During this same run, other flow bursts (not shown) are seen to originate in the tail and move Earthward but always at a different location. Without the coverage of a constellation, the scope and significance of these flow channels remain unknown.

Because the fast flows are bursty, they may likely come from localized reconnection. DRACO can determine the extent of the presumably local X-lines and will also be able to observe whether two or more small-scale X-lines can co-exist at any one time and whether these X-lines can develop into more global ones during major substorms. DRACO will provide the spacecraft spacing and distribution necessary to unravel both the spatial extent and temporal evolution of BBF's as well as their detailed role to the substorm.

Current Sheet Thickness and Evolution — Present theories that attempt to address the substorm onset question on the basis of current sheet instabilities require direct measurements of the current sheet thickness and intensity [e.g., Lui et al., 1991, Wang et al., 1990]. Attempts to model the current sheet thickness and density by inverting the observed magnetic field measured at more than one location during fortuitous conjunctions of spacecraft has lead to some success [Pulkkinen et al., 1991]. In addition, current measurement techniques in the tail using two spacecraft measurements [McComas et al., 1986] have given incontrovertible evidence for the existence of thin current sheets and their importance during substorms. However, the only possible way to ensure that the tail-current system is adequately monitored at the time and place where it actually becomes unstable is to simultaneously monitor its thickness at many different downtail distances. This necessitates a CLUSTER-like system at many different distances. One way to achieve that is to design for some orbits with enough separation in Z (~ 1-2 R_E) at different downtail distances. For current sheet densities of the order of 1 nA/m^2 which are typical of the cross-tail current, and intersatellite separations of 1 R_E such measurements can be made comfortably with 0.5 nT accuracy, i.e., well within the capabilities of conventional magnetometer designs.

Plasmoids and Flux Ropes — Plasmoids are large three-dimensional segments of the plasma sheet which are ejected down the tail in association with reconnection at the near-Earth reconnection site. When spacecraft are positioned in the tail beyond $X \sim -25\ R_E$ during magnetospheric substorms, plasmoids are detected with great regularity [e.g., Taguchi et al., 1998; Moldwin and Hughes, 1992; Slavin et al., 1993]. These large structures possess typical volumes and downtail speeds of $\sim 10^3$-10^4 cubic R_E and ~ 400-800 km/s, respectively. These dimensions have been inferred from a synthesis of single spacecraft observations, but we lack a clear view of the actual origin, structure, and evolution of plasmoids.

Schindler [1974] and Hones [1976] predicted the plasmoid phenomenon on theoretical grounds. As depicted earlier in **Figure 2**, these complex structures begin to form late in the substorm growth phase when reconnection at the near-Earth neutral line (NENL) is still limited to the closed magnetic flux tubes threading the plasma sheet [Taguchi et al., 1998]. The location of the NENL near the time of substorm onset is now known to be $X \sim -20$ to -30 R_E [Nagai et al., 1998]. Plasmoid ejection begins at the moment when the last closed field line in the plasma sheet merges, thus allowing the lobes to come together and begin reconnecting "open" field lines. It is the reconnection of the lobe field lines which liberates the large amounts of magnetic energy necessary to power substorm expansion phase phenomena in the inner magnetosphere and the ejection of plasmoids down the tail.
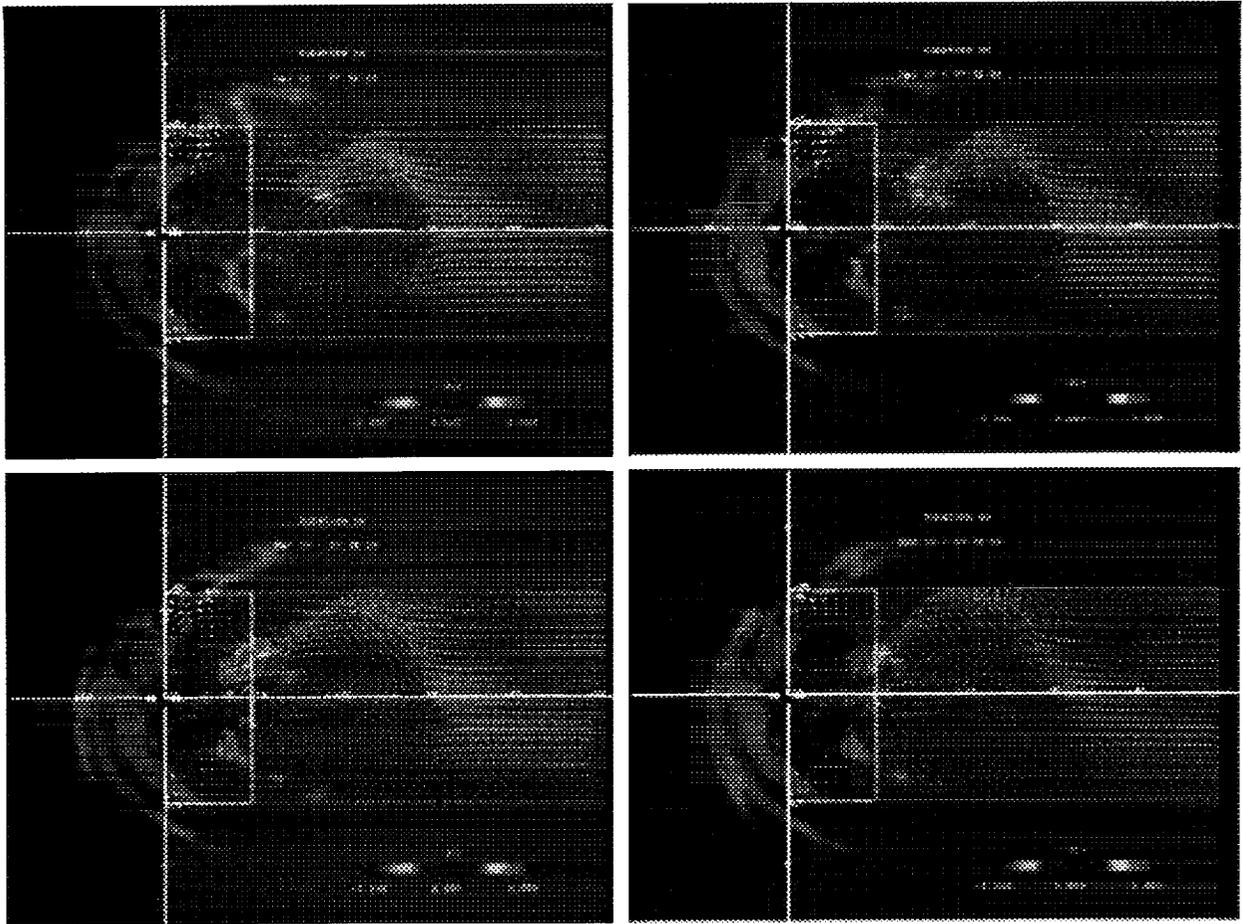
Figure 6. Four snapshots from an MHD simulation of the dynamic magnetotail; frames are approximately 1 minute apart. A flow burst moves from the deep tail toward the Earth where the flow brakes. As the flow slows, a current wedge forms that feeds current to the ionosphere. Such regionalized features recur sporadically in the modeled magnetotail during substorms. Figure is courtesy of C. Goodrich, UMd.

The classic plasmoid model invoked a 2-dimensional geometry, where the structure was simply a closed bubble of magnetic flux. The actual internal magnetic structure of plasmoids has been found to be quite variable; many possess a helical structure and intense core magnetic fields resembling magnetic flux ropes [Moldwin and Hughes, 1992; Slavin et al., 1998]. Such a spiraling of the plasmoid magnetic field had been predicted earlier from topological arguments [Hughes and Sibeck, 1987] involving the effects of the modest B_y magnetic field component in the tail on reconnection. However, few details concerning the 3-dimensional structure of plasmoids and their magnetic connectivity to the rest of the tail or how they evolve with time are known. However, the overall impression was that plasmoids exhibited "compression regions" in the lobes [Slavin et al., 1993].

The simple-minded static view of plasmoid formation and ejection has recently been overturned by new ISTP-era results. Ieda et al. [1998] has presented the first comprehensive survey of plasmoids in the Geotail magnetic field and

plasma data sets. The high-resolution measurements returned by Geotail clearly show that plasmoids grow rapidly in all three dimensions following their release. A particularly startling result is that Geotail frequently observes fast plasma flows within "young" plasmoids (i.e., at X>- $60R_E$) with Vy ~ 100 to 200 km/s which produces a rapid plasmoid expansion in the east-west direction following its release.

The Magnetospheric Multiscale mission with spacecraft separations in the tail of ~ 10^3 km will resolve the small-scale structure of plasmoid high field core regions. However, measurements from a constellation of spacecraft at distances of X ~ 10 to 40 R_E are necessary to determine the origins, dimensions, magnetic structure, stress balance and early evolution of plasmoids as well as their interaction with the surrounding magnetotail. The magnetic field, plasma and energetic particle measurements made across this region with spacings of 1-2 R_E will allow for determination of the nature of the neutral lines, magnetic field reconfiguration and plasma sheet flow field which lead to

Magnetospheric Constellation Mission...

plasmoid formation and ejection. This constellation of spacecraft will also provide direct measurements of the plasma flow and circulation within the plasmoid, larger scale magnetic field topology, the rate of plasmoid expansion and any exchange of plasma with the external tail and, possibly, the magnetosheath. The combined magnetic and plasma data sets will enable direct examination of local stress balance between the regions within the plasmoid and between the plasmoid and the rest of the tail. Energetic ion observations will be used to map the separatrix layers associated with the NENL and Distant Neutral Line (DNL) and determine their location relative to the individual plasmoids. The energetic ion data will also be used to remotely sense the motion of boundaries/regions using well-known finite Larmor radius techniques [e.g., *Owen et al.*, 1995]. Energetic electrons, buy virtue of their high velocities, will also be used as remote tracers of magnetic topology. Small X-lines should develop small-scale plasmoids or fluxropes. DRACO can observe whether more than one plasmoid/fluxrope can coexist at any one time and whether these plasmoids merge into more global ones at times.

In this manner, magnetotail constellation measurements will enable us to observe the plasmoid formation process, determine the forces which are responsible for its ejection, infer plasmoid dimensions, map their magnetic topology and magnetic connectivity with the rest of the magnetotail and, finally, ascertain how plasmoids evolve with time and downtail distance. Specific questions that DRACO can answer are: How much magnetospheric mass and energy is carried off by plasmoids? How are multiple plasmoids formed and released in rapid succession and how is the plasma sheet replenished so quickly? How are high magnetic field strength cores formed within plasmoids and what factors determine their magnetic topology? What are the causes of the rapid plasmoid expansion and downtail acceleration immediately following their release? What is the nature of the plasmoid-tail interaction and how does it influence neutral line motion and plasmoid ejection speed?

1.5 Nonlinear Dynamics of the Chaotic Magnetotail

We have been summarizing our current knowledge of the magnetotail, and the insufficiency of available observations. In this section, we identify the magnetotail as an example of a nonlinear system exhibiting chaotic behavior. In nonlinear dynamics, chaos is defined as behavior that is apparently random and irregular, but that is actually governed by a finite set of differential equations and therefore deterministic. Simple examples include the asynchronously driven pendulum, or a ball bouncing on a base plate that vibrates up and down to counteract dissipation and maintain the bounce, or a dripping water faucet. These systems are accurately described by simple sets of differential equations. The systems are precisely determinate,

yet they appear highly irregular. The magnetotail is certainly much more complex than these simple systems, and much more irregular in many ways. Nevertheless, some limited regularities of the magnetotail are loosely analogous to a nonlinear oscillation: for example, the recurrent cycle of stretching, then relaxation and plasmoid shedding that we identify with substorms. Magnetotail dynamics is of course inherently nonlinear.

Chaotic systems have the property of limited predictability, as distinct from the strong predictability of the small amplitude, synchronously driven pendulum. The linear pendulum, having been disturbed, eventually settles back to its original routine. By contrast, when the driving amplitude is sufficiently large, chaotic behavior results and the smallest disturbance of the pendulum switches it to a different but equally chaotic pattern. The pendulum's behavior is completely determined by the initial condition and forcing function, but one cannot predict its behavior for any considerable period without extremely precise knowledge of the initial drivers. The divergence between two slightly differing sequences grows exponentially, the difference growing with each successive interval by a roughly constant factor, so that the smallest uncertainty renders predictions useless after a finite period.

This illustrates the concept of a "horizon of predictability," shared by all chaotic nonlinear systems. In practical terms, the horizon of predictability is an impassable barrier. Atmospheric movements, governed by well-defined equations, are thought to be in a state of chaos. Improved knowledge of initial and boundary conditions has significantly improved atmospheric predictability in recent decades as improved space-based measurements have converged with huge improvements in computational capabilities. Ultimately, however, incremental improvements come up against the exponential divergence of minutely different initial conditions, and the "horizon of predictability" reaches a practical limit. Certain statistical features of climate, such as annual cycles of temperature and rainfall, are exempt from the limitations of chaos. Other large-scale processes may still allow long-range prediction; the more detail one asks for in a forecast, the sooner it will lose its validity.

The magnetotail has to date been studied at a primitive level in comparison with our lower atmosphere. Current observational knowledge of the magnetotail is perhaps akin to the meteorological knowledge of the early explorers, made from individual ships, widely separated in time and space. In contrast, theoretical work on the magnetotail is advanced, albeit relatively untested through confrontation with observations. One key motivation for the magnetospheric constellation mission is to bring the tools and lessons of nonlinear dynamics to the study of the magnetotail system. The foremost of these that is lacking at present is the measurement of initial and boundary conditions with resolution and accuracy commensurate with current and future generations of global simulation models.

1.6 Science Objectives and Questions

The scientific foundation of the Magnetospheric Constellation DRACO mission is the quest for an understanding of the nonlinear dynamics of the structured magnetotail. This understanding will flow from answering the question: **"How does the dynamic magnetotail control energy flow?"** This can be broken down into derivative questions:

- What processes control magnetotail structure and *dynamics?*
- How do magnetotail dynamics *respond* to extrinsic conditions as well as to internal instabilities?
- How do physical processes and regions *couple* over the hierarchy of scales?

A more detailed expansion of these questions under mission objective headings is given below.

1.6.1 Determine Dynamics

- Are there states approximating equilibria of the magnetotail?
- Does the magnetotail fluctuate strongly even when the solar wind is steady?
- How do these fluctuations depend on the pressure, speed, magnetization, and fluctuations of the solar wind?
- What is the nature of global magnetotail reconfigurations?
- How do magnetotail dynamics accelerate and transport energetic particles?

DRACO will make it possible to identify both equilibrium states and their fluctuating components as dynamic sequences.

1.6.2 Understand Responses

- Are magnetotail flow vortices generated spontaneously or in response to solar wind disturbances?
- Is the occurrence of kink, ballooning, tearing or reconnection instabilities determined by magnetotail boundary conditions?
- Are fast Earthward flows and associated currents the same disturbances that form and release plasmoids, and are they reliably triggered by specific solar wind variations?
- Is particle acceleration triggered or enhanced by solar wind discontinuity effects on magnetotail dynamics?

DRACO will permit us to unambiguously determine and characterize the magnetotail's unique responses to external and internal drivers.

1.6.3 Reveal Connections

- Does the plasma sheet collapse from the inside out (rarefactively), or from the outside in (compressively)?
- How are observed ionospheric current systems and auroral expansions connected to plasma flows, particle acceleration, plasma injections?
- How are disturbances communicated within the magnetosphere?
- What is the horizon of magnetotail predictability at present and can it be extended with improved knowledge of initial and boundary conditions?

DRACO's extended measurement network will provide the first vector field movies of the magnetotail, revealing the connections of causes-to-effects via both convecting and propagating disturbances.

1.6.4 Summary

Magnetospheric Constellation DRACO will for the first time clearly identify the boundary conditions that are associated with configuration instabilities of the magnetotail. In contrast with MMS, which will examine the role of local velocity space micro-instabilities, DRACO will provide a test of the macroscopic conditions for instability.

In summary, the overarching goal of the Magnetospheric Constellation DRACO mission is to reveal magnetotail *dynamics*, its *responses* to external conditions determined by the solar wind, and the *connections* within the magnetotail and to its boundaries. To achieve observational closure with theory-based global circulation models, leading to confidence in our physical description, we must observe the plasma sheet system as a coupled whole. This requires a network of measuring stations dense enough to resolve the principal vector field features of the magnetotail as they evolve under varying solar wind conditions.

2.0 Science Requirements

2.1 A New Leap in Magnetospheric Physics

This section provides a derivation of Magnetospheric Constellation DRACO mission requirements from the scientific objectives, as stated in the previous sections. A constellation mission is a fundamental departure from the prior state of the art in space physics. In the past, space exploration was conducted first from lone spacecraft and later from small numbers of widely separated spacecraft (i.e., ISTP), seeking to understand the gross coupling between principal regions. Now we have observations from small groups of spacecraft flying in tetrahedral formation (CLUSTER), examining the detailed structure and dynamics of specific regions such as the sites of reconnection

(MMS). Imaging missions like IMAGE, and others like TWINS, will give us global perspectives for emissive phenomena that can be characterized as scalar image fields.

A constellation mission will provide a qualitative and quantitative leap beyond these techniques to a distributed network of identical observing stations, providing dense vector field sampling of a large region of space. The constellation approach flows naturally from the history of dynamic meteorology, where a similar approach has allowed the testing of comprehensive theoretical models and made reliable prediction possible. It fits logically into the hierarchy of physical scales in space and completes the corresponding strategic hierarchy of mission architectures. It implies a set of considerations for data handling, visualization and synthesis that were heretofore unique to atmospheric meteorology, but now must be dealt with for future progress in space physics and the Sun-Earth Connection (SEC).

In this section, we show how the science objectives of the previous section lead inevitably to the requirement for a constellation mission. The deployment of a constellation of spacecraft will be most challenging in the area of resources. In place of the conventional stress on the development of unique and highly capable measurement instruments, a constellation must be based on techniques more akin to those of the consumer electronics industry. A variety of highly sophisticated devices must be designed into a durable and reliable package that can be reproduced and operated inexpensively. The art of designing a constellation mission then clearly lies in the definition of a highly capable but also cost-effective instrument package and spacecraft, capable of achieving the science objectives of the mission through deployment in unprecedented numbers. For any conceivable resource envelope, a trade clearly exists between the capability of each individual spacecraft and the scope and resolution of the constellation that can be deployed. We identify the measurement requirements for each spacecraft, then the required deployment density and domain. Finally, we identify the required instrument payload and spacecraft capabilities, implicitly prioritizing a maximal number of spacecraft.

2.1.1 Lessons Learned from Dynamic Atmospheric Meteorology

Earth's magnetosphere is a complex geophysical system formed by interactions between the magnetized solar wind and the neutral and ionized atmospheres and magnetic fields of the Earth. It is certainly valid and increasingly common to think of the magnetosphere as a part of the Earth's overall weather machine [Calder, 1974]. "Weather" may be defined simply as the cosmic dynamical phenomena that are of interest to humankind by virtue of their occurrence within space that we inhabit. Increasingly, we inhabit the space around the Earth out to the limits of our atmosphere and beyond, into the atmosphere of our star, the Sun. We also invest in the placement of robotic agents

within that space, whose survival is important to us for various practical reasons. Thus, magnetospheric phenomena are beginning to have relevance to our lives and are becoming more familiar to us in this space age.

A single view of the global aurora suggests strongly that it is fundamentally a turbulent fluid flow phenomenon, as shown in **Figure 7**. The global structure of the polar aurora is comparable to that of the global cloud cover of our planet, as exemplified in **Figure 8**. Clouds and aurora provide telltale identifications of fluid parcels with distinguishing characteristics of moisture content and particle precipitation, respectively. As parcels are transported and distorted, they reveal much about the flow patterns that exist within their parent fluids. Large-scale eddies and vortex flows are particularly obvious in time-lapse motion pictures of these phenomena.

The modern account of global atmospheric winds derives from the work of meteorologists over the past two and a half centuries. In the words of Nigel Calder [1974], "above all, the modern account is based on millions of measurements of conditions high over our heads, made by balloons, aircraft, and satellites." In combination with the theoretical work of Rossby, Starr, Charney, and Lorenz (some of which lead to a more general theory of chaos), and their working computer models of global circulation, a high level of understanding has been reached. Terms like jet stream, front, depression, pressure ridge, and even baroclinic instability, have entered the vocabulary of the general public through daily discussion by news media weather forecasters everywhere. Clearly, modern communication technologies, most recently geosynchronous satellite imaging, were enabling in the synthesis of worldwide data into meteorological understanding and predictive know-how.

In the troposphere, planetary rotation sets up a balance between the pressure and Coriolis forces, stabilizing against planet-wide Hadley convection, or thermal overturning of the atmosphere. However, the thermal conductivity of the atmosphere is insufficient to support the available energy flux. To move more heat from the equator to the poles, the system develops a baroclinic instability whose circulation permits the energy flux to be transported convectively, albeit in a complex 3-D pattern involving a mid-latitude overturning cell in addition to polar and equatorial cells. The mean meridional motions (in latitude) are illustrated in **Figure 7**. Superposed on these mean motions are the frontal and storm phenomena that make up mid-latitude weather. Sustained global and local monitoring of weather conditions, combined with sound theoretical underpinnings, have permitted weather prediction to become usefully accurate over time scales of up to a week or two, though useful climate predictions continue to elude us at present.

Magnetospheric meteorology is on a trajectory similar to that of tropospheric meteorology. Pioneering thinkers such as Dungey, Axford, Hines, and Nishida developed the basic description of the overall circulation of the magneto-
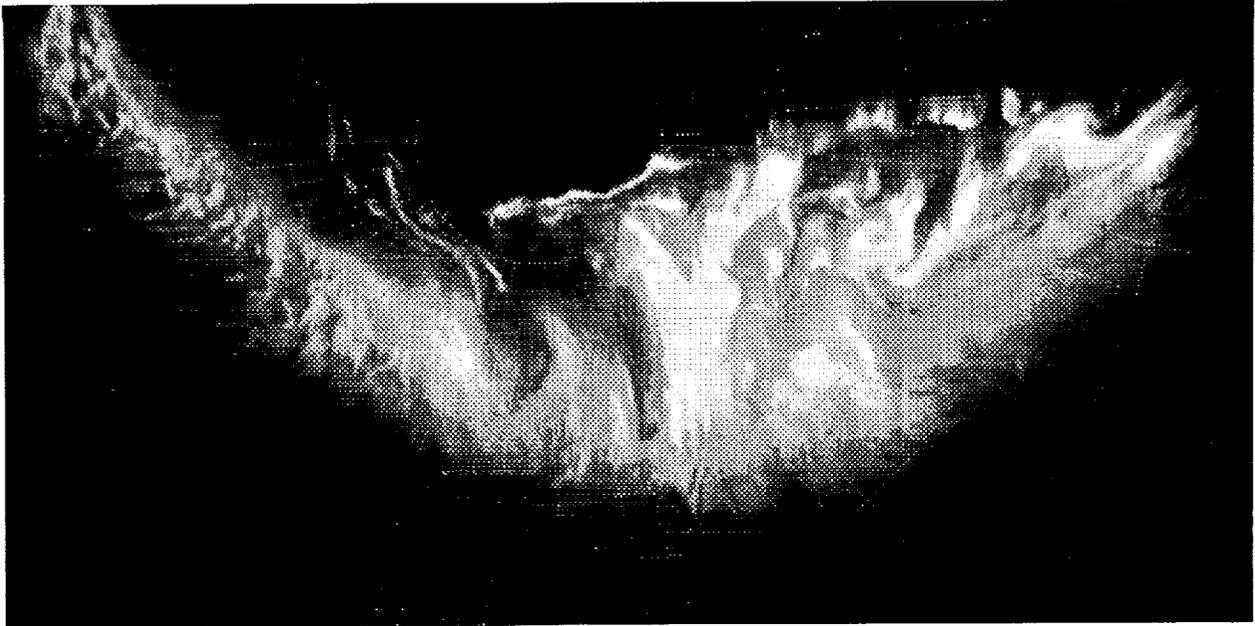
Figure 7. *This figure is an example of the global auroral structure during a significant magnetospheric disturbance. This image is courtesy of the Air Force Research Laboratories and was acquired in a stripwise fashion as the Defense Meteorological Spacecraft Program (DMSP) spacecraft moved along a relatively low Earth orbit.*

sphere. Corresponding to the Hadley cell for the magneto-sphere, this model of magnetospheric circulation gets the overall pattern correct, but overlooks much of the important and interesting dynamics. It was realized almost immediately [Dungey, 1966; McIlwain, 1967; see acknowledgments] that further progress on global dynamics would be limited with individual observing station (spacecraft) data. They recognized that literally "bunches" of spacecraft would have to be put in orbit to definitively understand the local and dynamic behavior of the magnetotail and its auroral plasmas. Since that time, considerable theoretical work has been accomplished and indeed, numerical models have been constructed of the magnetosphere and its dynamics, as exemplified in **Figure 1**. Nevertheless, the small number of multipoint simultaneous measurements has greatly hampered closure between models and observations. The true behavior of the magnetosphere eludes us and we have many competing theoretical ideas with no way of refuting most of them. Consequently, we have an unrelenting debate, and a poor basis for understanding and predicting magnetospheric dynamics.

The magnetosphere has many storm-like departures from the mean expected circulation. The basic driving force, analogous to the thermal driving of the troposphere, is the solar wind flow, which seeks to impart momentum to the outer layers of the magnetospheric plasma. Large cycles of magnetotail distension and collapse suggest an instability that might be called "barotensile" in recognition of the disruption of balance between plasma pressure and magnetic tension. Just as the true nature of the baroclinic instability emerged from millions of measurements of conditions throughout the troposphere, the true nature of mag-

netospheric configuration instabilities responsible for auroral substorms and storms will come from a program to obtain simultaneous global measurements. This will lead to a more complete understanding of the Sun-Earth system and eventually the capability to predict its behavior over longer time spans. We now need observations with a resolution in time and space that is commensurate with our knowledge of correlation scales in the plasma sheet, and of hydrodynamic wave propagation times across such scales: 2 R_E and 10 seconds. To achieve this, we must develop affordable means by which conditions can be measured at many points simultaneously and repetitively, and integrate them into space weather maps. *This is the goal of Magnetospheric Constellation DRACO (and all other constellation missions).*

2.1.2 Hierarchy of Scales and Mission Architectures

The progression from single satellites to constellations is driven by the hierarchical nature of magnetospheric phenomena. Spatial scales of magnetospheric phenomena range from kinetic scales associated with magnetic reconnection to whole-body (i.e., magnetospherewide) responses to solar wind waves and discontinuities. Associated with the hierarchy of spatial scales is a hierarchy of temporal scales, since large-scale phenomena tend to last longer than small-scale phenomena. Moreover, the scales are interrelated, one scale feeding into the next and vice versa.

The hierarchical nature of magnetospheric phenomena ex-
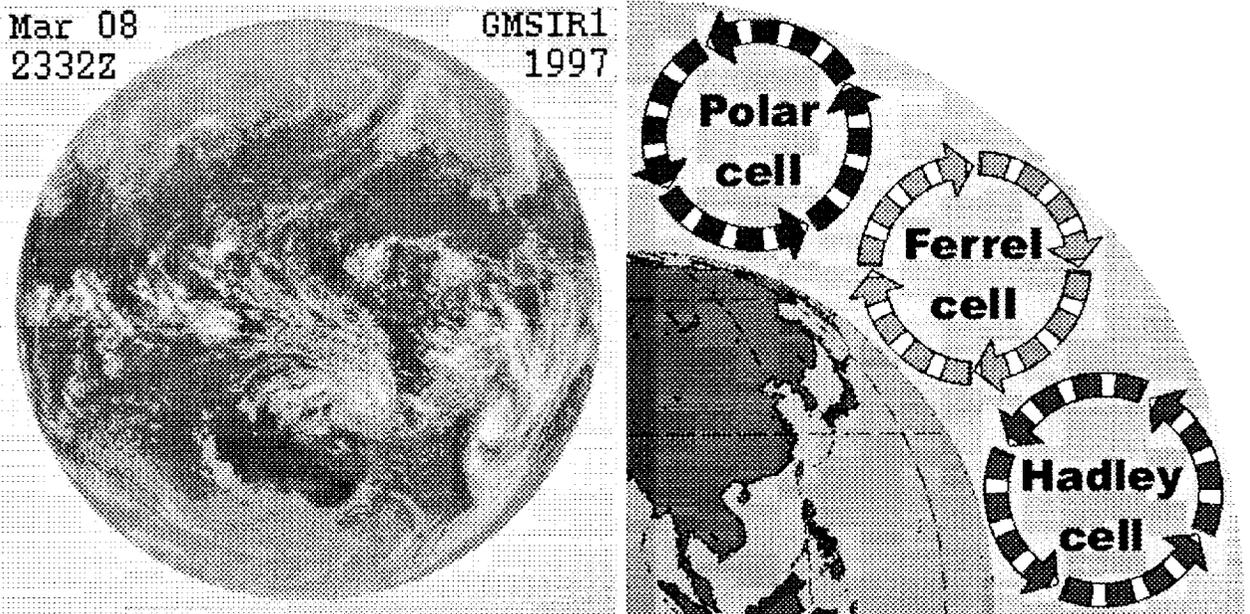
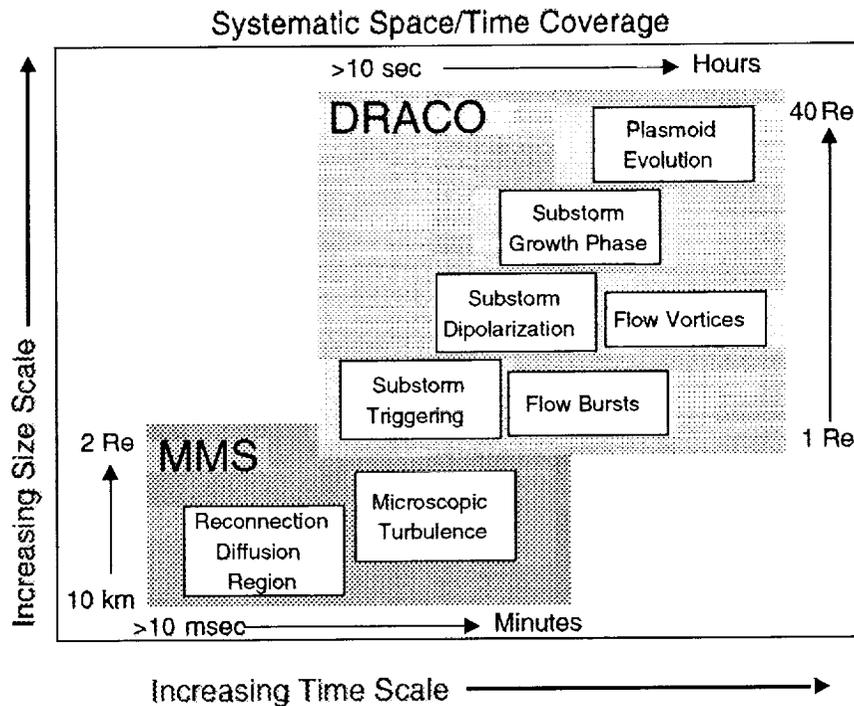**Figure 8.** *(Left Panel) An example of Earth's global cloud cover imaged in visible light, illustrating the complex circulation of our atmosphere in response to the flow of heat from Equator to pole, the baroclinic instability. (Right Panel) Mean meridional atmospheric flow, owing to the breakup of the Equator to pole cell proposed by Hadley, into three cells, leading to the formation of the Ferrel cell and mid-latitude weather. Figures are courtesy of the University of Washington Geophysics Program.*

emplifies a general property of astrophysical plasmas. *T. Tajima* [1997] remarks that the "hierarchical nature of plasma manifests itself as a kind of structure made up of levels of physical phenomena. But these are yet ultimately interrelated to each other." Tajima illustrates the point with the example of magnetic reconnection, a local process that occurs as a result of global dynamics and in turn gives rise to global dynamics.

Meteorological phenomena also exhibit a hierarchy of scales, which feed into each other. The analogy to meteorology helps explain why magnetospheric physics must advance by progressing from single satellites to constellations. Meteorology has approached the problem of understanding atmospheric phenomena by formulating the equations of motion of the atmosphere and developing an observational procedure for measuring the terms that enter these equations. The most important of the dynamical terms are wind, pressure, and temperature. For the most part, these quantities are invisible in the sense of being inaccessible through remote sensing. Meteorologists have found that the way to advance in the face of a hierarchy of dynamical scales driven by invisible forces is to establish an *in situ* observing network. The meteorological observing network has grown to become dense enough and broad enough to display atmospheric phenomena on all relevant scales. It is also broad enough to be able to follow weather-producing atmospheric phenomena through their life cycles. To achieve an adequate network, meteorology moved from single isolated stations to networks in which the number of nodes grew to encompass the phenomena.

Magnetospheric physics is in a closely analogous situation to meteorology with hierarchical dynamical modes and invisible dynamical parameters, which in this case also include electromagnetic fields. In this type of situation, the problem of data-theory closure has no known solution other than that developed in meteorology—a dense, broad network of *in situ* observing stations. In the magnetospheric context, this means moving from single satellites to networks of satellites—single satellites, then clusters, then constellations—until the magnetosphere itself is encompassed.

Figure 9 schematically illustrates the hierarchy of magnetospheric scales and how these scales relate to upcoming multispacecraft missions in the study of magnetospheric phenomena (Magnetospheric Constellation DRACO and Magnetospheric Multiscale). Characteristic spatial scales on the vertical axis increase from microscale, mesoscale, and macroscale, to global, spanning physical dimensions of 10 km to 40 R_E. These are deliberately vague to allow many phenomena to be included. "Microscale" roughly represents kinetic (nonmagnetohydrodynamic or velocity space) processes. "Mesoscale" represents phenomena that have scale sizes comparable to the internal structures of the magnetosphere. "Global" phenomena engage the whole magnetosphere. Scales for duration are represented by phenomena having those durations. Time scales for duration increase on the horizontal axes ranging from 10's of milliseconds to hours.

Systematic Space/Time Coverage

>10 sec ──────────► Hours

DRACO

Plasmoid Evolution

Substorm Growth Phase

Substorm Dipolarization

Flow Vortices

Substorm Triggering

Flow Bursts

40 Re

1 Re

2 Re

MMS

Microscopic Turbulence

Reconnection Diffusion Region

10 km

>10 msec ──────────► Minutes

Increasing Size Scale

Increasing Time Scale ──────────►

Figure 9. Hierarchy of scales in the magnetotail, illustrating the complementary design of various mission architectures in the study of representative phenomena.

Figure 9 indicates key processes and phenomena that MMS and Magnetospheric Constellation DRACO will address, demonstrating the different regions of space/time they will resolve. All scale sizes and durations are represented and phenomena at different scale sizes are related by mode of origin. This illustrates for the magnetospheric case the point that Tajima made about astrophysical plasma in general: They are hierarchical and their scales relate to each other. To understand the system fully, we must resolve all size/time scales systematically and, ideally, simultaneously.

At present, single satellites have only glimpsed the phenomena shown in **Figure 9**, and have not been able to resolve inherent space-time ambiguities. As such, single satellites only describe the state of phenomena that change slowly, such as the relatively slow-moving magnetospheric boundary layers, inverted V's, and diffusive changes in the ring current and radiation belts. For other phenomena, single satellites only give statistical information accumulated by multiple encounters with the phenomena on separate occasions. In meteorological terms, for other phenomena single satellites give climatologies rather than descriptions of actual weather systems.

CLUSTER-class missions such as MMS will be able for the first time to resolve the state and evolution of the

plasma physics of reconnection and turbulence down to microscopic scales (10 km). At the other end of the MMS range, it will also capture appreciable elements of such phenomena as substorm triggers and bursty flows. But there are important science questions that lie outside the portion of parameter space that presently planned cluster-class missions can explorer.

As outlined in the previous sections, many important processes are operating in the constellation-class domain covered by Magnetospheric Constellation DRACO. These include the magnetosphere's best-known and most energetic dynamical modes: the substorm. In addition, for instance, it is within this constellation-class domain that the global consequences of reconnection can be understood. Other constellation-class processes include manifestations of flux ropes.

In summary, the hierarchical, interdependent phenomena of astrophysical plasmas in general and of magnetospheric plasmas in particular drive a progression from single satellites to constellations. Meteorology has similar dynamics and has implemented a corresponding progression of atmospheric observing stations. Magnetospheric physics has passed through a single-satellite state and is on the brink of a cluster state. The time is right to plan for the constellation stage.

2.1.3 Complementary with Other Missions

NASA SEC missions are coordinated to provide knowledge about the magnetosphere at all relevant scales. The ISTP missions provided the most global coverage to date, establishing the importance of continuous solar and solar wind monitoring in conjunction with single-spacecraft observations at other strategically chosen locations. In the process, ISTP has also demonstrated the capability to remotely sense and image the energetic ions of the inner magnetosphere [Henderson et al., 1997, Jorgensen et al., 1997]. Now, the IMAGE and TWINS missions are putting in place the tools for routine dedicated imaging of the inner magnetospheric energetic ions as well as the cold plasmaspheric helium, low-energy ionospheric outflows, and the motions of the dayside magnetopause. However, imaging missions are unable to probe the magnetotail region, owing to the low plasma and neutral gas densities in that region. Even with increased sensitivities, magnetospheric imaging missions cannot make vector measurements of the magnetic field and plasma flow field, being limited to scalar quantities such as line-of-sight flux. These are extremely important in the magnetotail region.

The MMS mission will focus upon the microscale and velocity space processes that occur in magnetospheric boundary layers, including the thin magnetotail current sheet: reconnection, particle acceleration, and turbulence. These processes regulate the flow of mass, energy, and momentum from magnetotail lobe storage regions into the inner magnetosphere and ionosphere via high-speed plasma flows, energized particles, and field-aligned currents, thereby determining when and where geomagnetic disturbances will occur. MMS will discriminate between spatial and temporal phenomena and provide the local gradient observations needed to characterize and then identify these poorly understood microscale processes. Fundamentally, it will address the influence of microscale velocity space structure on the dynamics of the magnetosphere.

The Geospace Electrodynamics Connection (GEC) mission will define the nature of the connections linking the magnetosphere and the ionosphere. The key objectives of this mission include:

- Identifying the spatial and temporal scales over which the ionosphere and thermosphere respond dynamically to magnetospheric input,
- Establishing the route linking magnetospheric and ionospheric currents as a function of conductivity, and
- Defining how plasma flows between ionosphere and magnetosphere affect the dynamics of both regions.

Whereas the MMS and GEC missions will provide a wealth of information concerning the small-scale structure of processes in magnetospheric boundary layers and the ionosphere, neither mission will explore the global equilibrium, response to disturbances, and macroscopic configuration space instability of the magnetotail, nor its global link-

ages. Specifically, DRACO will focus on the global consequences of the reconnection process, the global control of its onset locations and trigger mechanism and evolution, and the causal links of (possibly) multiple reconnection sites. Only the dense network of vector measurement stations provided by DRACO can address these fundamental global issues, complementing the other STP missions. Fundamentally, DRACO will address the influence of macroscale configuration space conditions on the dynamics of the magnetosphere, complementing the other missions. All of the missions are described in web pages at http:// stp.gsfc.nasa.gov

2.1.4 Data Synthesis Considerations for Constellation-Class Missions

2.1.4.1 Novel Modeling, Data Handling and Assimilation Techniques. The Magnetospheric Constellation DRACO mission will provide multipoint *in situ* magnetospheric measurements of substantially different quality and quantity than any previous mission. The quality of the measurements lies not so much in the quality of the individual measurements—which are indeed comparable to previous missions—but in the fact that these observations are made in a coherent fashion on a large number of spacecraft simultaneously. Making optimal use of the measurements will require the development and application of new techniques. The implementation of the DRACO mission will result in a leap, similar in its importance to that made by the atmospheric physicists many decades ago. Individual weather observations were gathered into synoptic maps (summarizing a large number of individual observations). Later, the maps came to be further processed using spatial objective analysis and data assimilation. The analysis of individual spacecraft observations will become mostly obsolete and will be replaced by synoptic analyses that use observations from all satellites in the constellation. An example of the type of information that will be obtained from DRACO is shown in **Figure 10**, generated from the global simulation and visualization work of *Goodrich et al.,* [1999].

Figure 10 shows a snapshot of the magnetotail neutral sheet region from a global simulation, showing the formation of a strong Earthward flow in the evening sector. Arrows indicate the local flow vector, while color contouring indicates the flow of electric current into or out of the neutral sheet region, along magnetic field lines.

Techniques developed for the atmospheric sciences over the past decades can be borrowed to solve the new analysis challenges. This is critical for the success of DRACO because — as the atmospheric sciences show us — the development of these techniques can take decades and sometimes lead into dead ends. By exploiting the existing knowledge, DRACO will make these tools ready for the first magnetospheric multipoint mission in less than a decade. It is crucial for DRACO's success to include a strong modeling element right from the beginning. These analysis and
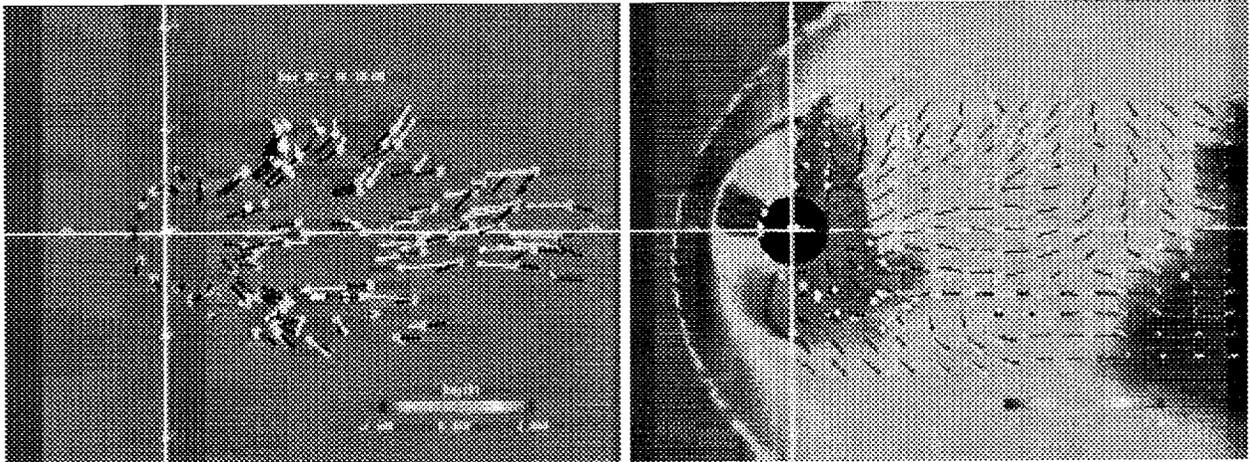
Figure 10. A single spacecraft snapshot gives good information at a point in space and time. A single spacecraft orbit gives good information but spread over a 3-day orbit. A constellation gives a dense set of data with good time resolution and spatial resolution adequate to resolve the main global features of the simulation (right panel). Figure is courtesy of C. C. Goodrich, from Goodrich et al. [1999].

assimilation tools need to be ready when the first DRACO measurements become available. The development of these tools will require substantial effort.

The first factor is the simultaneous data coverage of the magnetosphere. A significantly nonuniform distribution of the satellites will result in a loss of information in regions with sparse coverage, while an excessively dense concentration of the space probes in relatively small regions will not enhance the fidelity because of limited spatial resolution of the mathematical models. Therefore, the inversion methods must include a means of "filling in the gaps"; for example, using the predictions of the global statistical models in regions with poor spatial coverage. Similar principles have been successfully applied in consolidating multipoint ionospheric measurements in the Assimilative Mapping of Ionospheric Electrodynamics (AMIE) models. In this regard, simultaneous monitoring of the conditions of the incoming solar wind could greatly enhance the accuracy of the DRACO-based modeling. In spite of the fact that the DRACO measurements will be made mainly at low latitudes, the dynamic evolution of the orbits and distortions of the tail will provide sufficient information about structure normal to the orbital plane [*Tsyganenko*, 1998].

The second factor is the flexibility of the model representation; that is, its ability to reproduce a large variety of possible magnetic configurations. Substantial progress in this direction has taken place recently. A mathematically simple and general approach was developed to model the largest-scale geomagnetic field, produced by currents on the magnetospheric boundary. This magnetopause contribution is important throughout the magnetosphere and depends mainly on the dynamical pressure of the solar wind. The cross-tail electric current, flowing from dawn to dusk in the equatorial plasma sheet, is also critically important. The most recent mathematical models [e.g., *Tsyganenko and Peredo*, 1994], superpose the fields from

several equatorial current sheets with variable thickness and different radial profiles, all confined within a magnetopause with realistic shape and size. In addition, powerful new techniques became available recently, making it possible to take into account the seasonal/diurnal warping of the tail current and its twisting around the Sun-Earth line, induced by the reconnection of the geomagnetic and interplanetary magnetic fields [*Tsyganenko*,1998]. Now many more degrees of freedom can easily be introduced into the model, making it possible to magnetically map the effects of catastrophic reconfigurations of the magnetotail during disturbed periods. Further progress in this area is expected on the basis of the new deformation method [*Tsyganenko*, 1998], allowing one to greatly expand the variety of modeled magnetic configurations, including plasmoids and other transient features.

2.1.4.2 Data Assimilation in Dynamic MHD Modeling.
Data assimilation takes the synoptic mapping a significant step further by introducing the "first principle" dynamical MHD models into the analysis process. The underlying idea is that assimilation of data can minimize errors in both the data and the model, even when the model suffers from simplifying assumptions, and thus provide an optimal "map" of the physical state of the magnetosphere at any given time.

Data assimilation techniques have been successfully used in atmospheric and oceanographic models for some time [*Ghil et al.*, 1997], but never before in magnetospheric modeling. Data assimilation techniques take the observations distributed in time and space and merge them dynamically into the numerical model in order to determine as accurately as possible the instantaneous state of the magnetosphere. The primary objectives and needs for the data assimilation are our poor knowledge of the initial state that is used to start a model simulation and the fact that the simulated magnetosphere may gradually diverge in

time from its actual state. Data assimilation ensures that, in the course of time, the state of the simulation remains optimally close (in terms of a merit function) to the concurrent observations at the measurement points. The primary reason that data assimilation methods have not yet found their way into magnetospheric modeling is the scarcity of magnetospheric *in situ* measurements. The Magnetospheric Constellation DRACO mission will change that dramatically by providing for the first time a fairly dense grid of *in situ* data describing the MHD state of the entire modeled system. The fact that these observations are restricted to the vicinity of the tail plasma sheet is no major obstacle. Atmospheric models have to deal with similar unevenly distributed data sets and powerful methods exist to make optimal use of them [*Miller et al*, 1994; *Talagrand*, 1997].

The power of data assimilation has been demonstrated convincingly by the numerical weather prediction models which all use assimilation techniques. Employing these techniques in magnetospheric modeling will result in a dramatic breakthrough, since the data assimilation will serve as an ultimate test of the underlying model's quality. A systematic divergence of a model from the data will provide a clue to some intrinsic deficiency to be corrected. In addition, not only will the model improve overall, but also new knowledge will be gained about the physical processes, whose incomplete or wrong description had caused the model to fail. In short, the data assimilation forces a continuing reevaluation of our understanding of how the magnetosphere works. This is one of the primary reasons why the DRACO Mission should be implemented.

2.2 Mission Requirements

2.2.1 Measurement Requirements

The science objectives for DRACO are expressed in terms that identify the most fundamental measurements: magnetic field, plasma flow field, and energetic particle acceleration. These are the three basic measurements that DRACO will require. It may be objected that charged particles are accelerated by electric fields, so that electric field measurements are required as well. However, at the time scales of interest to DRACO (~ 10 sec), and in the region of interest to DRACO, the electric field may adequately be inferred from the plasma flow (transverse component) and from measurements of magnetic field variations (induced parallel component). Short time-scale phenomena can usually be best observed using electric field measurements to integrate instantaneously over the plasma velocity distribution. However, such phenomena are generally beyond the scope of DRACO and can be best diagnosed by missions devoting their resources to detailed microphysical observations. **Table 1** provides a compact summary of the measurement requirements for DRACO. A translation of these requirements into a straw man payload is provided in this section. It is the nature of DRACO science objectives to require coordinated measurements of all MHD

plasma state variables. These individual measurements cannot be exclusively associated with specific DRACO objectives; all contribute equally.

2.2.2 Orbit-Attitude Requirements

2.2.2.1 Orbit. DRACO must sample the magnetotail region from about 7 R_E to 40 R_E in the night side along the Sun-Earth line, and across the magnetotail east and west of the Sun-Earth line by ~ 10 R_E. This is based on the importance of phenomena within the region from geosynchronous orbit to beyond the convection reversal associated with substorm activity, near 25-30 R_E. Eccentric orbits with perigees near 2-3 R_E provide an optimal trade between orbit stability and economical transmission of commands and data. A set of orbits with apogees ranging from 7 to 40 R_E would provide all the coverage that is needed. The number of spacecraft required must be determined on the basis of detailed orbit modeling, which is reported below in the mission design section.

2.2.2.2 Attitude. Spacecraft attitude stability and control are required to within 5°. The attitude stability requirement is derived from the mission requirement for 10% absolute knowledge of the magnetic field. Data collection in shadows and shortly thereafter is not required, but it is highly desirable. Since thermal changes during shadows will affect the magnetometer and particle measurements, as spin rate changes, it is recommended (but not required) that spin rate data be obtained interchangeably from the Sun sensors and the Earth/Moon sensors (infrared detector).

2.2.3 Spatial Resolution and Number of Spacecraft

DRACO must provide a typical interspacecraft spacing (resolution) of ~ 2 R_E. Moreover, the distribution of interspacecraft spacing should be as narrow as practical, so that random "holes" and "bunches" in the spacecraft distribution are minimized. This requirement is translated into orbital strategy in Section 3.

2.2.4 Mission Duration

To achieve its science objectives, DRACO must have a mission lifetime of sufficient duration to observe magnetotail behavior during a variety of solar wind conditions and at least a sampling of typical solar wind disturbances, including co-rotating interaction regions and Coronal Mass Ejections (CME's). The entire constellation should be put into orbit with apogees in the local time range around local dawn. Initial activation would then be complete well in advance of the rotation of the tail across the constellation orbit pattern as the Earth orbits the Sun. This would produce a pioneering but ancillary study of the dawn flank of the magnetosphere and its interaction with the magnetosheath, early in the mission. This would be followed by a main mission phase as the constellation passes

Measurement	Range	Resolution	Time Resolution	Comments
3-Axis Magnetic Field	+/- 300 nT	0.1 nT	1 sec 1 min @ 100 Hz	Fluxgate technology exists
Plasma 2-D Temperature	10 - 2000 eV	20%	10 sec	Requires $180°$ field-of-view
Plasma Flux	$10^5 - 10^8$ $cm^{-2} s^{-1} sr^{-1}$ eV/eV	20%	10 sec	Electrostatic analyzer technology exists
Plasma 3-D Velocity Electron PAD	1 - 1000 km/s	20% $20°$	10 sec	Mass analysis significant but not absolutely required
Particle Energy	20 - 500 keV	20%	10 sec	Mass analysis significant but not absolutely required
Particle Flux	$1x10^0 - 1x10^6$ $cm^{-2} s^{-1} sr^{-1}$	20%	10 sec	Solid-state telescope technology exists
Particle Pitch Angle	$180°$	$20°$	10 sec	

Table 1. Measurement requirements.

through the center of the magnetotail over a period of roughly 4 months. This, in turn, would be followed by a study of the dusk flank and boundary layer interactions. All this would occur during the first 6 months of operation, and would achieve the minimum success criteria for the mission. Continued operations over a subsequent year would produce unprecedented studies of the day side magnetopause, magnetosheath, bow shock, and foreshock regions in the solar wind. Studies of these regions are of course considered to be ancillary science for DRACO, but would have high value, and would position DRACO for a second pass through the tail 1-2 yrs after launch.

2.2.5 Data Volume and Flow

The general data flow scenario calls for data from an entire orbit to be stored on board, and then downloaded quickly during perigee passes near the Earth. This will minimize the requirements for transmitter power and ground operations, but creates the need for onboard storage. **Table 2** presents the Magnetospheric Constellation DRACO science data accumulation rates and total data storage requirements per orbit, absent any data compression. Loss-less compression will be used routinely in practice, creating a factor of two contingency in the overall data volumes shown here, reducing the requirement for bulk memory on the spacecraft, and possibly reducing the downlink requirement from that reported here. The typical intrinsic instrument sampling rates will generate the acquisition of a quantity of data from a single spacecraft that is quite manageable by contemporary standards.

Data assimilation is greatly facilitated by homogeneity of the individual data sets in terms of time, energy, and angular resolution. Thus, the economic advantage of making all the spacecraft and instruments identical is synergistic with the overarching science goals for the mission. In place of time-variable burst mode data-taking, routine data products will include both high time resolution integrated data (moments), and lower time resolution detailed data.

DRACO's lower apogee orbits have reduced storage requirements in accord with the shorter orbital periods, the lowest apogee orbit having a period of ~ 12 hrs. Assuming identical spacecraft, the excess data storage capability in the lower orbits translates into considerable flexibility in the planning of downlinks. All of the lower apogee data can be transmitted during considerably shorter contact periods, or it can be accumulated for multiple orbits and transmitted using the same contact period as the higher apogee orbits. The opportunity also exists for triggered burst mode data to be collected at higher than normal time resolution, with the burst mode data stored in the contingency memory for the lower apogee orbits. Provision for burst mode collection can also be made for the higher apogee orbits when data compression is implemented, particularly if "lossy" compression of detailed data is used, as is becoming increasingly accepted for image data.

A summary of a possible scenario including burst data collection is shown in **Table 3**. The lowest apogee orbits can easily collect an amount of burst data per orbit equal to the routine data collection, assuming a data dump can take place once per perigee pass. Lower tracking availability will reduce the burst collection from those orbits. The highest apogee orbits (periods greater than 50 hours, i.e., apo-

Instrument	Basis (3 sec spin period)	Data Rate
Magnetometer (MAG)	16 vectors/spin @ 16bits/sample	768 bits/spin
Plasma velocity, ions	8 elevation x 11 azimuth x 16 energy x 8 bits/sample	11264 bits/spin
Plasma velocity, electrons	8 elevation x 11 azimuth x 16 energy x 8 bits/sample	11264 bits/spin
Energetic ions	4 elevation x 8 azimuth x 16 energy x 8 bits/sample	4096 bits/spin
Energetic electrons	4 elevation x 8 azimuth x 16 energy x 8 bits/sample	4096 bits/spin
Total/Spin		31488 bits/spin
Total/100 hrs.	Maximum apogee orbit (40 R_E) data accumulation	3.8 Gbit/orbit maximum

Table 2. Instrument data sampling rates.

gees greater than 20 R_E) must retain most of the memory available for routine data collection. However, they can easily accommodate an amount of burst data similar to that for the lower apogee orbits, simply by foregoing routine collection in the lower altitude parts of the orbit (r < 7 R_E).

2.2.6 Command Uplink

Instrument commanding will be minimal. All commands are time-tagged and uploaded to an onboard buffer in the Command and Data Process Unit (CDPU) for delayed implementation. Commands include clock updates, providing information on when to start and stop routine data collection, when to anticipate ground contact next (based on updated contact times), what criteria are to be used to trigger burst mode, and which quantity to burst on. Other options may include changes in the number of burst intervals, software uploads, and onboard processing options, but do not constitute standard commands during routine tracking sessions. In general, instrument mode changes will not be part of the routine commanding unless required for health and safety.

During initial activation, high-voltage instruments will be ramped and checked out during perigee pass contact periods, then turned over to automated operation for the rest of their lifetimes. While the first few spacecraft activations may be watched closely, this operation will become quite routine thereafter.

Orbit	Apogee = 7 R_E	Apogee = 40 R_E
Orbital Period (OP) =	15 hrs. min.	120 hrs. max.
Routine Accumulation Interval (RAI)	12 hrs. min.	100 hrs. max.
Burst Accumulation Interval (BAI)	12 hrs. (equiv. routine data)	20 hrs. (equiv. routine data)
Total collection per orbit	128 MByte	640 MByte

Table 3. DRACO Downlink Summary

Magnetospheric Constellation Mission...

2.3 Instrumentation Requirements and Strawman Payload Resources

The science requirements can be fulfilled with three principal measurement instruments: 1) Triaxial MAG 2) Electrostatic Analyzer (ESA) and 3) Solid State Telescope (SST). The instruments are based on current technology. Anticipated advances in technology can reduce the instruments' size and weight; such advances will increase the number of probes that can be released on a single launch, increase the capability for the same weight and power, and enhance the science return.

The unique aspects of the science payload for DRACO are:

- The high level of integration of instruments;
- The high level of integration of the spacecraft around the science instruments; and
- Special design considerations that will render the instrument suite manufacturable in large numbers and capable of rapid testing and calibration as a single unit.

The following discussion is a summary of instrument resource requirements. These are derived from current technology, with the addition of a strategy for integration to reduce weight and power down to a minimal amount. The strategy is to implement most of the electronics design on a single board of the spacecraft Data Processing Unit (DPU). **Table 4** summarizes those resources for the three instrument types.

2.3.1 Magnetometer

Triaxial fluxgate magnetometer capabilities that satisfy science requirements have been demonstrated in previous missions (Lunar prospector, FAST, WIND). Careful design for the DRACO mission can also reduce weight and power to make the magnetometer commensurate with nanosatellites. Ring cores of a few centimeters have been tested in the laboratory and low-weight copper windings have been flown previously (POLAR/Magnetic Field Instru-

ment (MFE)). A 16-bit digitization is sufficient. Noise levels based on previous flight experience and lab tests are ±0.05 nT. Two ranges are necessary: 1) a low field range (<1000 nT) for science and is noise-limited, and 2) a high field range (<16000nT), for backup attitude knowledge and ground testing of the unit but where digitization is limited (0.05 nT).

The mission will benefit from a Quality Assurance (QA) program that emphasizes the redundancy built into the large number of nanosatellites rather than in a single instrument realization. This makes instrument-commanding and mode-switching simpler and the instrument lighter. In accordance with this philosophy, a single drive (rather than the traditional triple-redundant) electronics circuitry can be used, which further reduces the power and weight of the instrument.

Early resolution of magnetic cleanliness issues has proven to be commensurate with a low-cost, high-performance flight unit. All known sources of magnetic material (including the possibility of broom magnets on the SST) must be compensated for early in the program. A clear understanding that there is no expectation for useful data collection during Radio Frequency (RF) operation, must be addressed. A primary consideration for magnetic cleanliness is the current from solar panels which demands careful electrical design and wiring.

Spacecraft shadow operations impart a change in the spin rate due to thermal contraction of the spacecraft body. Shadow data are not mission-critical, but occur in regions where the reconnection or current disruption processes erupt. Salvaging such data should be given careful consideration. One possibility is to use an Earth Infrared (IR) sensor to accurately track the spin rate, in addition to the Sun sensor. Automatic switching to the IR sensor once the Sun sensor signal degrades (shadow) will accomplish this goal at little added expense (or at no added expense if the IR sensor is already part of the Attitude Control Subsystem (ACS) system).

Instrument Type	Dimensions (mm)	FOV	Mass (g)	Power (mW)	Comments
MAG	Sensor: 10x10x10 Boom: 1000x20 Electronics: 76x96x40	N/A	200	300	Sensor, High Voltage Power Supply (HVPS) and analog electronics
Plasma Velocity Analyzer (PVA)	Sensor: 100x100x100 Electronics: 50x100x50	+90 x +10 +90 x +10 from radial	1200	1200	Sensor, boom and analog electronics
Energetic Particles Analyzer (EPA)	Sensor: 100x100x100 Electronics: 50x100x50	+90 x +10 from radial	800	600	Sensor, HVPS and analog electronics
CDPU	Logic: 90x90x50 Power: 90x90x50	N/A	500	600	Digital logic and power control

*Table 4. DRACO instrument resource allocations.*
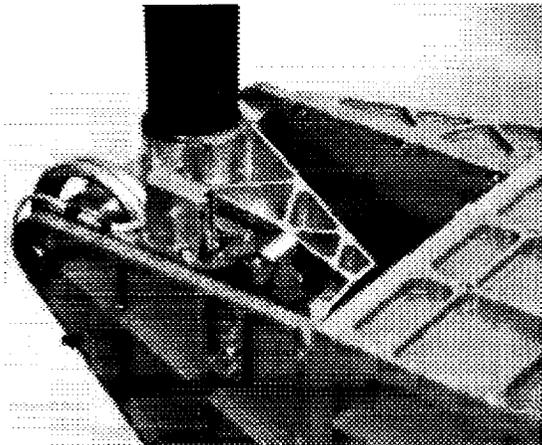
Figure 11. Lunar Prospector magnetometer boom latch.

A small (30 cm) boom deployable via centrifugal force shortly after release is expected to be necessary for cleanliness purposes. The weight of the boom (from carbon epoxy based on Lunar Prospector, FAST and POLAR heritage) is 100 grams and has been included in the magnetometer weight given above. An arm boom with a latch would be preferable to a telescopic boom, since it better maintains the MAG mounting orientation after release.

Figures 11 and 12 show the Lunar Prospector boom latch, and the ROSETTA lander magnetometer respectively. The DRACO sensor can be ~ 1.5 cm or smaller. Developing technologies will make possible even smaller and lighter magnetometer systems, but this is not essential to DRACO.

Onboard calibration is a significant component of the mission success. It is important to ascertain that two spacecraft provide identical values when no currents are present. Existing methods from cross-calibration of CLUSTER magnetometers can be used. These methods call for initial individual calibration of zero levels, gains and sensor orientations, followed by inter-calibration in low-current regions of the magnetosphere. The benefits from such a method can surpass any preflight ground testing with significant value added to the data. Automating this procedure is essential to limit costs.
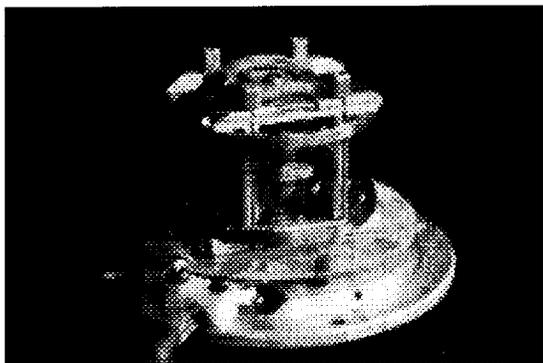

Figure 12. ROSETTA lander magnetometer at 50g.

2.3.2 Electro-Static Analyzer Plasma Instrument

The ESA instrument measures total ions and electrons at energies between 10 eV and 30 keV. The science requirements of Magnetospheric Constellation DRACO can be met with a single analyzer pair (one for ions and one for electrons) on each nanosatellite. These will collect measurements of the complete 3-D ion and electron velocity distributions during each spacecraft spin. Particles enter the analyzer over a ~ 180 degree Field Of View (FOV) and are selected in energy by the potential applied between the outer (0 Volts) and inner (0-3 kV, sweeping) concentric spheres. The particles are focused onto the Micro-Channel Plate electron multiplier (MCP).

The ~ 180 degree field of view is aligned with the spin axis so that a full 4π steradian solid angle can be covered each spin. The FAST plasma instrument illustrates the flight heritage of hardware that would be practical to fly on DRACO, while the Medusa plasma instrument for the Swedish Munin spacecraft shows that even smaller instrumentation is being developed currently (Munin total spacecraft mass = 6 kg). Both are based on the dual opposing top-hat concept. Figures 13 and 14 illustrate the assembly of 4 such ESA's for the FAST spacecraft, and the complete Munin spacecraft, weighing only 6 kg, and containing one Medusa ESA.

Incremental gains in weight and power reduction are expected from development funding using the top-hat instrument principle, or other related optics principles (e.g., the Munin Medusa instrument). However, breakthrough instrument advances may result from the development of
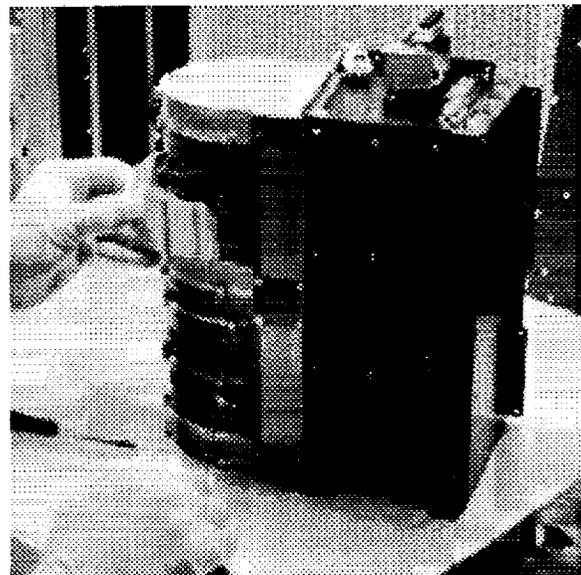
Figure 13. The FAST ESA mechanical structure, including four independent fast plasma analyzers.
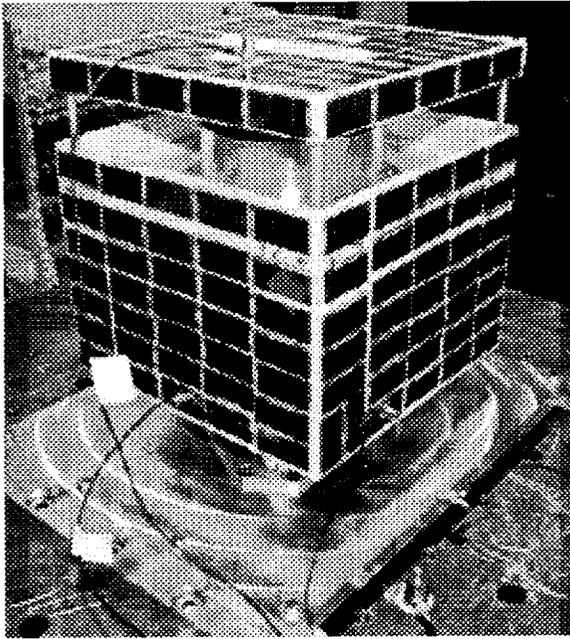
Figure 14. *The Munin structure with solar arrays and a single Medusa analyzer, with a total spacecraft mass of 6 kg.*

delta-doped detectors and other similarly motivated solid-state devices. That principle is expected to reduce the threshold of particle detection in solid-state detectors, which will allow solid-state telescopes to operate in the plasma energy range. This is a technology that should be pursued further for DRACO as instrument development funding becomes available.

2.3.3 Solid State Telescope for Energetic Particles

The principle of solid-state telescope detection of total ion measurements has a long heritage in previous missions and can be readily implemented in a way that meets the science requirements of DRACO at a weight and power commensurate with a 10-kg nanosatellite. Using WIND and Equator-S heritage detectors, each double-ended telescope would consist of a set of 3 semiconductor detectors. The detectors are fully depleted, ion-implanted silicon with low leakage current. One side detector measures ions, and the other side detector measures electrons. High-energy (400 keV- 1MeV) electrons are measured by the center detector. The operational principle is illustrated in **Figure 15**. Ions are stopped on one side using a Lexan foil and electrons are stopped on the other side using a small "broom" magnet. A pair of such detectors stacked together and using a common magnet yoke is also shown in **Figure 16** (one pair is shown as deployed on WIND). Analog electronics for pulse shaping amplifier A/D converter and coincidence logic are housed close to the detector, while digital electronics are housed at the spacecraft DPU.
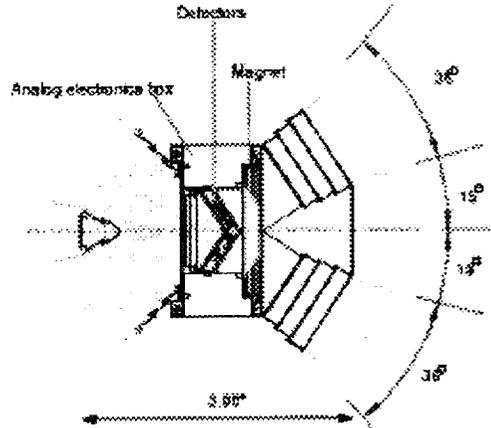
Figure 15. *Solid State Telescope (SST) operational concept.*

Increased capability can be achieved from new technologies utilizing miniature detector design and Application Specific Integrated Circuit (ASIC) technologies for analog and digital processing. Such capability entails full angular resolution and mass discrimination at no additional weight and power expense. These ASIC units have already been developed and tested and are slated for flight on upcoming NASA missions.

2.3.4 Signal/Noise Requirements

Figure 17 indicates the basis for sensitivity requirements, using data from recent missions (Geotail and WIND). These observations were obtained in the magnetotail from 8 to 30 R_E, spanning variations in flux by an order of magnitude for these representative examples. The pixel geometric factors for successful observations in this region range from 0.0001 cm2-sr-eV/eV to 0.01 cm2-sr-eV/eV per pixel
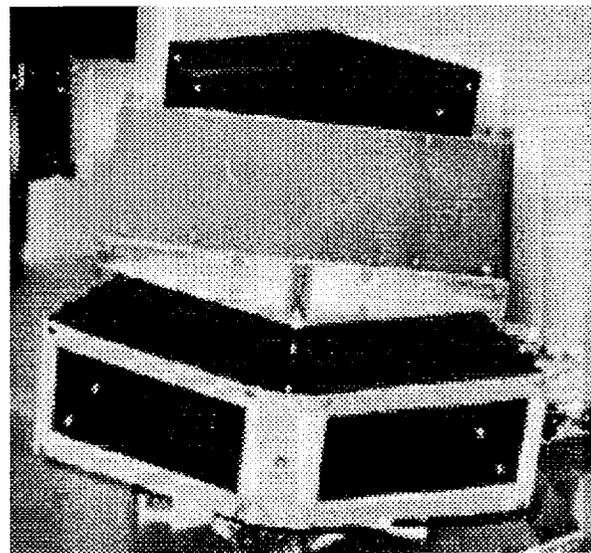
Figure 16. *WIND spacecraft realization of SST.*
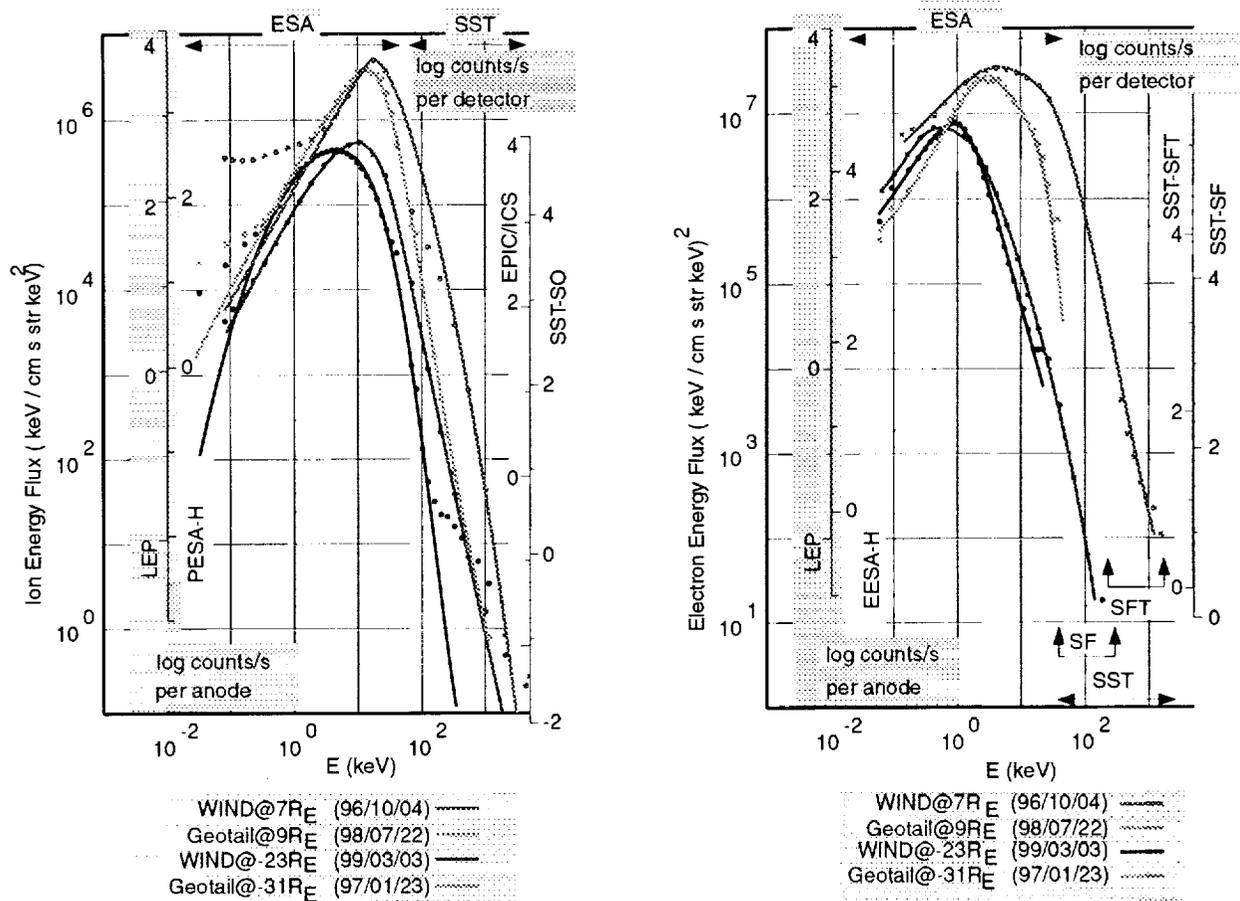
Figure 17. Peak fluxes (left side scales) and count rates (inner left and right side scales, also logarithmic) are shown both from the LEP, or low-energy plasma instrument, and EPIC/ICS, the energetic particle instrument, on Geotail. Similar results from WIND, closer to the Earth, are derived from the PESA/EESA (plasma instrument), and the SST (energetic particles instrument). Both data points and representative fits are shown. Data is courtesy of T. Mukai (LEP), D. Williams (EPIC), and R. P. Lin (PESA/EESA/SST).

for the plasma velocity analyzer, and from 0.01 to 0.1 cm2-sr-eV/eV for the energetic particles instruments.

To assure the required time resolution of 10 sec (~ 3 spins as currently planned) for plasma measurements having an accumulation time at full angular and energy resolution of 0.06 sec (16 energies, 11 azimuths) (elevation imaged on 8 anodes), we need = 18 s⁻¹ count rate to have meaningful statistics. This is readily attained for the range of GF's used on Geotail and WIND, as seen in **Figure 17**.

To assure the required time resolution for energetic particle measurements having an accumulation time at full angular and energy resolution of 0.08 sec (16 energies, 8 azimuths) (elevation imaged on 4 detectors), we need = 13 s⁻¹ count rate to have meaningful statistics. This is easily attained for electrons with the range of Geometric Factors (GF's) used on Geotail and WIND, as seen in **Figure 17**. For energetic ions, this is satisfied in the range up to a few

hundred keV, but some integration will be required for the high-energy ions, with GF's similar to those on Geotail and WIND.

Problematic noise sources for these measurements include ultraviolet (UV) leaks through the optics, and penetrating MeV electrons. The former can be reduced adequately with careful blackening and baffling. The latter are only a serious problem inside of 10 R_E, but adequate shielding close to the detectors must be included in the instrument designs, since the nanosatellite structure offers limited shielding external to the instrument.

3.0 Mission Design

The Magnetospheric Constellation DRACO mission can currently be implemented with 50 state-of-the-art satellites similar to NASA's Space Technology-5 (ST-5) space-

craft to provide the science floor mission. NASA invested considerable resources in nanosatellite technology development, as has private industry. The first nanosatellite launches occur in 2000. It is expected that judicious investments to close the gaps between current nanosatellite technical capabilities and the DRACO requirements will enable a maximum science mission with 100 satellites.

The Magnetospheric Constellation DRACO launches from Kennedy Space Center on a Delta 7925 H into a 185 km by 20 R_E transfer orbit. A specially designed dispenser ship, which carries the 50 to 100 spacecraft, provides the propulsion to raise the orbit perigee from 185 km to 3 R_E and delivers the spacecraft to orbits with a common perigee of 3 R_E and apogees ranging from 7 to 40 R_E.

3.1 Constellation Orbit Strategy

The Magnetospheric Constellation DRACO must sample the magnetotail region from about 7 R_E to 40 R_E, centered at midnight and extending east and west of the Earth-Sun line by about 10 R_E. The spacing of the spacecraft should be as uniform as possible, given the eventual random phasing of the spacecraft around their orbits. A nested group of orbits with a common perigee and apogees from 7 to 40 R_E provides this spacing. Thus, all of the spacecraft pass through a common region for economical telemetry downlinks. The 3 R_E perigee distance was chosen mainly for orbital stability and communication. Careful study of the constellation orbit options has been performed to determine the number of nanosatellites that will give adequate spatial coverage, as outlined in this section.

3.1.1 Orbit Studies

As a basis for quantitatively assessing this strategy, orbit modeling has been performed on a suite of up to 100 virtual spacecraft. In particular, this simulation addressed the spatial separations obtained using various orbital deployment strategies, with an eye toward meeting the mission measurement requirements with the minimum possible number of spacecraft. It was determined that the optimal deployment strategy is a distribution of single spacecraft in closely spaced orbits, with random placement of spacecraft in orbital phase.

Figure 18 illustrates the optimal strategy using 2-D plots of the probability density of the spacecraft in 1x1 R_E cells. The optimal approach is compared with another strategy that was considered, in which families of spacecraft are placed in common orbits. A much more uniform distribution results from the uniformly distributed approach. Of course, any orbit chosen will be susceptible to perturbations and evolve over time.

When the constellation is examined statistically in terms of the distance from each spacecraft to its nearest neighbor, the result is a histogram of nearest neighbor distances, as shown in **Figure 19**. Note that such a histogram would

DRACO Orbit Probability Density

Family (s R$_E$)   Y (R$_E$)   Uniform Spacing
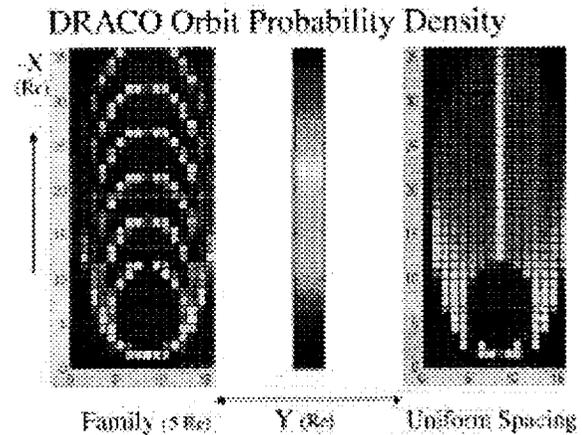
Figure 18. Density probability of 75 spacecraft in family (5 R_E spacing) and single (or random) spacecraft distributions of orbit apogees, both averaged over random distributions in orbital phase, with all perigees at 3 R_E and apogees extending to 35 R_E. The probability peak at apogee results from slow motion there.

— in the limit of a perfectly uniform grid of spacecraft (like that of a global simulation) — produce a delta function histogram with its peak density at the grid spacing distance. We adopted the most probable nearest neighbor distance as the effective spatial resolution of the constellation, and we sought a constellation whose distribution of nearest neighbor distances was as narrow as possible, and therefore as close as possible to an ideal grid of spacecraft. To avoid overly weighting the perigee legs of the orbits, nearest neighbor distances are computed only for the parts of the orbits with X<-10 R_E. For 75 spacecraft spread over the range from 10 to 35 R_E, in either distribution, the resolution is about 1.2 R_E. Relaxing the requirement to 2.0 R_E allows the number of spacecraft in the constellation to be reduced somewhat. When scaled to a distribution extending from 7 to 40 R_E, the mission science goal is a constellation of 100 spacecraft with resolution of 1.2 R_E. However the descope floor that just satisfies the mission requirement for 2 R_E mean spacing is 50 spacecraft.

It can be seen from **Figure 19** that as the number of spacecraft decreases, the mean spacing increases, as expected. By distributing the apogees appropriately, it is possible to level the spacecraft probability, as suggested by **Figure 18**, in the radial dimension. This produces a narrower distribution of spacings, and a more uniform constellation distribution overall, than shown here.

3.1.2 Constellation Evolution

One of the important considerations about this constellation configuration is how long it will stay together when the orbits evolve. To check this we have calculated orbits including moments of the Earth's gravitational field up to the fourth geopotential coefficient, J4, and including lunar and solar gravitational effects.
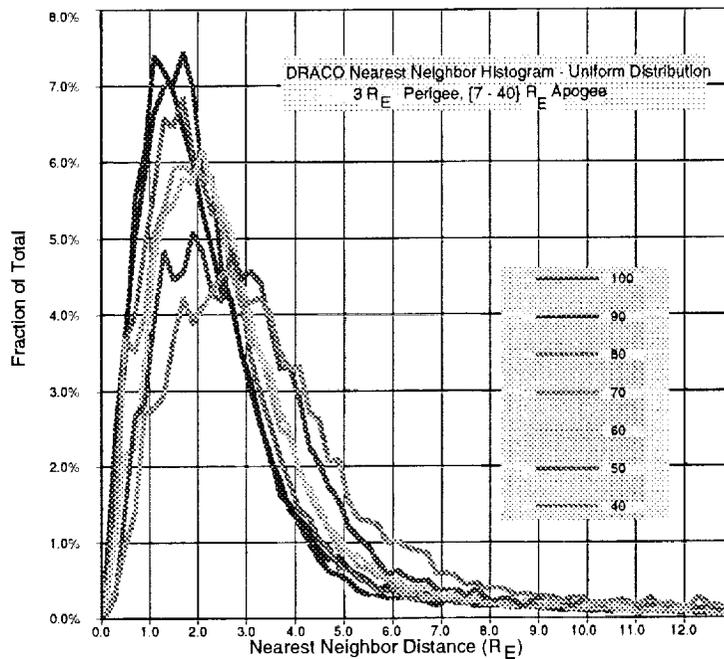
Figure 19. Histograms of nearest neighbor distances for a fleet of varying spacecraft with orbital apogees over the range from 7 40 R_E.

The evolution of the constellation orbits is affected by orbital insertion uncertainties, by lunar and solar perturbations, and by differential precession among the different orbits. Insertion uncertainties will produce some initial spread of the orbits away from the targeted alignments. Lunar/solar perturbations will cause the outer orbits to drift away from the initial orbital plane. **Figure 20** summarizes and illustrates the manner in which the orbit inclination will evolve over the first 2 years. Differential precession will spread the inner orbits relative to the outer orbits, splaying the overall constellation out in local time. **Figure 21** illustrates and summarizes the orbital precession effects for orbit inclination of 10° (and a slightly different constellation design).

3.1.3 Deployment Strategy

The strategy for orbital deployment supports a single launch of up to 100 nanosatellites using a Dispenser Ship (DS) spacecraft that contains and deploys the individual nanosatellites. The DS is designed to fit within a Delta II fairing, and to hold up to 105 nanosatellites. The baseline mission design assumes that each nanosatellite is equipped with sufficient propulsion to reach its final orbit from a suitable drop-off orbit attained by the DS. The propulsion allocation between the DS and the nanosatellites is a subject for future trades.

3.1.4 Radiation Environment

The expected radiation environment for spacecraft in the DRACO orbits is an additional consideration for the orbital deployment strategy and has been evaluated. The total ionizing dose for a 2-year mission is 100 k-rad. **Figure 22** shows the radiation dose-depth curves for a 12.5 R_E apogee orbit. It can be seen that this environment, while significant, is comparable to other mission dose requirements, notably POLAR. This environment will require trades between shielding (increased mass) and custom electronics (increased cost).

3.2 Instrument Accommodations

The ST-5 instrument provides the required mechanical accommodations for DRACO payload's footprints and fields of view. It also provides power and data storage. **Table 4** summarizes the instrument resource requirements.

3.3 Spacecraft Description

The information contained in this section is from NASA GSFC's ST-5 proposal, modified to accommodate the Magnetotail Constellation payload. The spacecraft platform is spin stabilized with body mounted solar arrays. The basic
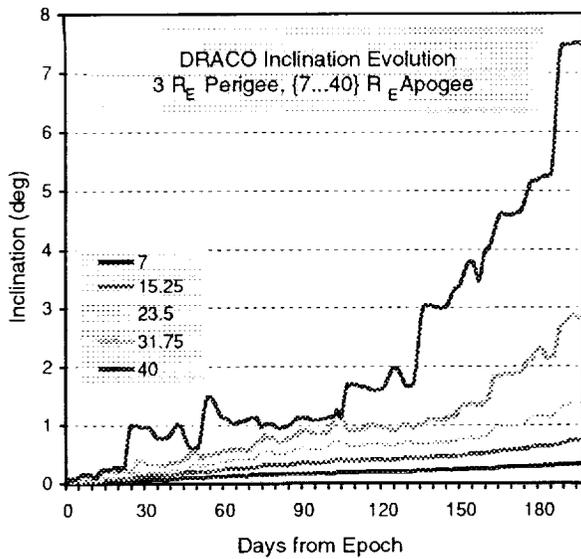
Figure 20. *Evolution of typical Magnetotail Constellation orbits over 2 years.*

structure is an octagonal prism 20.0 cm in height and 41.6 cm in diameter across the flat facets (44.0 cm including the stowed magnetometer) and 45.0 cm across the vertices. The overall height in the launch configuration with both the Global Positioning System (GPS) and whip-type Ultra High Frequency (UHF) antennas stowed is 29.0 cm from the base of the balance weights to the top of the X-band antenna. **Figure 23** shows the deployed spacecraft. **Table 5** summarizes the spacecraft component and mass list. Note that the ST-5 instrument mass is identical to the

Magnetospheric Constellation instrument mass allocations.

3.3.1 Subsystem Description and Performance

Table 6 summarizes the predicted ST-5 subsystem sizing requirements, component capabilities, and integrated performance results for the spacecraft functions. Each subsystem is discussed in detail in the following.

3.3.1.1 Spacecraft Mechanical Subsystem. The mechanical subsystem consists of a structural bus, deployables, and a launch vehicle deployment/release mechanism. The graphite/cyanate ester composite bus structure consists of a removable, high-conductivity honeycomb sandwich top deck, to which most of the spacecraft equipment is mounted:

- a composite honeycomb sandwich bottom deck; and
- sidewalls constructed of thermally isolated filament wound composite shell.

Components will be attached to the top and bottom decks with aerospace fasteners and/or adhesives. Aluminum radiation shielding, 0.218 cm, is provided for sensitive components Command and Data Handling (C&DH), transponder, power supply electronics, and A Formation Flying and Communications Instrument/Global Positioning System (AFFCI/GPS) to restrict the total dose to 50 k-rads. Software-commanded deployable structures include the magnetometer boom and the GPS and UHF antennas. The magnetometer boom deployment is repeatable to 0.25 degrees (each axis).
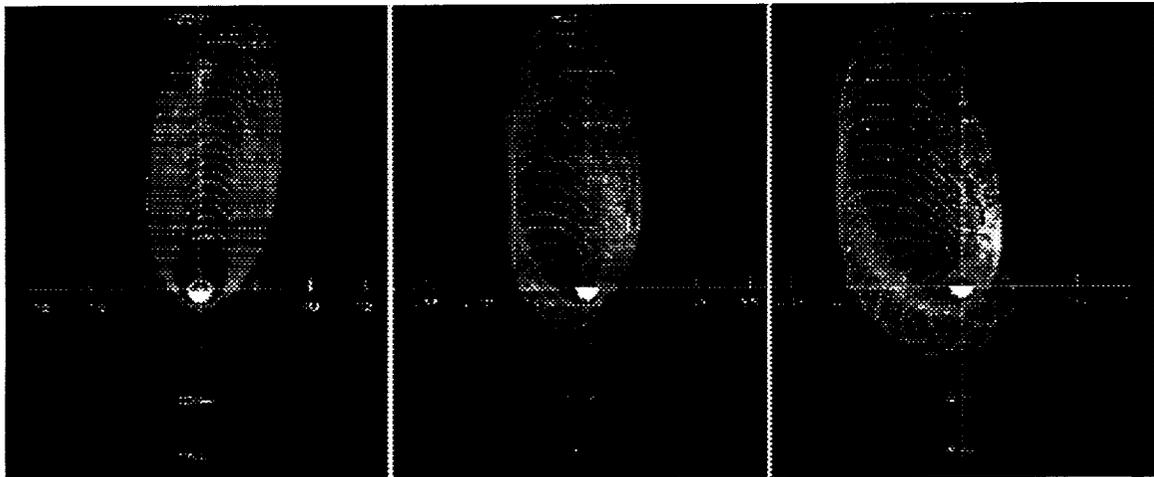
Figure 21. *Drift of a constellation of 21 spacecraft over a 2-year period owing to differential precession of lines of apsides, for orbit inclination of 10°. Spatial frequency of occurrence along each orbit is color-coded in arbitrary units a) at launch, b) after 1 year, and c) after 2 years. The precession of the constellation shown here is much more rapid than for DRACO, because this constellation has perigee at low Earth orbit. It is provided as an extreme case reflecting the fastest possible precession in the event that lower perigees are used for DRACO.*

Magnetospheric Constellation Mission...

Figure 22. Constellation DRACO radiation environment. Orbital parameters are given in terms of apogee and perigee altitudes, and correspond to 12.5 R_E x 3 R_E geocentric distance.

3.3.1.2 Electrical Power Subsystem. The Electrical Power Subsystem (EPS) consists of three major components: the solar array, the battery, and the control electronics. Triple junction Gallium Arsenide (GaA's) solar cells with 26% beginning-of-life (BOL) efficiency and conductive covers populate two separate cell strings on each of the eight solar panels (total array area of 832.0 cm²). E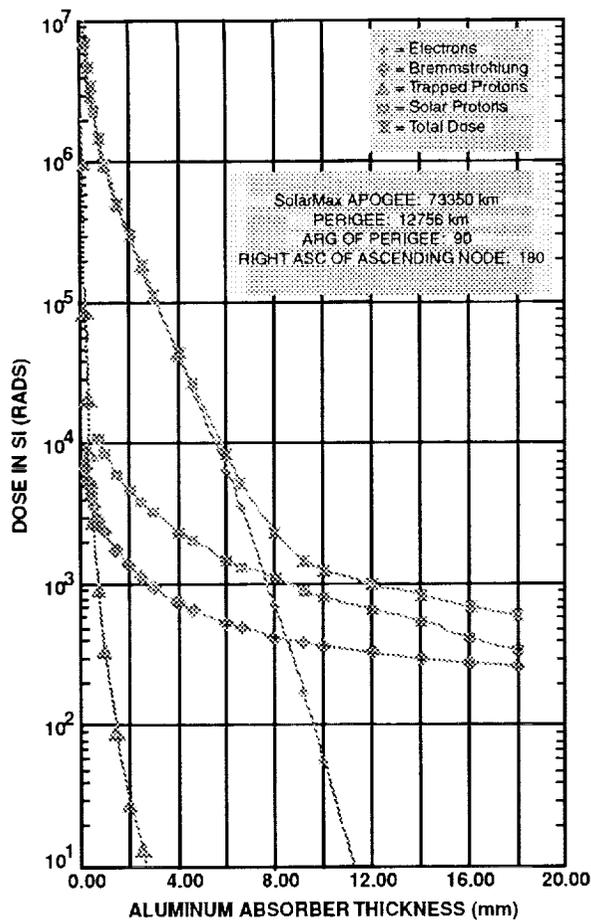ach string is connected to a separate battery cell. Flexible circuit interconnects provide electrical connection for the solar cells on one of the eight panels. Standard wire interconnects are used on the remaining panels.

A two-cell, 42 W-hr lithium ion battery supplies power during eclipse and for in-Sun "peaking" loads exceeding the solar array capability. Connecting each battery cell to a separate solar cell string incorporates charge protection.

Rate solar cell string incorporates charge protection. String voltage is limited to 4.10V by solar array string regula-

tors, which assure full charge at the maximum battery cell voltage of 4.10V and a maximum battery total voltage of 8.2V. The C&DH, which monitors individual cell voltages and reduces spacecraft total load when necessary, accomplishes discharge voltage control. Power conditioning and control electronics regulate solar array output and supply regulated power to spacecraft loads.

3.3.1.3 Thermal Control System. The thermal control system (TCS) is primarily passive and includes heaters, multilayer insulation (MLI) blankets, fillers, thermistors, and variable emittance coatings. The interior of the solar array panels is insulated with MLI as are the interiors of the top and bottom decks, aside from cutouts for a single radiator on each deck. The battery will be insulated to maintain 25 °C at the minimum expected temperature of -30 °C. One heater provides 0.15W to the magnetometer and a second provides 0.5W to the transponder oscillator. External coatings, including the radiator coatings, are electrically conductive, and all MLI layers are grounded to the structure.

3.3.1.4 Propulsion System. Trade studies were completed to explore the most efficient way to put each nanosatellite into its desired orbit. This study weighed the merits of putting all the propulsion on the deployer ship, all on the nanosatellites, or some combination of the two. Viable versions of each scenario were judged to be nearly equal in merit.

In case some propulsion is required for each nanosatellite, advanced engineering studies have already shown that such new systems are feasible. The nanosatellite propulsion system consists of a miniature cold gas thruster system and a 15.2 cm diameter titanium Gaseous Nitrogen (GN2) propellant tank. Within the operating pressure range from 1500 psia BOL to 100 psia, the cold gas thruster system can provide a total velocity increment of 5.5 m/s. The system can deliver a minimum impulse bit of 45 mN-s at 1000 psi. The system provides a maximum vacuum thrust of 1.32 N at 1500 psia and a maximum impulse of 109 N-s at a specific impulse of 60 seconds, providing a total delta Vee capability of 5.5 m/s. The ST-5 propulsion system will require modification if the individual satellites need to provide the propulsion for apogee changes after deployment from the dispenser ship.

3.3.1.5 Guidance, Navigation, and Control Subsystem. The Guidance, Navigation, and Control (GN&C) subsystem incorporates a mini +/- 90 degree field-of-view Sun sensor, a nutation damper, and also uses the science magnetometer. The attitude control system software actuates the cold gas thrusters via the C&DH subsystem to perform minor orbit adjustments and spin axis precession control. Spin-synchronized pulses are used for precession control, while continuous firing is used for orbit raising. A simple passive nutation damper damps thruster-induced nutation.

	Quantity	Component	Mass Ea. Unit (kg)	Total Mass (kg) Subsystem Actual	Dimensions (cm)	Mass of Subsystem
INSTRUMENTS	1 1 1 1 1	Magnetometer MAG Electronics, etc. MAG Boom Electron Detector Proton Detector	0.150 0.800 0.750 0.500 0.500	0.150 0.800 0.750 0.500 0.500	4 x 4 x 6 10 x 20 x 5 50L x 3 10 x 10 x 7 10 x 10 x 7	2.700
COMM	1 1 1	Transponder, X-band X-band Antenna Amp-Diplexer (HPA)	0.150 0.100 0.160	0.150 0.100 0.160	5 x 7 x 5 x 5 7L 2 x 4 x 4	0.410
GN&C	1 1 1 1 1	Sun Sensor Nutation Damper CCNT GPS Antenna UHF Antenna	0.250 0.100 1.550 0.100 0.100	0.250 0.100 1.550 0.100 0.100	2 x 2 x 2 4 x 4 x 1 15 x 6 x 18 6 x 6 x 5 .2 x .2 x 20	2.050
PROPULSION	1 1 1 1	Thruster Tank Cold Gas Propulsion Misc.	0.130 0.560 0.200 0.500	0.130 0.560 0.200 0.500	1.75 OD x 2.2	1.440
THERMAL	1	Thermal	0.760	0.760	N/A	0.760
C&DH	1	C&DH box	1.800	1.800	2 x 18 x 36	1.800
POWER	1 1	Battery Solar Array	1.000 1.258	1.000 1.258	6.35 x 6.35 x 11.8	2.258
MECH	1 1 1	Separation Device Balance Weights Structure	0.200 0.500 1.815	0.200 0.500 1.815	N/A	2.515
MISC	1 1	Radiation Shielding Harnesses (all)	0.244	2.684 1.329	N/A	4.013
Totals				17.946		

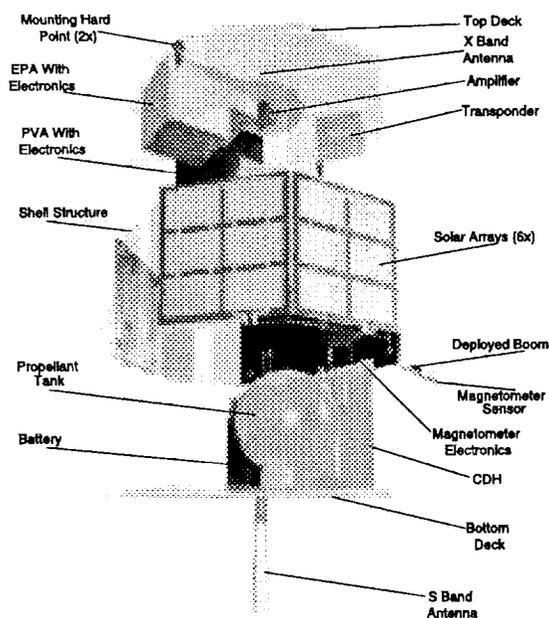Table 5. ST-5 spacecraft component and mass summary.

Figure 23. Conceptual view of the Space Technology-5 satellite for Magnetotail Constellation.

3.3.1.6 Command and Data Handling Subsystem. The C&DH subsystem is an Essential Servicing Node (ESN)-based system, which resides on one side of a double-sided card. The ESN multichip module (MCM) contains an ASIC chip as its central device. Embedded in the ASIC is a general purpose bus computer with the UTMC UT69R000 16-bit RISC processor as its core and a number of industry standards as its onboard peripherals. In addition to the devices contained in the ASIC, the MCM contains several memory storage devices used for instruction and data storage and an analog subcircuit used to support analog signal measurements.

The C&DH system sends commands, gathers telemetry data, stores data in Consulting Committee for Space Data Systems (CCSDS) packets, time tags data, and transmits stored data to the ground. The card consists of:

- an ESN multichip module, acting as the MHz processor which processes commands, makes data packets, and performs ACS computations;
- multiple RS422 interfaces which gather telemetry and distribute commands to the science instruments and to the space-to-ground and space-to-space communications systems;
- a memory section containing 80 Mbits of D-RAM;
- an ACS interface for the Sun sensor and thruster;
- a housekeeping interface which reads analog data from the power system and thermistors and controls heaters;

- a communications interface, which sends CCSDS packet telemetry to the ground and receives and processes CCSDS packet commands.

3.3.1.7 Communications Subsystem. The space-to-ground communications system consists of the Aero-Astro X-band transponder and diplexer. The transponder is used to downlink all science and housekeeping data to the ground once per orbit, to receive ground commands, and for two-way coherent Doppler tracking with the ground.

3.3.1.8 Flight Software Subsystem. The flight software is based on the operating system for the low-power ESN Central Processing Unit (CPU) used on the MAP mission. All flight software resides in a single 16-bit UT69R000 ESN microprocessor with a configuration similar to that of the MAP housekeeping remote services node, and uses the "C" language and assembly level programming.

3.4 Dispenser Ship

The details presented herein for the Magnetospheric Constellation DS are given by *Lieberman* [1999b]. That report also references and draws upon the Magnetospheric Constellation Mission Document [*Lieberman*, 1999a]. The actual mission design and DS designs have changed and may change further as a result of future studies. The orbits upon which the following details are based are not necessarily the orbits presented in Section 3.1. In case of discrepancies, the information given in earlier sections takes precedence over the materials in this section.

3.4.1 Orbital Maneuvers of the Dispenser Ship

Six methods for placing the nanosatellites in orbit were studied. The final orbit selected was the least complicated and minimized the nanosatellites propellant mass requirements.

For the orbit selected, the Delta places the DS in an elliptical orbit whose parameters are perigee 185 km, apogee 20 R_E with inclination of 28.7 deg. The DS performs an apogee burn and raises the perigee to 1000 km and makes a small change in the inclination. A second apogee burn raises the perigee to 3 R_E and removes 21.2 deg of inclination. The parking orbit of the DS is 3 R_E perigee, 20 R_E apogee, 7.5 deg inclination with the line of apsides lies in the ecliptic. From the parking orbit, several nanosatellites are released with their spin axes aligned to the DS perigee velocity vector. The nanosatellite kick motors are ignited at perigee. Some nanosatellites will raise their apogees and others will fire in retrograde direction to lower their perigees.

Although the details presented in this report are based on delta-V capability for the nanosatellites, it has not been determined at this stage of formulation if this capability

Subsystem/Component	Design	Subsystem/Component	Design
Structure _Clearance Envelope (cm³)_ _Launch Loads (g's each axis, flight)_ _Min. Fundamental Axial Frequency_ _Min. Fundamental Lateral Frequency_ _Radiation Total Dose Absorbed at 3 months_	_43x31x45_ _>15_ _>134 Hz_ _134 Hz_ _50 krads_	_Propulsion_ _Velocity Increment (m/s)_ _Guidance, Navigation and Control_ • Pointing Accuracy, Sun Line to Spin Axis, Sun Acquisition Mode (deg.) • Spin Rate Knowledge, initial (% rpm) • Spin Axis Pointing Accuracy, Ground Based Control Mode +/- deg. • Knowledge (+/- deg.)	_5.5_ _.90 +/- 3.0_ _+/- 0.1_ 2.5 1.0
Spacecraft Deployment _Separation Velocity (m/s)_ _Maximum Tipoff Rate (deg./sec.)_ _Spin Rate at Separation (rpm)_ _Spin Rate Pre Delta-V_	_0.66_ _1.0_ _28 +/-_ _10%_ _20 +/-_ _10%_	_Control (+/- deg.)_ • Spin Rate Knowledge On-Orbit (% rpm) • GPS Orbit Determination 3-D RMS (m) • PreDelta-V Spin Axis (Pointing +/- deg.)	_1.5_ _+/- 0.1_ 100 2.5
Power (Solar Array at 25 °C) _Power required, orbit average (W)_ _Energy Storage Required (W-hr)_ _Voltage Regulation Range_	_21.4_ _42.0_ _5.0 +/-_ _4.0%_	_Command and Data Handling_ • PROM (kWord) • EEPROM (kWord) • Data RAM (kWord) • Instruction RAM (kWord) • Data Recorder Size (Mbits)	_32_ _128_ _64_ _164_ _80_
Thermal (Solar Flux = 1285 w/m² Cold, 1418 w/m² Hot _Internal Equipment Operating (°C)_ _Internal Equipment Non-Op (°C)_ _Solar Array Operating °C)_ _Solar Array Non-Op (°C)_ _Duration of Elipse (hrs.)_ _Radiator Area for 25 W (cm²)_	_-5 to +25_ _-5 to +28_ _-77 to +28_ _-77 to +40_ _2.1_ _600_	_Communications (Space-Ground)_ _Data Rate (at 5.0 Re, 1.5 W, BER 1x 10⁻⁵ (kbits/sec)_ _Link Margin with 11 M Antenna (dB)_ _Total Data Downlinked (Mbit)_ _Space to Ground Transmit Time (min.)_	_100_ _5.5_ _640_ _107_

Table 6. _Spacecraft requirements and design capabilities._

will be the final nanosatellites requirement. Another option under consideration is to design the DS with the capability to ensure proper nanosatellite orbit insertion. Having the nanosatellite orbits determined solely by how and when they are released from the mother ship could have significant impact on the requirements and design for a release mechanism.

3.4.2 Nanosatellite Orbital Maneuvers and Mission Operations

Four nanosatellite release mechanisms have been proposed. The kinematics of release were simulated; the simulations show that all four will provide a noninterference separation of the nanosatellite from the DS. All four require a discrete electrical command, which will cause the force holding the nanosatellite to the DS to cease to exist in a short period of time — approximately 1 msec. The command will be given simultaneously to up to 14 nanosatellites. When released, the rotating nanosatellites will "fly" tangentially away from the DS. The angular rate will be approximately the same as that of the DS. The command receivers of the separated units will be turned on; however, only one will have its transmitter on. After the nanosatellite's kick motor has fired (the one with the active transmitter), the ground station — using the nominal burn trajectory for a reference orbit — will point its antenna at the nanosatellite. The Doppler shift of the transmitted signal will be used to determine the nanosatellite orbital velocity and by analysis the ground station will be able to determine the nanosatellite's orbit.

When the nanosatellites are dispensed, they will be se-
lected such that no two satellites will be transferred into
an orbit with same apogee. This requirement will assure
1) the ground station has adequate time to track the
nanosatellites and, 2) the true anomaly of satellites in the
same orbit will be different. If 10 nanosatellites are dis-
pensed at 2 R_E separation, no more than four will be in an
orbit whose apogee is less than 20 R_E. Thus, the ground
station will be able to get the 30 minutes of tracking per
nanosatellite needed to get "good" data for each of the four
"lower" apogee nanosatellites before they leave the search
field. The ground station can then turn its attention to the
remaining six nanosatellites destined for the higher apo-
gees. Approximately 200 (325-120) minutes (33 minutes
per satellite) are available to track the remaining six
nanosatellites.

3.4.3 Dispenser Ship Overview

The heart of the system is the C&DH system. The X-band
receiver, located in the Communications Subsystem, re-
ceives the ground commands. They are decoded and stored
in the C&DH as relative or absolute time commands. The
ACS sensors send attitude signals to the C&DH, where
they are processed to determine the actuator commands
(five thrusters) that are needed to maintain attitude con-
trol or to maneuver the DS to a new attitude. The C&DH
issues release commands to the nanosatellites via the arm
and fire relays. The C&DH also sends commands to the
main thruster during each of the two orbit change maneu-
vers. Finally, the C&DH processes and formats housekeep-
ing, status, and health and safety telemetry for transmis-
sion to the ground. Each subsystem is briefly described in
this section; a more detailed discussion of the dispenser
ship can be found in the full report [Lieberman, 1999a].

3.4.3.1 Mass and Power Summary. Table 7 summa-
rizes the mass and power budgets of the DS concept. The
mass and power figures apply to the DS exclusive of the
DRACO nanosatellites.

3.4.3.2 Mechanical Configuration. Figure 24 shows the
mechanical configuration of the nanosatellite DS. The blue
ring at the top is the 130 watt solar array. Above the array
is the X-band omni antenna. Located on the top ring are
three coarse Sun sensors, Earth sensors and a fine Sun
sensor.

In this version, 92 nanosatellites are located in individual
bays. There are 14 bays per tier and seven tiers, a total of
98 bays. Since the lift mass of the Delta only permits a
payload of 92 nanosatellites, six bays will be empty. Lo-
cated in the area around the base of the DS are the main
thruster, three additional coarse Sun sensors, and four
small thrusters. The propulsion tanks, power regulators
and the avionics are housed in the interior of the DS.

**3.4.3.3 Attitude Control Subsystem (ACS)
Description.** The ACS uses an Earth sensor and fine Sun
sensor for attitude references and to measure the spin rate.
The ring laser gyro is used as attitude reference to precess
the spin axis to a desired attitude and for sensing and con-
trolling the nutation of the DS. The normal mission atti-
tude of the spin axis is perpendicular to the ecliptic except
during the portion of the orbit when the nanosatellites are
to be released. Before release, the DS will be commanded
to precess the spin axis to be parallel to the velocity vector
at perigee. The nanosatellites will be released close to peri-
gee. Precession will be accomplished by actuating the bi-
propellant thrusters.

The six coarse Sun sensors' output provides the position of
the Sun with respect to the DS. This information from the
coarse Sun sensors will be used during the initial stabili-
zation phase after the DS has been released from the launch
vehicle. To precess the spin axis of the DS from the release
attitude to the normal operational attitude (perpendicu-
lar to the ecliptic), the thrusters are used.

**3.4.3.4 Command and Data Handling (C&DH)
Subsystem.** The C&DH avionics module is based on a cen-
tral processor. The subsystem also has a solid-state recorder
to store data that will be transmitted to the ground sta-
tions for distribution to the end user. The avionics module
includes interfaces to the ACS, the power subsystem, and
the communications subsystems as well as the release ac-
tuators. The avionics module sends commands, gathers te-
lemetry data, processes the data, stores the data using
CCSDS packets, time tags the data, and transmits the
stored data to the ground. The avionics module is a proces-
sor-based system which processes commands, packetizes
the data, performs the timekeeping functions, performs
ACS computations and controls power. The avionics mod-
ule contains 2.0 Gbits of Random Access Memory (RAM),
and interfaces to the ACS subsystems Earth/Sun Sensor
(analog data), Attitude Thruster (pulse command), Orbit
Thruster (single pulse), the latch valves and the pyro ac-
tuated valves. The housekeeping functions include read-
ing the thermistors, pressure transducers, and voltage and
current monitors, and gathering other analog telemetry.
These functions will be handled using a 12-bit A/D con-
verter. The Uplink/Downlink interface is connected directly
to the transmitter and receiver. This interface sends CCSDS
packet telemetry to the ground antennae, and receives
CCSDS packet commands from the ground antennae and
processes them.

The avionics module is an MCM stack. It is composed of
six functional interfaces, each of which performs separate
functions required by the avionics module. These functions
are the processor, the memory, the actuator interface, the
ACS interface, the housekeeping interface, and the com-
munications interface. The development of these interfaces
will require the extensive use of Field Programmable Gate
Arrays (FPGA's). These FPGA's will be developed in a low-
power technology.

Subsystem	Mass (kg)	Power (watts)
ACS	7.1	13.8
C&DH	12	2
Communications	7.8	7.2
Power	5.6	32
Propulsion	50	-
Harness	4.5	0
Thermal	4.5	5
Structure	131	0
Total as Designed	216.9	60

Table 7. DS final as-designed mass and power.

3.4.3.5 Communications Subsystem. The communication system for the DS consists of a transmitter, receiver and an omni antenna. It operates in the X band. The link analysis shows positive margin with an 11-meter ground station antenna and an omni antenna on the DS. The G/T ratio for the ground segment must be 35.4 dB/K in the X band. The Effective Isotrophic Radiated Power (EIRP) from the DS is 1.76 dbw (1.5 watts to the antenna). To be compliant with the
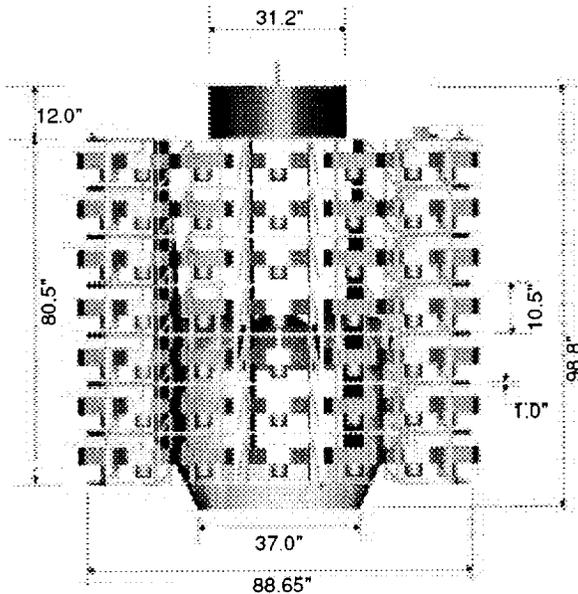

Figure 24. Conceptual mechanical configuration for nanosatellite dispenser ship.

system requirement, using one-way Doppler for tracking, the oscillator must be stable to 5×10^{-8} per day. The down link transmission rate can be as high as 100 Kb/sec and the command rate is baselined as 1 Kb/sec. (NB: downlink rates of up to 640 Kbps have been determined to be feasible, since this study).

3.4.3.6 Power Subsystem. The power subsystem consists of three main elements: the solar array, which converts solar energy to electrical power, the regulators, which, as the name implies, reduce the variation of the voltage on the power bus, and the lithium hydride battery. The output to the bus will be 28 +/- 7V DC. The solar array is sized to deliver 130 watts off the array at BOL. The power subsystem provides no power to the nanosatellites. The power subsystem provides power through eclipses up to 40 minutes.

3.4.3.7 Propulsion Subsystem. The DS propulsion provides 202 kg of bipropellant and operates while the DS is spinning at 30 rpm. The system will be used for adding delta-V, precessing the spin axis, controlling the spin rate and maintaining attitude control. The large thruster will be used for delta-V maneuvers and the smaller thrusters will be used for the other functions. The pyro valves are opened after the DS has been placed in orbit by the launch vehicle. The thrusters will not fire until the latch valves are commanded open. The main engine latch valve will be kept closed and opened when a delta-V maneuver is imminent. The other latch valves will be left open and closed only if a thruster malfunctions. The thrusters are fired infrequently and therefore the orbital average power is negligible.

3.4.3.8 Structure. The DS structure consists of the inner structure and seven berthing rings. The inverted cone at the base of the internal support transition cylinder interfaces with the launch vehicle payload adapter fitting. Attached to this cylinder are seven vertical gussets, which support the seven nanosatellite berthing rings. Detailed views of these structures are shown in the full report [Lieberman, 1999a].

3.4.3.9 Inner Structure. The propulsion system's four tanks and the large thruster are carried by the inner structure. The four small thrusters are located on the lower berthing ring. Two of the thrusters are for spin control, a third is used for precession control and the fourth is a backup for the precession control thruster. In addition, the inner structure carries the three coarse Sun sensors.

3.4.3.10 Thermal Subsystem. The DS thermal requirements can be accommodated with a passive thermal control system (blankets, heaters, and coatings). The MLI will be used on top and bottom to reduce losses and gains from the environment. The cylindrical sides (shell) of the DS are not insulated. Heaters and MLI may be used to maintain propulsion lines and thrusters during orbit changes.

A top-level thermal analysis has been completed. For components that are mounted externally, have a high watt density, or have tight temperature control requirements, a more detailed model would need to be completed.

Preliminary results indicate that the nanosatellites mounted in the top ring run slightly warmer than the others, while the ones in the bottom ring run the coolest. The DS temperature is set by the high energy absorbed by the shell and its conductive coupling to the birdcage. The design described is reliable and appears to meet temperature requirements for the DS as well as the nanosatellites. Further parametric analysis will be conducted with a more detailed model

3.5 Integration and Test

Of particular importance to the DRACO mission will be innovation in the way in which the payloads (nanosatellites) are integrated to the dispenser ship. The normal way of integrating payloads to the main spacecraft would result in an unacceptably long and costly integration period. This section discusses ways of approaching this issue. It will be assumed that each nanosatellite bus and instrument suite will be delivered as a single, ready-to-integrate system. Furthermore, each nanosatellite must not take longer than 1 or 2 days to be fully integrated to the DS. This is necessary, because the integration of 92 nanosatellites taking 2 days each would be 184 days, or 6 months of 7-day per week operation if the nanosatellites are integrated in a serial fashion. If several nanosatellites could be integrated in parallel, this would reduce the integration time, but could increase integration cost due to higher manpower requirements.

One approach to mitigating this issue is to design the nanosatellite for rapid integration thru the use of highly automated processes and test equipment. This would require development of automated test equipment and processes, or would require that the design process take into account the use of existing test equipment and processes to optimize the ability to quickly test the "sciencecraft."

Another approach is to accept more risk in the process by only completely testing every nth unit and performing reduced testing on the other units. This approach means that more risk must be accepted.

3.6 Mission Operations

The operation of a constellation of identical nanosatellites requires different concepts than for single spacecraft missions. The nanosatellites may be constrained in the amount of functions they can perform on board by the lack of processing power. The large number of spacecraft requires automation on the ground in order to keep the staffing to a reasonable level and offers an opportunity for changes in risk management. The loss of a few spacecraft over the mission lifetime is tolerable for this mission.

Routine operations commence after the nanosatellites have reached their operational orbit. Anomalies or infrequent events such as eclipse only interrupt routine operations.

3.6.1 Space/Ground Communications

There are several options for space/ground communications services: dedicated stations, commercial networks, NASA stations, large antennas, smaller antennas, etc. This operations concept assumes the use of a commercial network of 11-meter antennas. The commercial network would have a number of these antennas distributed around the world. Communications would only occur around perigee. At times during the mission, there may be as many as two dozen spacecraft near perigee at the same time. The multiple stations would be able to handle some of these spacecraft. Spacecraft with smaller apogees could skip a contact, and dump their data at the next perigee. Loss of some data during these infrequent "traffic jams" would be acceptable — the overall data completeness requirement will be ~ 95%.

The ground stations will provide telemetry, commanding, and tracking services. The real-time housekeeping data will be extracted from the downlink data and sent to the operations center in real-time. Playback science and housekeeping data and tracking data will be sent to the operations center after the contact, sharing the bandwidth with other station users.

3.6.2 Planning and Scheduling

The scheduling of the ground stations depends on how the ground station services are provided. One option would be to let the ground station provider schedule the contacts within provided guidelines for data completeness and frequency of tracking data collection. The ground station provider would have the flexibility to adjust the contacts within these guidelines, which potentially could result in lower costs to the project. The ground station provider would provide the schedule to the operations team so that they could identify uplink opportunities and support data accounting.

3.6.3 Commanding

The spacecraft will be commanded every contact to initiate the downlink of data. Since the ground station schedule is subject to change, particularly for the spacecraft with distant apogees, the spacecraft cannot initiate the downlink. The instrument scripts may be updated once every month. The instrument script may be as simple as timed tagged commands or could be a more sophisticated set of instructions for the onboard system to interpret. Software loads may be performed if problems are identified after launch that can be addressed by the flight software. The data system will automatically uplink new loads or instrument scripts to the constellation. The loads will have a time window within which each spacecraft must be updated. The system will automatically send and verify the load during regularly scheduled contacts. The operators will be

alerted of any spacecraft that is not updated when the window closes.

3.6.4 Housekeeping Data Processing

The data system will automatically process the housekeeping data and identify limits violations and improper configurations. The system will be capable of processing data from multiple spacecraft simultaneously. The data system will also process status information from the ground station and identify any missing or poor quality data. Problems will be ranked according to severity. Significant problems will result in an immediate alert to the operations team. If the operations team members are not present, the system will use a pager to notify them. The data system will process all of the housekeeping data and produce standard analysis reports. These reports will compare telemetry parameters across time and across spacecraft. Spacecraft engineers will be able to generate custom reports as well.

3.6.5 Science Data Processing

The science data is automatically level-zero processed when it is received from the ground station. This processing removes overlaps in the data and identified missing data. Operators are alerted in the event that a significant amount of data is missing. The system will have data accounting tools to assist the operators in visualizing the data loss and its distribution over the constellation. The operators will work with the ground station network to attempt to recover lost data that exceeds requirements. They may adjust the scheduling priorities if some part of the constellation is losing more data than other parts. The data will be automatically processed into standard products and archived in the science center. It will be distributed to science users electronically or, for large amounts of data, on physical media.

3.6.6 Operations Staffing

The mission operations staff (not including the science operations staff) for the Magnetospheric Constellation DRACO can be relatively small. The spacecraft are performing survey missions and have limited reconfiguration capability. The ground systems are automated, performing all routine functions. The operations team will primarily handle exceptions that have been flagged by the data system. The operations team's primary concern will be for common problems that have the potential to affect all of the members of the constellation. The nominal operations staff will be about six people. It will include one or two spacecraft engineers, a science liaison member, a data accounting person, and an orbit expert. The operations staff will work 40 hours per week, and at least one member will be on call for automated alerts during off-hours.

3.6.7 Special Operations

At launch, the operations team will be augmented with personnel from the spacecraft development and test functions. The ground data system may include more ground stations or larger ground stations, to check out and track the spacecraft after deployment. The ground system will also have to operate the DS during this phase of the mission. The deployment operations may be adjusted (e.g., to change the number of spacecraft deployed at a time, or change the frequency of deployment), based on the experience with the first few deployments.

In the event of an anomaly, the operations team may request the assistance of the spacecraft developers to identify the cause of a problem and to develop corrective action or workarounds. The spacecraft developer will be responsible for maintaining the flight software throughout the mission. To assist in the anomaly resolution, the operations team may use larger ground antennas to communicate with the spacecraft over longer periods of time, rather than just at perigee.

3.7 Status and Schedule

The current STP funding profile supports a launch in September 2010. Implementation will begin in 2006. Technology development is expected to continue through 2005. The schedule for the project is shown in **Figure 25**.

4.0 Mission-Enabling Technology Development

To realize the Magnetospheric Constellation mission, a number of enabling technologies must be developed and matured. These technologies are listed below:

- Low-mass, low-power, C&DH systems;
- Miniaturized, low-power, radiation-hardened analog and digital electronics;
- Advanced propulsion systems;
- Avionics on a chip;
- Lightweight, high-capacity batteries;
- Lightweight, low-power communications components;
- Software tools for autonomous ground operations of satellite constellations;
- Data acquisition, distribution and visualization from constellations.

In addition to these technologies, new tools and methodologies must be developed for manufacturing large numbers of research grade instruments and satellites at low cost, and testing and integrating these large numbers of nanosatellites in a reasonable amount of time. These particular issues will be discussed in greater detail in the sections to follow.

4.1 Instrumentation

Development of instrument technologies and instruments of mass and power commensurate with a nanosatellite class mission are well underway by Department of Defense (DOD), NASA and various other institutions and agencies, both U.S. and international. Some instruments, such as magnetometers, are already close to the mass and power needed for a constellation mission. The issues of most significance in the development of instruments for a constellation mission are recurring cost and capability to be manufactured in large quantities in a reasonable period of time. The current paradigm of a 2-3 year instrument development, fabrication and qualification period with costs typically in the several hundred thousand to over $1 million cost range is clearly unacceptable when one wishes to fabricate and qualify as many as 100 identical sets of instruments. It is this "manufacturability" issue that most needs to be addressed by the Magnetospheric Constellation DRACO mission, especially in light of the possibility that some instrument technologies may require new designs to achieve the cost and "manufacturability" requirements.

The strategy to be pursued by the Magnetospheric Constellation mission includes the following options:

- NASA Research Announcements (NRA's) initiated and funded through DRACO formulation efforts;
- Leveraging of NASA Headquarters-initiated and funded NRA's (directed DRACO funding to supplement these efforts);
- Participation in, or leveraging of, other proposal opportunities such as the Cross-Enterprise Program;
- Spinoff from the ST-5 nanosatellite Constellation Trailblazer project under the New Millennium Program;
- Restructuring the typical spending plan for STP missions in order to fund preliminary designs for early mission development.

Another approach under consideration involves the partnering of scientists and instrument developers with the developers and builders of spacecraft buses to create an integrated "sciencecraft." This approach will be discussed in a little more detail in the next section.

4.2 Nanosatellite Development

In contrast to instruments, a number of technologies (as listed above) needs to be developed and matured before a nanosatellite meeting the DRACO requirements can be realized. As with the instrument technologies, a number of agencies and institutions, both domestic and international, are actively working on nanosatellite technologies. In many cases, these technologies are being funded at the subsystem level of development (e.g., avionics on a chip or miniaturized propulsion systems), with emphasis placed on the technology of most interest by the organization providing the money. The DRACO mission will track these activities and wherever possible leverage these development efforts. One

potential near-term opportunity is to work closely with the recently awarded ST-5 mission, nanosatellite constellation Trailblazer. Efforts are already underway to establish a relationship with the ST-5 project office at Goddard Space Flight Center.

The same issues of nonrecurring cost and "manufacturability" apply to the spacecraft. In addition, however, there is the issue of integration and testing at the laboratory level (instruments and spacecraft). Although some efforts at development have begun in these areas (e.g., National Research Opportunity (NRO) Directors Innovation Initiative NRO000-99-R-0176), the issue as it applies to DRACO must be addressed. Although the spacecraft "manufacturability" issues can be addressed through the use of NRA's and Requests for Proposals (RFP's), a more integrated approach has been suggested for the DRACO mission.

It is thought that all of the manufacturability issues might be addressed by teaming a science group with a spacecraft vendor. In this fashion, an integrated approach can be taken from the beginning, at the design level. Innovative methods of testing must be developed to greatly reduce the time required; this can be accomplished through hardware design, software development or a combination of both. Test methods and hardware can be designed concurrently with the instrument and spacecraft development process. Instrument and spacecraft designs would be influenced by how easily and quickly integration could be done. At the present time, it is not clear what mechanism would be used to create or encourage the partnership of the science teams and the spacecraft teams.

4.3 Constellation Operations Management and Autonomy

In order to manage a large constellation of nanosatellites during the operations phase at a reasonable cost, a significant degree of autonomy on the ground as well as on board the nanosatellites will be required. There is already an existing base of experience and knowledge, along with the hardware and software tools, that resides in the commercial world — in particular, the Iridium communications constellation. It is expected that the DRACO formulation efforts will learn and build upon this knowledge base, developing new tools and methods as required for a scientific constellation. To the extent that the commercial world is aware of the push for future science missions that consist of large constellations of spacecraft, there is already some evolution of the ground operations tools and methodologies to accommodate this.

In the area of spacecraft autonomy, there is already a significant amount of interest in this area, with work being funded through numerous channels. The DRACO mission will require as a minimum the capability for onboard error detection and correction and the ability to operate for days or weeks at a time without ground intervention, but to a large extent these capabilities already exist. A greater
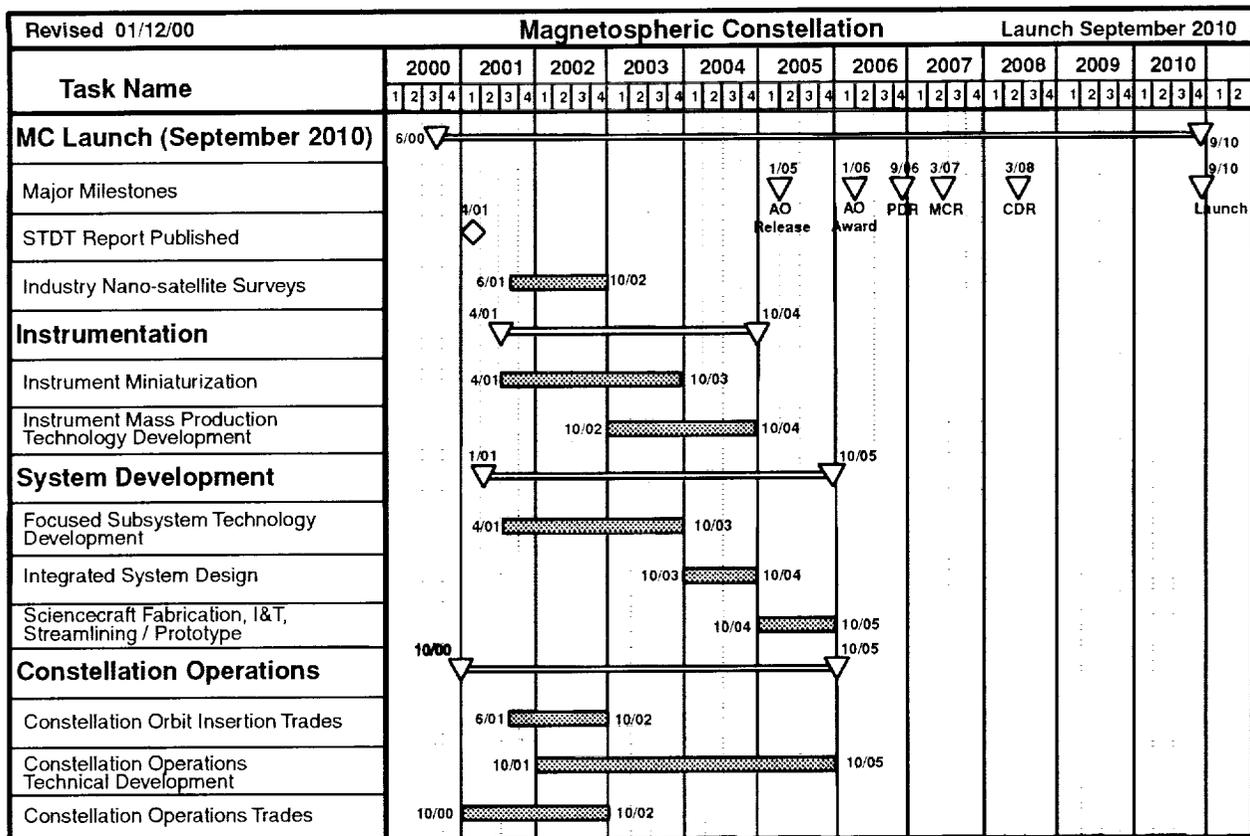
Magnetospheric Constellation — Launch September 2010

Task Name	Schedule (2000–2010)
MC Launch (September 2010)	6/00 → 9/10
Major Milestones	1/05 AO Release; 1/06 AO Award; 9/06 PDR; 3/07 MCR; 3/08 CDR; 9/10 Launch
STDT Report Published	4/01
Industry Nano-satellite Surveys	6/01 – 10/02
Instrumentation	4/01 – 10/04
Instrument Miniaturization	4/01 – 10/03
Instrument Mass Production Technology Development	10/02 – 10/04
System Development	1/01 – 10/05
Focused Subsystem Technology Development	4/01 – 10/03
Integrated System Design	10/03 – 10/04
Sciencecraft Fabrication, I&T, Streamlining / Prototype	10/04 – 10/05
Constellation Operations	10/00 – 10/05
Constellation Orbit Insertion Trades	6/01 – 10/02
Constellation Operations Technical Development	10/01 – 10/05
Constellation Operations Trades	10/00 – 10/02

Figure 25. Magnetotail Constellation development schedule.

degree of sophistication will be required for the DRACO mission and it is possible that new requirements will be levied in this area as the formulation effort progresses. At the current time, however, the exact degree of autonomy and detailed requirements for the DRACO Mission has not been determined beyond the basic requirements mentioned above.

4.4 Advanced Data Assimilation and Handling Techniques

It is widely recognized that the data sets generated by constellation missions require data management and handling techniques that are outside the current experience with space missions. Nevertheless, the problem is not qualitatively different from that associated with the conduct of atmospheric meteorology research and monitoring.

The most fundamental problem is the visualization of both scalar and vector field information from a large number of observing stations. Some techniques developed for meteorology will be directly transferable to use with constellation data sets. Others will require new techniques, for example, the visualization of magnetic field information that is not present in atmospheric meteorology.

The next step beyond basic visualization is the assimilation of the data into global circulation models. This will allow for instantaneous comparison with such models, extrapolation of the observations into other parts of the system outside the constellation, and projection or forecasting of system behavior for comparison with actual observed system evolution. This is a complex process, which has been discussed in much more detail in the section on science objectives, above.

Because the treatment of constellation data is so foreign to space physics, there is a significant need for the development of appropriate tools, borrowing wherever possible from prior work along the same lines that has already been completed in meteorology. As an integral part of the technology development effort for DRACO, developments along these lines should be supported at appropriate institutions with expertise in visualization and assimilation of data. Researchers who are active in the global simulation of magnetotail processes should undertake a significant amount of this work. They are in a position to generate simulated data sets, to introduce realistic errors in them, and then to develop the means to reassimilate the simulated data back into the same model that generated it, or other independent models.

Appendix A: Selected References

Aggson, T.L., J.P. Heppner, and N.C. Maynard, Observations of large magnetospheric electric fields during the onset phase of a substorm, J. Geophys. Res., **88**, p. 3981, 1983.

Akasofu, S.-I., The development of the auroral substorm, Planet. Space Sci., **12**. pp. 273-282, 1964.

Angelopoulos, V., C.F. Kennel, F.V. Coroniti, R. Pellat, H.E. Spence, M.G. Kivelson, R.J. Walker, W. Baumjohann, W.C. Feldman, J.T. Gosling, and C.T. Russell, Characteristics of ion flow in the quiet state of the inner plasma sheet, Geophys. Res. Lett., **20**, pp. 1711-1714, 1993.

Angelopoulos, V., C.F. Kennel, F.V. Coroniti, R. Pellat, M.G. Kivelson, R.J. Walker, C.T. Russell, W. Baumjohann, W.C. Feldman, and J.T. Gosling, Statistical characteristics of bursty bulk flow events, J. Geophys. Res., **99**, pp. 21257-21280, 1994.

Angelopoulos, V., F.V. Coroniti, C.F. Kennel, M.G. Kivelson, R.J. Walker, C.T. Russell, R.L. McPherron, E. Sanchez, C.-I. Meng, W. Baumjohann, G.D. Reeves, R.D. Belian, N. Sato, E. Friis-Christensen, P.R. Sutcliffe, K. Yumoto, and T. Harris, Multi-point analysis of a bursty bulk flow event on April 11, 1985, J. Geophys. Res., **101**, pp. 4967-4989, 1996.

Angelopoulos, V., T.D. Phan, D.E. Larson, F.S. Mozer, R.P. Lin, K. Tsuruda, H. Hayakawa, T. Mukai, S. Kokubun, T. Yamamoto, D.J. Williams, R.W. McEntire, R.P. Lepping, G.K. Parks, M. Brittnacher, G. Germany, J. Spann, H.J. Singer, and K. Yumoto, Magnetotail flow bursts: Association to global magnetospheric circulation, relationship to ionospheric activity and direct evidence for localization, Geophys. Res. Lett., **18**, p. 2271, 1997.

Ashour-Abdalla, M., L.M. Zelenyi, V. Peroomian, and R.L. Richard, Consequences of magnetotail ion dynamics, J. Geophys. Res., **99**, pp. 14891-14916, 1994.

Ashour-Abdalla, M., L.M. Zelenyi, V. Peroomian, R.L. Richard, and J.M. Bosqued, The mosaic structure of plasma bulk flows in the Earth's magnetotail, J. Geophys. Res., **100**, p. 19191, 1995.

Baker, D.N., T.I. Pulkkinen, R.L. McPherron, J.D. Craven, L.A. Frank, R.D. Elphinstone, J.S. Murphree, J.F. Fennell, R.E. Lopez, and T. Nagai, CDAW 9 analysis of magnetospheric events on May 3, 1986: Event C, J. Geophys. Res., **98**, pp. 3815-3834, 1993.

Baker, D.N., T.I. Pulkkinen, V. Angelopoulos, W. Baumjohann, and R.L. McPherron, Neutral line model of substorms: Past results and present view, J. Geophys. Res., **101**. p. 12975, 1996

Baumjohann, W., and G. Paschmann, Determination of the polytropic index in the plasma sheet, Geophys. Res. Lett., **16**, pp. 295-298, 1989.

Baumjohann, W., G.G. Paschmann, and C.A. Cattell, Average plasma properties in the central plasma sheet, J. Geophys. Res., **94**, pp. 6597-6606, 1989.

Baumjohann, W., G.G. Paschmann, and H. Luhr, Characteristics of high-speed ion flows in the plasma sheet, J. Geophys. Res., **95**, pp. 3801-3809, 1990.

Baumjohann, W., A short update on the present-day near-Earth neutral line model, J. Atmos. Sol.-Terr. Phys., **62**, 2000.

Berchem, J., J. Raeder, and M. Ashour-Abdalla, Interactive visualization of numerical simulation results: A tool for mission planning and data analysis, in: Visualization techniques in space and atmospheric sciences, E.P. Szuszczewics and J.H. Bredekamp Eds. NASA SP-519, 1995.

Birn, J., M. Hesse, and K. Schindler, MHD simulations of magnetotail dynamics, J. Geophys. Res., **101**(A6), p.12939, 1996.

Borovsky, J.E., R.C. Elphic, H.O. Funsten, and M.F. Thomsen, The Earth's plasma sheet as a laboratory for flow turbulence in high-beta MHD, J. Plasma Phys., **57**, p. 1, 1997.

Calder, Nigel, The Weather Machine, Penguin Books, Middlesex, UK, 1974.

Cattell, C., I. Roth, and M. Linton, The effects of low frequency waves on ion trajectories in the Earth's magnetotail, Geophys. Res. Lett., **22**, pp. 3445-3448, 1995.

Dungey, J., Inaugural Lecture as Professor of Physics at Imperial College, 1966; quote courtesy of W. J. Hughes.

Fairfield et al., Geotail observations of substorm onset in the inner magnetotail, J. Geophys. Res., **103**, p. 103, 1998.

Frank, L.A., and W.R. Paterson, Survey of electron and ion bulk flows in the distant magnetotail with the Geotail spacecraft, Geophys. Res. Lett., **21**, pp. 2963-2966, 1994.

Ghil, M. and P. Malanotte-Rizzoli, Data assimilation in meteorology and oceanography, Adv. Geophys., **33**, p. 141, 1997.

Ghil, M., K. Ide, A.F. Bennett, P. Courtier, M. Kimoto and N. Sato (Eds.), Data Assimilation in Meteorology and Oceanography: Theory and Practice, Meteorological Society of Japan and Universal Academy Press, Tokyo, 496 pp., 1997.

Goertz, C.K., and W. Baumjohann, On the thermodynamics of the plasma sheet, J. Geophys. Res., **96**, pp. 20991-20998, 1991.

Goodrich, C.C., et al., Interaction between the inner and mid-tail regions in MHD simulations of substorms, EOS Trans. AGU, 80(46), p. 871, 1999.

Haerendel, G., Disruption, ballooning or auroral avalanche on the cause of substorms, in First International Conference on Substorms, ESA SP-335, p. 417, 1992.

Hayakawa, H., A. Nishida, E.W. Hones, and S.J. Bame, Statistical characteristics of plasma flow in the magnetotail, J. Geophys. Res., **87**, pp. 277-283, 1982.

Henderson, M.G., G.D. Reeves, H.E. Spence, R.B. Sheldon, A.M. Jorgensen, J.B. Blake, and J.F. Fennell, First energetic neutral atom images from POLAR, Geophys. Res. Lett., **24**, p. 1167, 1997.

Hones, E.W., Jr., The magnetotail: Its generation and dissipation, Physics of Solar Planetary Environments, ed. by D.J. Williams, 557-571, AGU, Washington DC, 1976.

Hones, E.W., Jr., G. Paschmann, S.J. Bame, J.R. Asbridge, N. Sckopke, and K. Schindler, Vortices in magnetospheric plasma flow, Geophys. Res. Lett., **5**, p. 2069, 1978.

Hones, E.W., Jr., and K. Schindler, Magnetotail plasma flow during substorms: A survey with IMP 6 and IMP 8, J. Geophys. Res., **84**, pp. 7155-7169, 1979.

Hones, E.W., Jr., J. Birn, S.J. Bame, J.R. Asbridge, G. Paschmann, N. Sckopke, and G. Haerendel, Further determination of the characteristics of magnetospheric plasma vortices with ISEE 1 and 2, J. Geophys. Res., **86**, p. 814, 1981.

Hoshino, M., T. Mukai, A. Nishida, Y. Saito, T. Yamamoto and S. Kokubun, Evidence of two active reconnection sites in the distant magnetotail, J. Geomag. Geoelectr., **48**, p. 515, 1996.

Huang, C.Y., C.K. Goertz, L.A. Frank, and G. Rostoker, Observational determination of the adiabatic index in the quiet time plasma sheet, Geophys. Res. Lett., **16**, pp. 563-566, 1989.

Huang, C.Y., L.A. Frank, G. Rostoker, J. Fennell, and D.G. Mitchell, Nonadiabatic heating of the central plasma sheet at substorm onset, J. Geophys. Res., **97**, pp. 1481-1495, 1992.

Hughes, W.J., and D.G. Sibeck, On the three-dimensional structure of plasmoids, Geophys. Res. Lett., **14**, pp. 636-639, 1987.

Ieda, A., S. Machida, T. Mukai, Y. Saito, T. Yamamoto, A. Nishida, T. Terasawa, and S. Kokubun, Statistical analysis on the plasmoid evolution with Geotail observations, J. Geophys. Res., **103**, p. 4,453, 1998.

Jacquey, C., J.A. Sauvaud, and J. Dandouras, Tailward propagating cross-tail current disruption and dynamics of the near-Earth tail: A multi-point measurement analysis, Geophys. Res. Lett. **20(10)**, p. 983, 1993.

Jorgensen, A.M., H.E. Spence, M.G. Henderson, G.D. Reeves, M. Sugiura, and T. Kamei, Global energetic neutral atom (ENA) measurements and their association with the Dst index, Geophys. Res. Lett., **24**, p. 3173, 1997.

Krimigis, S.M., and E.T. Sarris, Energetic particle bursts in the Earth's magnetotail, in Dynamics of the Magnetosphere, edited by S. Akasofu, pp. 599-630, D. Reidel, Dordrecht, Holland, 1979.

Li, X., D.N.Baker, M.Temerin, G.D. Reeves, and R.D. Belian, Simulation of dispersionless injections and drift echoes of energetic electrons associated with substorms, Geophys. Res. Lett., **25(20)**, p. 3763, 1998.

Lieberman, A., NASA-GSFC Magnetospheric Constellation Mission Document, NASA GSFC Code 730, 30 March 1999a.

Lieberman, A., Final Report: Nanosat Dispenser Ship Performance Feasibility Study for the Magnetospheric Constellation Mission, NASA GSFC Code 730, Swales Aerospace report SAI-RPT-284, 22 July, 1999b.

Lopez, R.E., and A.T.Y. Lui, A multi-satellite case study of the expansion of a substorm current wedge in the near-Earth magnetotail, J. Geophys. Res., **95**, pp. 8009-8017, 1990.

Lopez, R.E., H.E.J. Koskinen, T.I. Pulkkinen, T. Bösinger, R.W. McEntire, and T.A. Potemra, Simultaneous observation of the poleward expansion of substorm electrojet activity and the tailward expansion of current sheet disruption in the near-Earth magnetotail, J. Geophys. Res., **98(A6)**, p. 9285, 1993.

Lui, A.T.Y., Plasma transport in the Earth's magnetotail, in Modeling Magnetospheric Plasma Processes. Geophys. Monogr. Ser., vol. 62, edited by G.R. Wilson, pp. 41-54, AGU, Washington DC, 1991.

Lui, A.T.Y., C.-L. Chang, A. Manofsky, H.-K. Wong, and D. Winske, A cross-field current instability for substorm expansions, J. Geophys. Res., **96**, pp. 11389-11401, 1991.

Lui, A.T.Y., Current disruption in the Earth's magnetosphere: Observations and models, J. Geophys. Res., **101(A6)**, p.13067, 1996.

Mauk, B.H., Quantitative modeling of the "Convection Surge" mechanism of ion acceleration, J. Geophys. Res., **13**, p. 423, 1986.

Maynard, N.C., W.J. Burke, E.M. Basinska, G.M. Erickson, W.J. Hughes, H.J. Singer, A.G. Yahnin, D.A. Hardy, and F.S. Mozer, Dynamics of the inner magnetosphere near times of substorm onsets, J. Geophys. Res., **101**, pp. 7705-7736, 1996.

McComas, D.J., C.T. Russell, R.C. Elphic, and S.J. Bame, The near-Earth cross-tail current sheet: Detailed ISEE 1 and 2 case studies, J. Geophys. Res., **91(A4)**, p. 4287, 1 April 1986.

McIlwain, C.E., Comments and speculations concerning the radiation belts, in Proceedings of the Joint IQSY/COSPAR Symposium, London, 1967, Part 1, MIT Press, Cambridge, MA, USA, p.303, 1967.

McPherron, R.L., C.T. Russell, and M.P. Aubrey, Satellite studies of magnetospheric substorms on August 15, 1968, 9, Phenomenological model for substorms, J. Geophys. Res., **78(16)**, pp. 3131-3149, 1973.

Miller, R.N., M. Ghil, and F. Gauthiez, Advanced data as simulation in strongly nonlinear dynamical systems, J. Atmos. Sci., **51**, p. 1037, 1994.

Moldwin, M.B., and W.J. Hughes, On the formation and evolution of plasmoids: A survey of ISEE 3 data, J. Geophys. Res., **97**, p. 19259, 1992.

Moore, T.E., R.L. Arnoldy, J. Feynman, and D.A. Hardy, Propagating substorm injection fronts, J. Geophys. Res. **86**, p. 6713, 1981.

Mukai, T., M. Fujimoto, M. Hoshino, S. Kokubun, S. Machida, K. Maezawa, A. Nishida, Y. Saito, T. Teresawa, and T. Yamamoto, Structure and kinetic properties of plasmoids and their boundary regions, J. Geomag. Geolectr., **48**, p. 541, 1996.

Nagai, T., Observed magnetic substorm signatures at synchronous altitudes, J. Geophys. Res., **87**, pp. 4405-4417, 1982.

Nagai, T., M. Fujimoto, Y. Saito, S. Machida, T. Teresawa, R. Nakamura, T. Yamamoto, T. Mukai, A. Nishida, and S. Kokubun, Structure and dynamics of magnetic reconnection for substorm onsets with Geotail observations. J. Geophys. Res., **103**, p. 4419, 1998.

Nakamura, R., D.N. Baker, D.H. Fairfield, D.G. Mitchell, R.L. McPherron, and E.W. Hones Jr., Plasma flow and magnetic field characteristics near the midtail neutral sheet, J. Geophys. Res., **99**, pp. 23591-23601, 1994.

Nishida, A., T. Mukai, T. Yamamoto, Y. Saito, and S. Kokubun, GEOTAIL Observations of the reconnection process in the distant tail in geomagnetically active times, J. Geophys. Res., **100**, p. 23663, 1995.

Ohtani, S., K. Takahashi, L.J. Zanetti, T.A. Potemra, R.W. McEntire, and T. Iijima, Tail current disruption in the geosynchronous region, in Magnetospheric Substorms, Geophys. Monogr. Ser., vol. 64, edited by J. R. Kan, T.A. Potemra, S. Kokubun, and T. Iijima, pp. 131-140, AGU, Washington DC, 1991.

Ohtani, S., S. Kokubun, and C.T. Russell, Radial expansion of the tail current disruption during substorms: A new approach to the substorm onset region, J. Geophys. Res., **97**, pp. 3129-3136, 1992.

Ohtani, S.-I., Earthward expansion of tail current disruption: Dual-satellite study, J. Geophys. Res., **103**(A4), p. 6815, 1998.

Owen, C.J., J.A. Slavin, I.G. Richardson, N. Murphy, and R.J. Hynds, Average motion, structure and orientation of the deep magnetotail determined from remote sensing of the edge of the plasma sheet boundary layer with E > 35 keV ions, J. Geophys. Res., **100**, p. 185, 1995.

Pulkkinen, T.I., et al., A study of magnetic field and current configurations in the magnetotail at time of a substorm onset, Plant. Space Sci., **39**, p. 883, 1991.

Quinn, J.M., and D.J. Southwood, Observations of parallelion energization in the equatorial region, J. Geophys. Res., **87**, p. 10536, 1982.

Reeves, G.D., R.W.H. Friedel, M.G. Henderson, A. Korth, P.S. McLachlan, and R.D. Belian, Radial propagation of substorm injections, International Conference on Substorms-3, ESA SP-339, pp. 579-584, 1996.

Robert, P., R. Gendrin, S. Perrault, and A. Roux, GEOS 2 identification of rapidly moving current structures in the equatorial outer magnetosphere during substorms, J. Geophys. Res., **89**, pp. 819-840, 1984.

Roux, A., S. Perraut, A. Morane, P. Robert, A. Korth, G. Kremser, A. Pederson, R. Pellinen, and Z.Y. Pu, Role of the near Earth plasmasheet at substorms, in Magnetospheric Substorms, Geophys. Monogr. Ser., vol. 64, edited by J.R. Kan, T.A. Potemra, S. Kokubun, and T. Iijima, pp. 201-214, AGU, Washington DC, 1991.

Schindler, K., A theory of the substorm mechanism, J. Geophys. Res., **79**, p. 2803, 1974.

Sergeev, V.A., T. Bosinger, and A.T.Y. Lui, Impulsive processes in the magnetotail during substorm expansion, J. Geophys. Res., **60**, pp. 175-185, 1986a.

Sergeev, V.A., R.J. Pellinen, T. Bosinger, W. Baumjohann, P. Stauning, and A.T.Y. Lui, Spatial and temporal characteristics of impulsive structure of magnetospheric substorm, J. Geophys. Res., **60**, pp. 186-198, 1986b.

Sergeev, V.A., R.J. Pellinen, and T.I. Pulkkinen, Steady magnetospheric convection: A review of recent results, J. Geophys. Res., 1996.

Slavin, J.A., M.F. Smith, E.L. Mazur, D.N. Baker, T. Iyemori, and E.W. Greenstadt, ISEE 3 observations of traveling compression regions in the Earth's magnetotail, J. Geophys. Res., **98**, p. 15425, 1993.

Slavin, J.A., D.H. Fairfield, R.P. Lepping, A. Szabo, M.J. Reiner, M. Kaiser, C.J. Owen, T. Phan, R. Lin, S. Kokubun, T. Mukai, T. Yamamoto, H.J. Singer, T. Iyemori, and G. Rostoker, Simultaneous WIND, GEOTAIL and GOES 9 observations of magnetic field dipolarization and bursty bulk flows in the near-tail during a substorm, Geophys. Res. Lett., **24**(8), p. 971, 1997.

Slavin, J.A., D.H. Fairfield, M.M. Kuznetsova, C.J. Owen, R.P. Lepping, S. Taguchi, T. Mukai, Y. Saito, T. Yamamoto, S. Kokubun, A.T.Y. Lui, and G.D. Reeves, ISTP observations of plasmoid ejection: IMP 8 and Geotail, J. Geophys. Res., **103**, p. 119, 1998.

Song, Y., and R.L. Lysak, Turbulent generation of auroral currents and fields — A spectral simulation of two-dimensional MHD turbulence, in Modeling Magnetospheric Plasma, T.E. Moore and J.H. Waite (eds.), p. 197, AGU, Washington D.C., 1988.

Spence, H.E., and M.G. Kivelson, Contributions of the low-latitude boundary layer to the finite width magnetotail convection model, J. Geophys. Res., **98**, pp. 15487-15496, 1993a.

Spence, H.E., L.A. Frank, W.R. Paterson, and M.G. Kivelson, The Galileo Earth-1 flyby: Comparison of the finite width tail convection model with observations, 1993 Fall AGU meeting, EOS Trans. **74**, p. 544, 1993b.

Stern, D.P., and N.A. Tsyganenko, Uses and limitations of the Tsyganenko magnetic field models, **73**, p. 489, 1992.

Swift, D.W., Numerical simulation of the generation of electrostatic turbulence in the magnetotail, Geophys. Res., **86**, p. 2273, 1981.

Taguchi, S., J.A. Slavin, M. Kiyohara, M. Nosé, G.D. Reeves, and R.P. Lepping, Temporal relationships between midtail traveling compression regions and substorm onset: Evidence for near-Earth neutral line formation in the late growth phase, JGR, **103**, 26607-26322, 1998.

Tajima, T., Astrophysical Plasmas, Frontiers in Physics series, Addison Wesley, 1997.

Talagrand, O., Assimilation of observations, an introduction, J. Meteo. Soc. Japan, **75**, p. 191, 1997.

Tsyganenko, N.A., A magnetospheric magnetic field model with a warped tail current sheet, Planet. Space Sci., **37**, pp. 5-20, 1989.

Tsyganenko, N.A., Modeling of twisted/warped magnetospheric configurations using the general deformation method, J. Geophys. Res., **103** (A10), p. 23551, 1998.

Tsyganenko, N.A., Modeling the Earth's magnetic field confined within a realistic magnetopause, J. Geophys. Res., **100**, p. 5599, 1995.

Tsyganenko, N.A., and M. Peredo, Analytical models of the magnetic field of disk-shaped current sheets, J. Geophys. Res., **99**, p. 199, 1994.

Tsyganenko, N.A., and A.V. Usmanov, Determination of the magnetospheric current parameters and development of experimental geomagnetic field models based on data from IMP and HELIOS satellites, Planet. Space Sci., **30**, p. 985, 1982.

Wang, X., A. Bhattacharjee, and A.T.Y. Lui, Collisionless tearing instability in magnetotail plasmas, J. Geophys. Res., **95**(A9), p. 15047, 1 September 1990.

Appendix B: Acronyms and Abbreviations

ACS — Attitude Control Subsystem
AFFCI/
GPS — A Formation Flying and Communications Instrument/Global Positioning System
AMIE — Assimilative Mapping of Ionospheric Electrodynamics
ASIC — Application Specific Integrated Circuit
BAI — Burst Accumulation Interval
BBF — Bursty Bulk Flows
BOL — Beginning of Life
CCE — Charge Composition Explorer
CCSDS — Consulting Committee for Space Data Systems
C&DH — Command and Data Handling
CDPU — Command and Data Processing Unit
cm — centimeter
CME — Coronal Mass Ejection
CPU — Central Processing Unit
dB/K — decibel/Kelvin
DMSP — Defense Meteorological Spacecraft Program
DNL — Distant Neutral Line
DOD — Department of Defense
DPU — Data Processing Unit
DRACO — Dynamic Response and Coupling Observatory
DS — Dispenser Ship
EIRP — Effective Isotropic Radiated Power
EPA — Energetic Particles Analyzer
EPIC/ICS — Energetic Particles and Ion Composition/Ion Composition System
EPS — Electrical Power Subsystem
ESA — Electrostatic Analyzer
ESN — Essential Servicing Node
FOV — Field of View
FPGAs — Field Programmable Gate Arrays
GaAs — Gallium Arsenide
GEC — Geospace Electrodynamics Connection
GFs — Geometric Factor
g — gram
GN2 — Gaseous Nitrogen
GN&C — Guidance, Navigation and Control
GPS — Global Positioning Satellite
GSFC — Goddard Space Flight Center
HLBL — High-Latitude Boundary Layers
HVPS — High-Voltage Power Supply
IR — Infrared
ISTP — International Solar Terrestrial Project
Kb/sec — Kilobits/seconds
LEP — Low Energy Plasma
LLBL — Low-Latitude Boundary Layers
m — meter
MAG — Magnetometer
MCM — Multi-Chip Module
MCP — Micro-Channel Plate
MCSTDT — Magnetospheric Constellation Science and Technology Definition Team

MFE — Magnetic Field Experiment
MHD — Magnetohydrodynamic
MLI — Multi-Layer Insulation
mm — millimeter
MMS — Magnetospheric Multiscale
NASA — National Aeronautics and Space Administration
NENL — Near Earth Neutral Line
NRA — NASA Research Announcement
NRO — National Research Opportunity
OP — Orbital Period
PSBL — Plasma-Sheet Boundary Layers
PVA — Plasma Velocity Analyzer
QA — Quality Assurance
RAI — Routine Accumulation Interval
RAM — Random Access Memory
RF — Radio Frequency
RFP — Request For Proposal
rpm — Revolutions Per Minute
SCW — Substorm Current Wedge
SEC — Sun-Earth Connection
SECAS — Sun-Earth Connection/Advisory Subcommittee
SP — Spin Period
SST — Solid State Telescope
STDT — Scientific and Technology Definition Team
STI — Scientific and Technical Information
STP — Solar Terrestrial Probes
TCS — Thermal Control System
UHF — Ultrahigh Frequency
UV — Ultraviolet
W — Watt